Univerzita Karlova v Praze
Matematicko-fyzikální fakulta

DIPLOMOVÁ PRÁCE

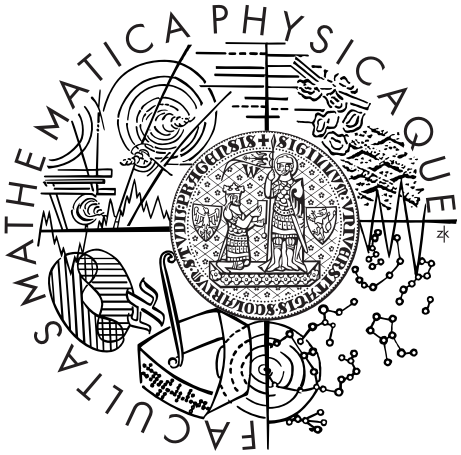

Milan Klicpera

Magnetokrystalová anizotropie ve sloučeninách TbTX

Katedra fyziky kondenzovaných soustav

Vedoucí diplomové práce: doc. Mgr. Pavel Javorský, Dr.

Studijní program: Obecná fyzika
Specializace: Fyzika kondenzovaných soustav a materiálů

Praha 2011

Charles University in Prague
Faculty of Mathematics and Physics

MASTER THESIS

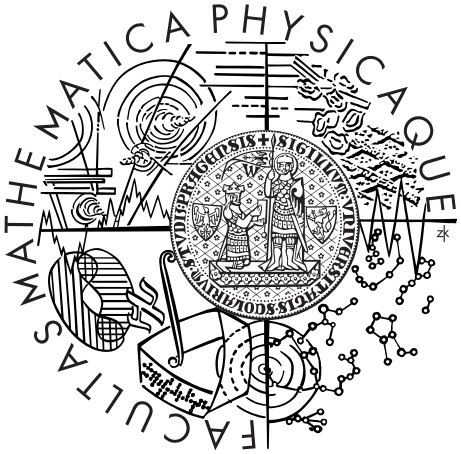

Milan Klicpera

The magnetocrystalline anizotropy in the TbTX compounds

Department of Condensed Matter Physics

Supervisor of master thesis: doc. Mgr. Pavel Javorský, Dr.

Study programme: General physics
Specialization: Physics of Condensed Matter and Materials

Prague 2011

In this place, I would like to thank to everybody who helped me during the work on this thesis.

I am most grateful to my supervisor, Doc. Mgr. Pavel Javorský, Dr. He supported me and he always had the time for my questions about my study and work on my thesis. He helped me to understand the studied problematic as well as experimental technics which I used during my work. I am also thankful to him for the assistance with interpreting the results of individual measurements and last, but not least for the help with writing this thesis.

I am very thankful also to other members of the Department of Condensed Matter Physics of the Faculty of Mathematics and Physics of Charles University in Prague. Above all, I am grateful to Doc. RNDr. Stanislav Daniš, Ph.D. for his help with X-ray diffraction and especially low temperature X-ray diffraction experiments and RNDr. Jiří Prchal, Ph.D. for his guidance of my electrical resistivity measurements and for his teaching me how to use the pressure cell.

My gratitude also belongs to Ing. Eva Šantavá, CSc. from the Institute of Physics of the Academy of Sciences of the Czech Republic for introducing me to the problematic of magnetic properties measurement.

I want to thank to Dr. Inés Puente Orench for her help with the powder neutron diffraction experiment provided in Institut Laue-Langevin, Grenoble, France.

I would like to thank also my colleagues Mgr. Jiří Kaštil, Mgr. Petr Čermák, Mgr. Jan Fikáček and Bc. Marie Kratochvílová for their collaboration in some experiments and daily work.

Prohlašuji, že jsem tuto diplomovou práci vypracoval samostatně a výhradně s použitím citovaných pramenů, literatury a dalších odborných zdrojů.

Beru na vědomí, že se na moji práci vztahují práva a povinnosti vyplývající ze zákona č. 121/2000 Sb., autorského zákona v platném znění, zejména skutečnost, že Univerzita Karlova v Praze má právo na uzavření licenční smlouvy o užití této práce jako školního díla podle §60 odst. 1 autorského zákona.

V ..... dne ..... Podpis autora

Název práce: Magnetokrystalová anizotropie ve sloučeninách TbTX
Autor: Milan Klicpera
Katedra: Katedra fyziky kondenzovaných soustav
Vedoucí bakalářské práce: doc. Mgr. Pavel Javorský, Dr.
e-mail vedoucího: javor@mag.mff.cuni.cz

Abstrakt: Předmětem této práce je studium strukturních, magnetických a transportních vlastností série TbNi(Al,In) jež povede k nalezení souvislostí mezi magnetokrystalovou anizotropií a mřížovými parametry struktury sloučenin TbTX. Polykrystalické vzorky $TbNiAl_{1-x}In_x$ byly připraveny tavením. Na vzorcích byla provedena fázová a strukturní analýza. Provedli jsme měření magnetizace, susceptibility, měrného tepla, elektrického odporu, nízkoteplotní rentgenové difrakce a práškové neutronové difrakce. Z neutronové difrakce jsme určili mřížové parametry a propagační vektory série. Hlavní propagace je (000) a druhá slabší komponenta má propagační vektor $(\frac{1}{2}\ 0\ \frac{1}{2})$. Změna magnetokrystalové anizotropie z jednoosého na planární typ nastává pro sloučeninu s x mezi 0.4 a 0.5.

Klíčová slova: magnetizace, rentgenová a neutronová difrakce, elektrický odpor.

Title: The magnetocrystalline anizotropy in the TbTX compounds
Author: Milan Klicpera
Department: Department of Condensed Matter Physics
Supervisor: doc. Mgr. Pavel Javorský, Dr.
Supervisor's e-mail address: javor@mag.mff.cuni.cz

Abstract: The subject of this work is the study of structural, magnetic and transport properties of the TbNi(Al,In) series to finding connections between magnetocrystalline anisotropy and lattice parameters of the structure of the TbTX compounds. Polycrystalline $TbNiAl_{1-x}In_x$ samples were prepared by melting. The phase and crystal structure analysis were provided on samples. We performed the measurements of the magnetization, susceptibility, specific heat, resistivity, low temperature X-ray diffraction and powder neutron diffraction. From the neutron diffraction data we refined lattice parameters and propagation vectors of the series. The main propagation is (000) and second weaker component has the propagation vector $(\frac{1}{2}\ 0\ \frac{1}{2})$. The change of the magnetocrystalline anisotropy from uniaxial to planar type occurs for compounds with x between 0.4 and 0.5.

Keywords: magnetization, X-ray and neutron diffraction, electrical resistivity.

Contents

Introduction

Intermetallic compounds of elements with partially filled f-electron shells show numerous effects such as the Kondo effect, heavy fermion behavior, coexistence of superconductivity and long-range magnetic order, mixed valence and complex magnetic ordering.

Ternary RTX compounds (R = rare earth, T = transition d-metal, X = p-metal) form a large group of intermetallics showing interesting magnetic properties mainly at cryogenic temperatures. A great importance in the study of these compounds has an influence of a chemical pressure on their structural and magnetic properties. The substitution of one element by another one leads to a change of structural parameters and can also change the number of conduction electrons in the system. As a consequence, the magnetic structure can change as well. This is due to the fact that the magnetic ordering in rare-earth compounds is mediated mainly by the electrons in the conduction band. Moreover, it appears that the different size of the substituted elements, that have the same number of conduction electrons, not only leads to a change of the lattice parameters, but can lead also to a change of magnetic structure.

This work is focused on the structural and magnetic behavior of $TbNiAl_{1-x}In_x$ pseudo-ternary series, where aluminium is being substituted by indium. This series belong to the large group of RTX compounds crystallizing in the hexagonal ZrNiAl-type of structure. The motivation of the study of TbNi(Al,In) series originates from previous studies of the TbTX compounds. Based on the investigation of magnetic structures in TbTX, all TbTAl have magnetic moments along the c-axis while TbTIn perpendicular to the c-axis. The transition between the easy-axis and easy-plane type of anisotropy should thus occur in the TbNi(Al,In) series. We have been looking for the connection between the change of lattice parameters, especially the c/a ratio, and magnetic structure.

During the present study, the polycrystalline samples with selected concentrations x have been prepared, their structure has been verified using X-ray diffraction, the distribution of elements has been found by EDX probe, the transport and magnetic properties were obtained by resistance, magnetization and heat-capacity measurement, the magnetic structure has been investigated by the low-temperature X-ray diffraction in static magnetic field and especially by the neutron diffraction experiment. The main goals of this work are: the examination of the influence of the substitution in TbNi(Al,In) series on the crystal and magnetic properties, finding the relation between crystal and magnetic structure and the generalization to the whole TbTX series.

This thesis is organized in the following way. The basic information about lanthanides, magnetic interactions, magnetic structures and brief introduction to X-ray and neutron diffraction are written in chapter 1.Theory. Results already known before we started to collect the results for this thesis are included in chapter 2.Previous results. Used techniques for sample preparation and obtaining the experimental data are described in chapter 3.Experimental details. Chapter 4.Results and discussion represents the main part of the thesis showing all experimental data and their discussion. The main results reached in this work are then placed in chapter 5.Conclusions.

1. Theory

1.1 Lanthanides

Lanthanides, the elements between lanthanum (La^{57}) and lutetium (Lu^{71}), together with scandium (Sc^{21}) and yttrium (Y^{39}) form a group historically known as rare earths. Lanthanides usually form trivalent cations Ln^{3+} in compounds. In addition, (Ce^{58}) can lose its single f electron to form tetravalent cation with the stable electronic configuration of xenon (Xe^{54}). Also, Eu^{63} can gain an electron to form divalent cation with the $4f^7$ configuration which has the extra stability of a half-filled shell, and Yb^{70} which form also divalent cation because of an effort to fill completely $4f$ shell. Strictly speaking, both boundary elements lanthanum and lutetium have been labeled as $5d$ elements, because they both have a single valence electron in the d shell. However, both elements are often included in any general discussion of the chemistry of the lanthanide elements. Lanthanum, yttrium and lutetium are mostly considered as $4f$ elements with empty(full) $4f$ shell, so as a non-magnetic analogue. The electronic structure of the lanthanide elements, with minor exceptions, is [Xe] $6s^2$ $4f^{\mathrm{N}}$.

Table 1.1: The atomic electron configuration of lanthanides and an electron configuration and atomic radius of their Ln^{3+} cations [1].

Element	Atomic configuration [Xe]	Electron configuration	Radius (pm)
Ce	$4f^1 5d^1 6s^2$	$4f^1$	102
Pr	$4f^3 6s^2$	$4f^2$	99
Nd	$4f^4 6s^2$	$4f^3$	98.3
Pm	$4f^5 6s^2$	$4f^4$	97
Sm	$4f^6 6s^2$	$4f^5$	95.8
Eu	$4f^7 6s^2$	$4f^6$	94.7
Gd	$4f^7 5d^1 6s^2$	$4f^7$	93.8
Tb	$4f^9 6s^2$	$4f^8$	92.3
Dy	$4f^{10} 6s^2$	$4f^9$	91.2
Ho	$4f^{11} 6s^2$	$4f^{10}$	90.1
Er	$4f^{12} 6s^2$	$4f^{11}$	89
Tm	$4f^{13} 6s^2$	$4f^{12}$	88
Yb	$4f^{14} 6s^2$	$4f^{13}$	86.8
Lu	$4f^{14} 5d^1 6s^2$	$4f^{14}$	86.1

The $4f$ orbital is located relatively deeply inside the atom and is shielded from $5d$ and $6s$ electrons. As a consequence of this, the chemistry of the elements is largely determined by their size, which decreases gradually from 102 pm (La^{3+}) to 86 pm (Lu^{3+}) with increasing atomic number, the so-called lanthanide contraction (see Table 1.1 according to Goldschmidt [1]). Near the atomic nuclei well-localized $4f$ electrons have only little effect on chemical bonding, however, the more fundamental importance to the magnetic behavior. All the trivalent lanthanide ions, except lutetium, have unpaired f electron(s). The magnetic

moments deviate considerably from the spin-only values because of the strong spin-orbit coupling. Neighbors ions and electrons of the lanthanide ion produce the electrostatic field, so-called crystal field (CF), which has the effect on the $4f$ electrons. CF causes splitting of the multiplet of lanthanide ion into $2J+1$ levels. Crystal field splitting is rather small for the lanthanide ions and is less important than spin-orbit coupling in regard to energy levels [2]. Because of the shielding of the f orbital, the coupling with molecular vibrations is weak. Consequently the spectra of lanthanide ions are rather weak and the absorption bands are similarly narrow.

1.2 Magnetic interactions

Exchange interactions are responsible for the ordering of magnetic moments in solids. Exchange interactions are divided into two basic types: direct and indirect. Special and important type of indirect interaction is called as RKKY. Well-arranged picture of these three exchange interactions according to Ashcroft [3] is shown in the Figure 1.1.

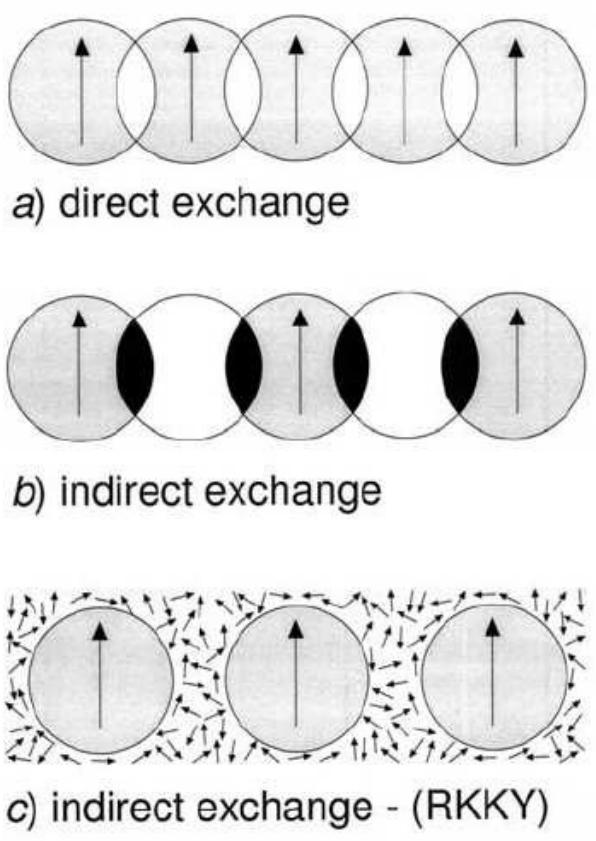

Figure 1.1: The basic types of exchange interactions: the direct, the indirect and the indirect RKKY exchange interaction [3].

The exchange interaction between two ions can be expressed by Heisenberg model as:

$$\hat{H}_{ij} = -\,2\,\mathrm{J}_{ij}\,\hat{S}_i\,\hat{S}_j, \tag{1.1}$$

where J_{ij} is the exchange integral between the spins S_i and S_j. The total Hamiltonian for the whole system is then:

$$\hat{H}_{\mathrm{ex}} = -\sum_{i \neq j} \mathrm{J}_{ij}\, \hat{S}_i\, \hat{S}_j, \tag{1.2}$$

The direct exchange interaction which is decisive for $3d$ elements, in the case of $4f$ metals is not very important because of negligible direct overlap of the $4f$-electronic wave functions. As mentioned in Section 1.1, $4f$ electrons are well-localized inside the atom and shielded by $5d$ and $6s$ electrons.

Much more important in these systems therefore are the indirect interactions. There are various types of these interactions, one important of them - conduction electrons mediate RKKY interaction. The electrons are spin polarized because of the presence of magnetic moments in their surrounding. Owing to properties of conduction electrons, this type of interaction is oscillating according the distance from the original magnetic ion. The polarized electrons then interact with the neighboring magnetic moments. The Hamiltonian of this interaction is:

$$\hat{H}_{\mathrm{RKKY}} = -\frac{1}{2} \sum_{i,j} \mathrm{J}(R_i - R_j)\, J_i\, J_j, \tag{1.3}$$

where we sum over all rare-earth ions with the moment J_i. J(R_i - R_j) is the effective exchange parameter.

Another type of the indirect exchange was proposed by Campbell [4]. This type is based on the coupling between $4f$-moments by the $5d$ rare earth electrons. As a consequence of the f-d exchange coupling, a positive local d-moment is induced. Because of the delocalized $5d$ electrons of the rare earth and the overlap of wave functions, one can take into account direct exchange interaction. In compounds with transition metals, the exchange between rare-earth $5d$-states and d-states of the transition metal has to be furthermore considered. This type of interaction prefers ferromagnetic coupling, reflected e.g. in a positive value of the paramagnetic Curie temperature.

1.3 Magnetic ordering

Mutual magnetic interactions between magnetic ions may lead to their regular arrangement. The magnetic order can, however, occur only at sufficiently low temperatures where magnetic interactions outweigh the thermal chaos. Above the magnetic ordering temperature the compounds behave as paramagnets. In paramagnetic materials, the dipole moments are randomly oriented due to thermal fluctuations. The total magnetic moment of the substance in zero external magnetic field is consequently zero. In the non-zero field, we observe flipping of individual dipole moments in the direction of the applied field and the total magnetic moment of the substance forms in this direction. The temperature dependence of magnetic susceptibility $\chi(T)$ in the paramagnetic state is described by Curie-Weiss law:

$$\chi \;=\; \frac{M}{H} \;\doteq\; \frac{\mathrm{N_A}\, \mu_0\, \mu_B^2\, \mu_{\mathrm{eff}}^2}{3\, \mathrm{k_B}\, (T - \theta_{\mathrm{P}})} + \chi_0 = \frac{\mathrm{C}}{(T - \theta_{\mathrm{P}})} + \chi_0, \tag{1.4}$$

where μ_{eff} is effective magnetic moment, θ_{P} is paramagnetic Curie temperature, and χ_0 is a parameter which includes the Pauli paramagnetic contribution to susceptibility and Van Vleck susceptibility. In the case of the polycrystalline material χ_0 also depends on the magnetocrystalline anisotropy.

In addition to the above mentioned paramagnetism of compounds containing magnetic ions, we observe also the paramagnetism of conduction electrons (Pauli paramagnetism) [4]. However, this contribution to the overall magnetization is much less evident and is manifested mainly in the materials without magnetic ions.

At the so-called critical temperature (the Curie temperature T_{C} for ferromagnetic, the Néel temperature T_{N} for antiferromagnetic compounds) the magnetic interactions become stronger then thermal fluctuation. The magnetic dipoles begin to orientate and this phenomenon may lead to the ordering of magnetic moments in compounds.

Ferromagnetic materials exhibit a spontaneous magnetization with magnetic domains in which the magnetic dipoles are identically oriented. The domain has a spontaneous magnetic moment, a non-zero magnetic moment even in zero external magnetic field, which is caused by regular arrangement of magnetic dipoles (see Figure 1.2a). In zero external magnetic field, the direction of the magnetic moments of each domain is different. Thus, the resulting magnetic moment of the compound is zero. In a weak external field boundaries of domains that have magnetic moments oriented in the direction of the field are expanding. At higher magnetic fields the magnetic moments in domains are progressively oriented in the direction of external magnetic field.

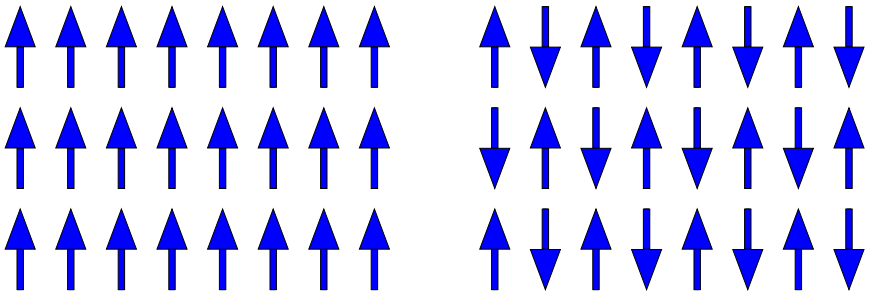

(a) Ferromagnetic ordering. (b) Antiferromagnetic ordering.

Figure 1.2: The basic types of magnetic ordering.

Magnetic domains occur also in antiferromagnetic materials. In this case, however, spins are arranged antiparallel as can be seen in Figure 1.2b. In zero external magnetic field the total magnetic moment of the domain and also the total magnetic moment of the substance are equal to zero. In the non-zero external magnetic field moments gradually move in the direction of the field and the total magnetic moment of the substance will point in the direction of the external field. Sufficiently strong magnetic field can then lead to a reorientation of the moments and the transition to the ferromagnetic state.

Another possibility of magnetic ordering is ferrimagnetic state or in other words uncompensated antiferromagnetism. Unlike the previous antiferromagnetic type of ordering in this case magnetic moments do not have the same size and because of that the magnetic moment of the domain is non-zero in zero external magnetic field.

1.4 X-ray and neutron scattering

The importance of scattering as very powerful method for determining atomic structures in solids is constantly increasing in the last few decades. Beam of X-rays, electrons or neutrons is mostly used as a radiation. Generally, there are two types of the scattering - elastic (diffraction) and inelastic. There are many scattering techniques whose are becoming increasingly popular in last time, but due to used methods in this work we focus only on brief description of X-ray and neutron elastic diffraction.

According to the Bragg's model of diffraction, a given reflection is associated with a set of evenly spaced sheets running through the crystal. The orientation of a particular set of sheets is identified by its three Miller indices ($h\ k\ l$), and let their spacing be noted by d. The incident radiation with a wavelength λ is scattered on electrons for X-ray radiation, on nuclei and in the case of magnetic scattering on electrons for beam of neutrons. The wave of the incident radiation scatters in atoms in periodic sets of planes and the scattered wave superpose coherently, resulting in diffracted intensities of the beam distributed in specific directions due to the constructive interference.

For a given crystal structure, the positions of the nuclear reflections are given by Bragg's law:

$$\lambda = 2\, d_{hkl}\, \sin\theta, \tag{1.5}$$

where θ is the angle between the normal to the hkl–plane and the direction of interacting radiation.

The measured intensities of the reflected radiation depends on the structure of a crystal which is represented by the structure factor F_{hkl}:

$$I \approx |F_{hkl}|^2. \tag{1.6}$$

The expressions of the structure factor are different for X-ray radiation, neutrons and magnetic scattering of neutrons. This distinction is caused by the different way of scattering on the crystal. X-ray radiation is scattered on electrons and because of that is the structure factor given by:

$$F_{hkl} = \sum_i f_{at}(\vec{q})\, \mathrm{e}^{-2\pi i \vec{q}.\vec{r}_i}\, \mathrm{e}^{-W_i}, \tag{1.7}$$

where we sum over the primitive cell. The parameter $f_{at}(\vec{q})$ is the atomic dispersion factor which is given as the Fourier transformation of the electronic charge density $\rho(\vec{r})$:

$$f_{at}(\vec{q}) = \int_V \rho(\vec{r})\, \mathrm{e}^{i\vec{q}.\vec{r}}\, \mathrm{d}\vec{r}. \tag{1.8}$$

The scattering vector $\vec{q}$ is the vector in reciprocal space, $\vec{r}_i$ is the position of an atom i in the primitive cell. The expression e^{-W_i} is the square root of the Debye-Waller factor. W_i involves the mean square displacement of the atom around its equilibrium position, this displacement is dependent on the temperature.

The structure factor for neutron diffraction (scattering on nuclei) is given by:

$$F_{hkl} = \sum_i \mathrm{b_c}\, \mathrm{e}^{-2\pi i \vec{q}.\vec{r}_i}\, \mathrm{e}^{-W_i}, \tag{1.9}$$

where b_c is a coherent scattering length. In contrast to X-ray radiation, where the atomic dispersion factor $f_{at}(\vec{q})$ is a function of the charge density, in the case of neutron scattering the parameter b_c is random with respect to the specific element and it can moreover vary within different isotopes of a given element. The scattering lengths are tabulated, for example in [5].

The neutrons are particles with spin and because of that they may interact also with the magnetic moments in the matter (spin-spin interaction). Interaction with the moments forming a magnetic structure in a material leads to additional diffraction patterns, similar to the ones obtained by diffraction on a periodic crystal structure. Usually we can observe both - the crystalline (nuclear) and the magnetic structure of a material using the same probe. The magnetic structure factor F_M is given by:

$$F_M = \frac{\gamma\, e^2}{2\, m_e\, c^2} \sum_j f_j(\vec{q})\, m_j\, e^{i\vec{q}.\vec{r}_j}\, e^{-W_j}, \tag{1.10}$$

where the sum is over all the magnetic moments within the unit cell. The parameter $f_j(\vec{q})$ is the magnetic form factor of atom j and m_j is the magnetic moment. The $f_j(\vec{q})$ function decreases with increasing $\vec{q}$ (and thus with the scattering angle), similar to $f_{at}(\vec{q})$ for the X-ray diffraction. In contrast, the scattering lengths b_c is $\vec{q}$-independent.

2. Previous results

2.1 *RTX* compounds

RTX compounds crystallize in many different structures and, on the other hand, there is also a large number of compounds that crystallize in the same structure type. Most common types are the orthorombic TiNiSi structure, the hexagonal AlB_2 structure and the hexagonal ZrNiAl structure (more for instance in [6]).

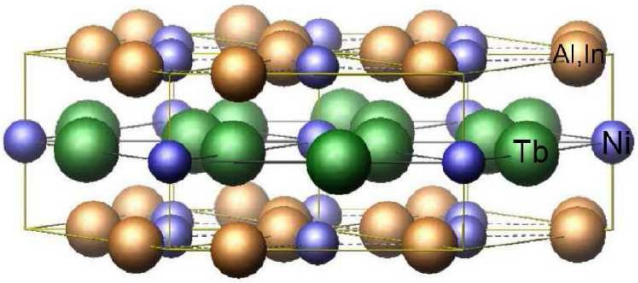

Atomic fraction coordinates:

Tb(3g):	Tb_1:	x_{Tb}	0	$\frac{1}{2}$
	Tb_2:	0	x_{Tb}	$\frac{1}{2}$
	Tb_3:	$-x_{Tb}$	$-x_{Tb}$	$\frac{1}{2}$
Ni(2c):		$\frac{1}{3}$	$\frac{2}{3}$	0
Ni(1b):		0	0	$\frac{1}{2}$
Al-In(3f):		$x_{Al(In)}$	0	0

Figure 2.1: Hexagonal ZrNiAl-type of structure (space group $P\bar{6}2m$). In our case structure of TbNi(Al,In). Fraction coordinates are also written in Figure. The positions of terbium atoms (Tb_1,Tb_2 and Tb_3) are equivalent from the symmetry.

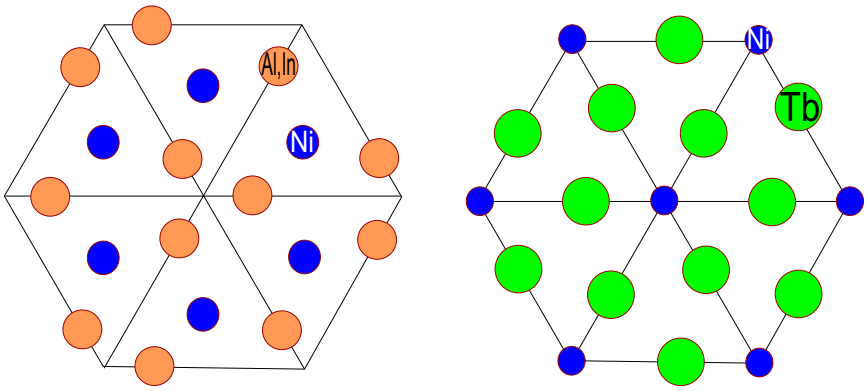

(a) z = 0 (b) z = $\frac{1}{2}$

Figure 2.2: Basal plane of ZrNiAl structure at layer z = 0 and z = $\frac{1}{2}$. The rare-earth atoms are placed in positions with orthorhombic symmetry.

Many ternary *R*NiAl, *R*CuAl, *R*PdAl, *R*NiIn, *R*CuIn, *R*PdIn, *R*AuIn, *R*RhSn and *R*PdTl series and their substitutions crystalize in ZrNiAl-type of structure (see Figures 2.1 and 2.2). Their investigation shows various magnetic properties ranging from non-magnetic valence fluctuators (e.g. CeNiAl [7]) to materials with complex magnetic structures, often characterized by the existence of frustrated magnetic moments (e.g. in most *R*NiAl compounds [8], CePdAl [9] or TmCuAl [10]). One of the essential characteristics of these materials is the magnetocrystalline anisotropy. The anisotropy is given mainly by crystal field acting on rare-earth ions and is largely influenced by the parameters of the crystal structure. Among these *RTX* compounds the strongest anisotropy is observed in terbium compounds - Tb*TX* (see e.g. [11]). Because of a systematic study of Tb*TX* series

we have data for a compilation Figure 2.3. From this Figure one can assume the flipping of magnetic moments from the direction parallel to the c-axis to the basal plane with decreasing c/a ratio.

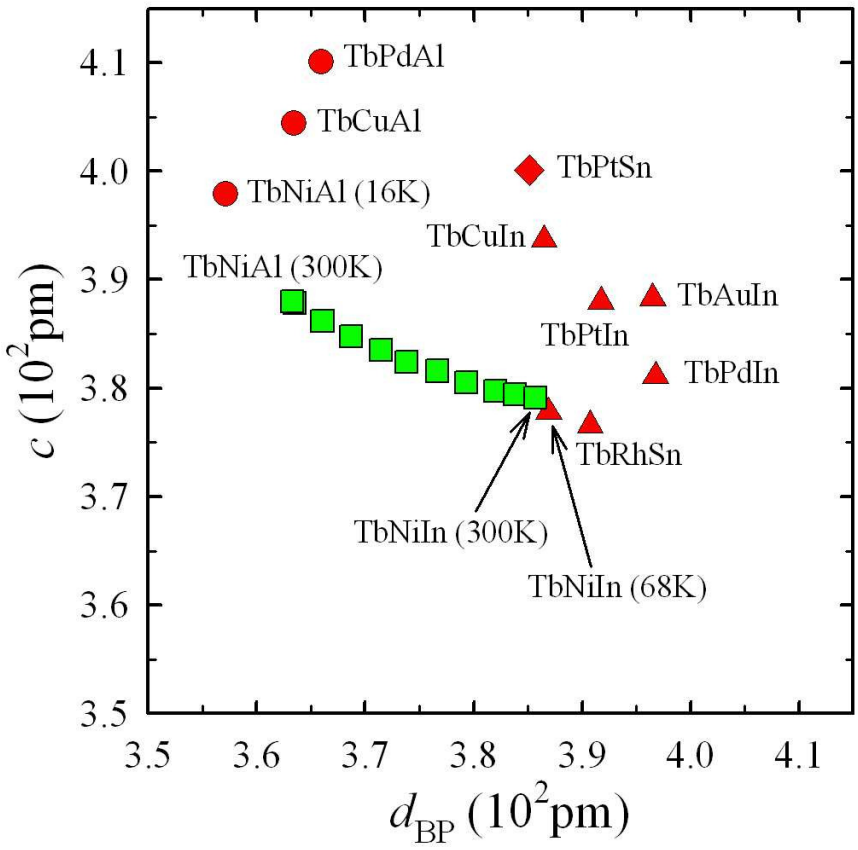

Figure 2.3: Magnetocrystalline anisotropy in TbTX compounds studied until now. d_{BP} is the distance between Tb atoms in the basal plane. The symbol '$\circ$' means Tb moments along the c-axis, the symbol '$\triangle$' Tb moments perpendicular to the c-axis and '$\diamond$' more complex behavior of magnetic moments pointing out of any principal crystallographic direction. The symbol '$\square$' indicate data measured by X-ray diffraction at 300 K in this work. The compounds occurring in the Figure were previously studied by X-ray and neutron diffraction: TbPdAl [12], TbCuAl [13], TbNiAl (16 K) [14] TbPtSn [15], TbCuIn [16], TbAuIn [17], TbPdIn [18], TbPtIn [19], TbRhSn [20], TbNiIn (68 K) [21].

A very interesting and surprising development of magnetic behavior was observed in the $R\mathrm{Ni}_{1-\mathrm{x}}\mathrm{Cu}_{\mathrm{x}}\mathrm{Al}$ series with R = Tb [13], Er [22], Dy [23], Nd [24] and Pr [25]. The transition between the magnetic order in RNiAl and RCuAl is rather complex and unusual. In particular, the loss of the long-range magnetic order in the concentration range between x $\simeq$ 0.6 and 0.8 was observed in all the five series. Nickel and copper are neighbors in the periodic table, their size is not much different, however the Cu atoms bring more d-electrons to the system. This change of the number of d-electrons can cause the change of the magnetic order from antiferromagnetic to ferromagnetic (for instance in Tb(Ni,Cu)Al system [13]), or even the flip of magnetic moments from the direction parallel with the hexagonal c-axis to basal plane. This flip was observed for the Er(Ni,Cu)Al series, ErNiAl is antifferomagnet with Er moments perpendicular to the hexagonal c-axis [26, 27] and ErCuAl is ferromagnet with Er moments along the c-axis [26]. A somewhat surprising finding was the influence of this substitution in the sys-

tem Dy(Ni,Cu)Al, where both parent compounds exhibit very similar behavior, characterized mainly by the dominant ferromagnetic moment of Dy along the c-axis (DyNiAl orders ferromagnetically with weaker antifferomagnetic component [8] and DyCuAl orders ferromagnetically [28]), but at the Ni-Cu concentration between 40 - 60% dominant antiffermagnetic ordering appears [29, 27, 23].

A structural discontinuity in the concentration evolution of the lattice parameters was found in the $R\mathrm{Ni}_{1-\mathrm{x}}\mathrm{Cu}_{\mathrm{x}}\mathrm{Al}$ series (R = Er [22], Dy [29]). A common property of this discontinuity is the absence of similar values of the c/a ratio (see Figure 2.4). A similar behavior of lattice parameters was also observed for other compounds where similar c/a values were absent (for more details see [30]). Despite the fact that the rule is correct for many $RT\mathrm{Al}$ compounds, there are also exceptions that do not follow this rule, for instance: $\mathrm{Ce}_{1-\mathrm{x}}\mathrm{Y}_{\mathrm{x}}\mathrm{PdAl}$ or $\mathrm{TbPd}_{1-\mathrm{x}}\mathrm{Ni}_{\mathrm{x}}\mathrm{Al}$ [12]. These exceptions could be discussed considering substituted atoms with a too much different radii (Ce-Y, Pd-Ni).

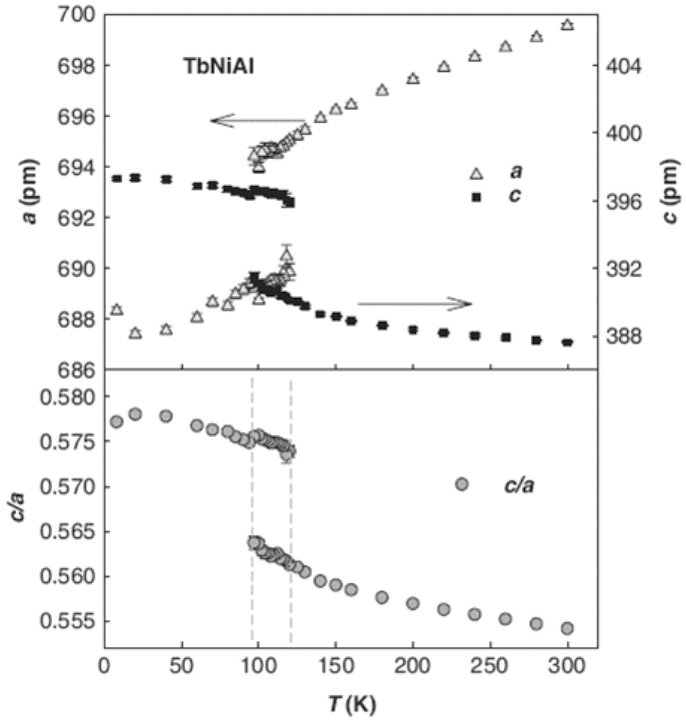

Figure 2.4: The temperature dependence of lattice parameters of TbNiAl. 'The forbidden region of c/a' can be seen at the bottom graph. The region of coexistence of two structure phases observed in small temperature range is marked by two vertical dashed lines [12].

Another studied series with d-metal substitution were $R\mathrm{Pd}_{1-\mathrm{x}}\mathrm{Ni}_{\mathrm{x}}\mathrm{Al}$ systems. Unlike the Ni–Cu substitutions, palladium has a larger atom volume than nickel, but the same number of free electrons in unfilled d-orbital. The different volume of Pd and Ni atoms causes a significant change of lattice parameters, although the c/a ratio remains almost unchanged. The change of lattice parameters causes i.a. drastically diminishing of the magnetic moment for R = Ce [31] or the violation of 'forbidden region of the c/a ratio' in R = Tb [12]. The magnetic structures in the $\mathrm{TbPd}_{1-\mathrm{x}}\mathrm{Ni}_{\mathrm{x}}\mathrm{Al}$ series remain almost unchanged [32].

2.2 TbNiAl

TbNiAl shows the structural phase transition around 110 K. There is a coexistence of two crystallographic phases with high and low c/a ratio in a limited temperature region (see Figure 2.4) [12]. The inelastic neutron scattering revealed that the CF potential has a very similar strength as well as symmetry above and below this structural transition [33]

The study of a single crystal as well as polycrystalline samples of TbNiAl by neutron diffraction and magnetization measurements demonstrates, that TbNiAl orders antiferromagnetically with Tb magnetic moments aligned along the c-axis below $T_{\mathrm{N}} = 44.6$ K [14, 34]. A propagation vector is $(\frac{1}{2}\ 0\ \frac{1}{2})$, but one third of moments remains reduced to almost zero due to a geometrical frustration. This suppression we can see at Figure 2.5a, where $\frac{2}{3}$ of the Tb moments (*regular* moments) are arranged in zigzag chains in the hexagonal basal plane (large circles) that separate the remaining $\frac{1}{3}$ of Tb moments (small circles).

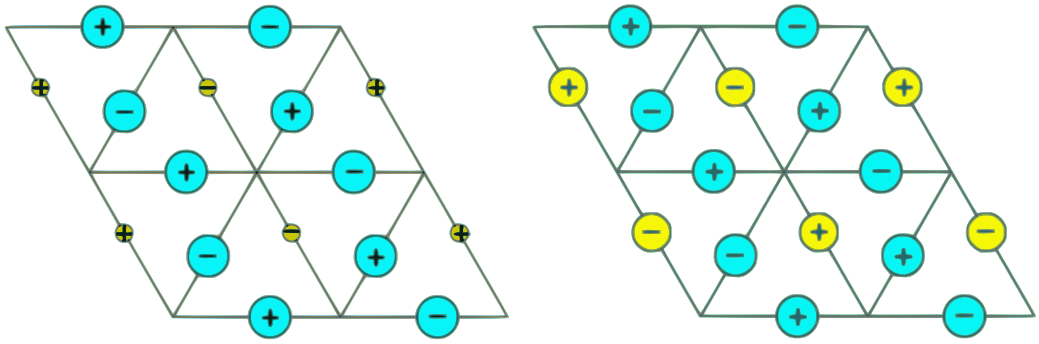

(a) $T_1 < T < T_{\mathrm{N}}$ (b) $T < T_1$

Figure 2.5: The magnetic structure of TbNiAl above and below magnetic phase transition T_1. The magnetic moments are oriented along the c-axis [14].

The frustrated moments start to propagate along different equivalent direction, e.g. with propagation vector $(-\frac{1}{2}\ \frac{1}{2}\ \frac{1}{2})$, below further magnetic phase transition at $T_1 = 23.5$ K. The strong frustration is removed below T_1, and finally all Tb moments reach the same value at 2 K (see Figure 2.5b).

The dynamic techniques, AC-susceptibility and muon spectroscopy (μSR), have given results that are mostly consistent with the neutron diffraction data. μSR picked up a precursor to the ferromagnetic phase transition even in zero field at a temperature where neutron scattering does only see a paramagnetic state (see Figure 2.6). The transition around $T_{\mathrm{N}} = 47$ K is clearly identified in the data as magnetic ordering. A third maximum of the relaxation rates $\lambda_{1,2}$ is found at $T = 58$ K, which does not correspond to a phase transition observable with neutron diffraction [35].

The antiferromagnetic ordering in TbNiAl can be relatively easy disrupt. The metamagnetic transition to a ferromagnetic state occurs when applying external magnetic field of $\simeq 0.4$ T along the c-axis at 2K. The magnetization data point to very strong uniaxial magnetocrystalline anisotropy with an anisotropy field above 35 T. The magnetic structure is almost insensitive to magnetic fields applied perpendicular to the c-axis (at least up to 5 T) [14], as can be seen in Figure 2.7. The antiferromagnetic structure of TbNiAl can also be easily disrupted by substitution of yttrium ($Tb_{1-x}Y_xNiAl$ [36]) or copper ($TbNi_{1-x}Cu_xAl$ [13]).

Already a few percent of Y or Cu substitution leads to the ferromagnetic order. The isoelectronic substitution in $TbPd_{1-x}Ni_xAl$ [32] leads to only subtle changes of propagation of 'frustrated moments' below T_1. The direction of Tb magnetic moments along the c-axis is retained for all these series and all concentrations.

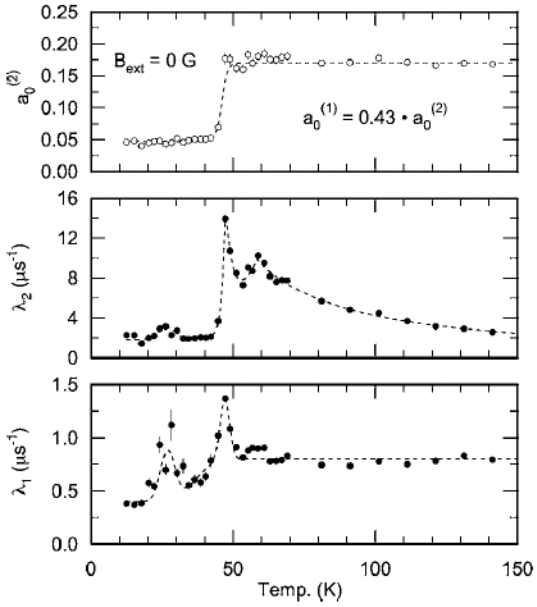

Figure 2.6: Muon relaxation rates λ_1, λ_2 and asymmetries $a_0{}^{(1)}$, $a_0{}^{(2)}$ in zero magnetic field. Maxima are observed at 27, 47, and 58 K. First two maxima correspond to magnetic phase transitions in accordance with neutron diffraction experiment, meaning of third maximum at 58 K is not clarified. Lines are guides to the eye [35].

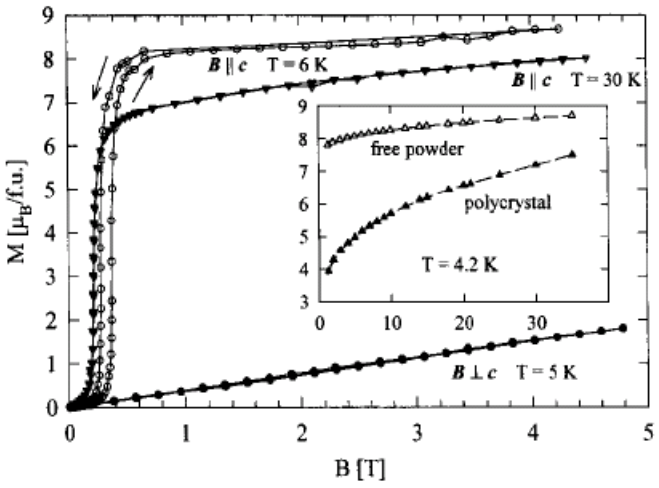

Figure 2.7: Magnetization curves of TbNiAl measured with magnetic field applied along and perpendicular to the c-axis show strong uniaxial magnetocrystalline anisotropy [14].

2.3 TbNiIn

TbNiIn orders magnetically around $T_{\mathrm{ord}} = 70$ K and the AC-susceptibility indicated additional magnetic phase transitions at $T' = 59$ K and $T_1 = 29$ K (see Figure 2.8) [21]. However, the neutron diffraction experiment shows only two magnetic phase transition at temperatures of 68 and 26 K [37]. The magnetic ordering can not be simply described as ferromagnetic or antiferromagnetic, but complex non-collinear structure. The main-maximum observed in χ'_{ac} at T' shifts to lower temperatures with increasing magnetic field (see Figure 2.9a) which indicates the antiferromagnetic ordering. On the other hand, an extreme at T_{ord} with increasing magnetic field disappears and with higher field (above 0.1 T) appears again and shifts to higher temperatures which indicate the complex magnetic order [38].

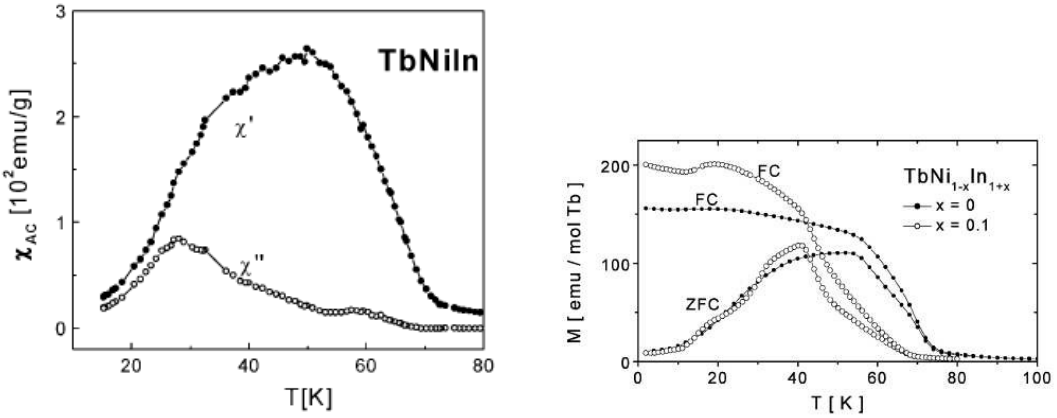

(a) (b)

Figure 2.8: Magnetic measurements of TbNiIn: (a) The temperature dependence of AC-susceptibility. (b) The temperature dependence of magnetization. Data taken from Reference [21].

As inferred from neutron diffraction, the Tb moments lie within the basal plane perpendicular to the c-axis (see Figure 2.9b) and form a non-collinear structure with (0 0 0) propagation below T_{ord}. All moments have the same size, they are magnetically equivalent. Additional weaker component with much lower Tb moments develops below T_1. The propagation vector of this modulated phase was determined as $(\frac{1}{2}\ 0\ \frac{1}{2})$ by Gondek [37]. But according to Ehlers [38], the propagation vectors of modulated phase are at least three: $(\frac{1}{4}\ \frac{1}{4}\ \frac{1}{4})$, $(\frac{1}{4}\ 0\ \frac{1}{4})$ and $(\frac{1}{4}\ 0\ \frac{1}{2})$.

TbNiIn unlike TbNiAl does not undergo structural phase transition [38]. The temperature dependence of lattice parameters is exactly opposite as compared to TbNiAl, the lattice parameter a decreases and c increases with increasing temperature (see Figure 2.10).

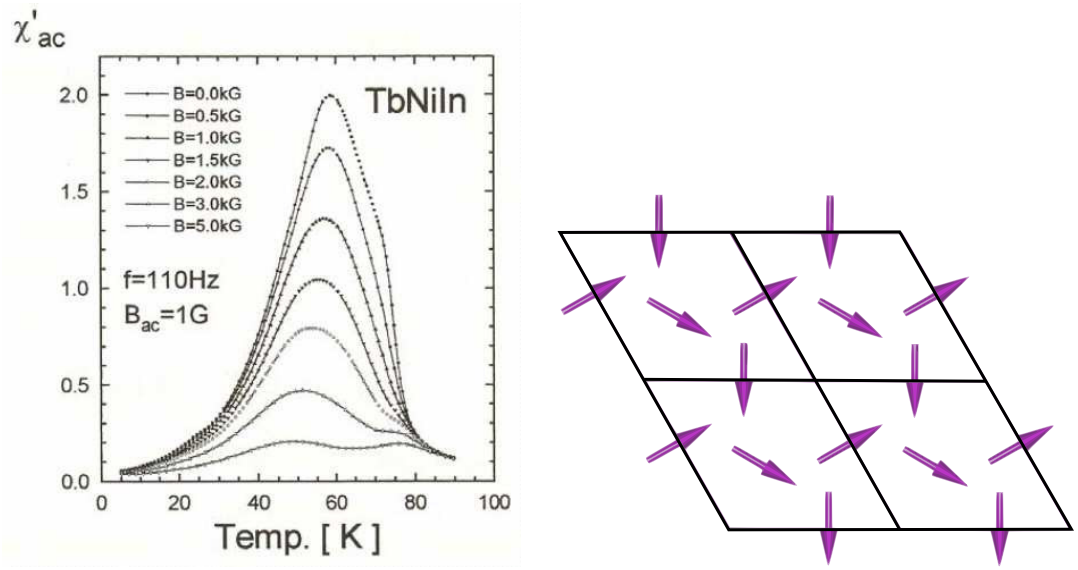

(a) (b)

Figure 2.9: Magnetic measurements of TbNiIn: (a) The temperature dependence of the real part of AC-susceptibility in the magnetic field. (b) The magnetic structure determined from neutron diffraction. Tb moments lie in the basal plane. Data taken from Reference [38].

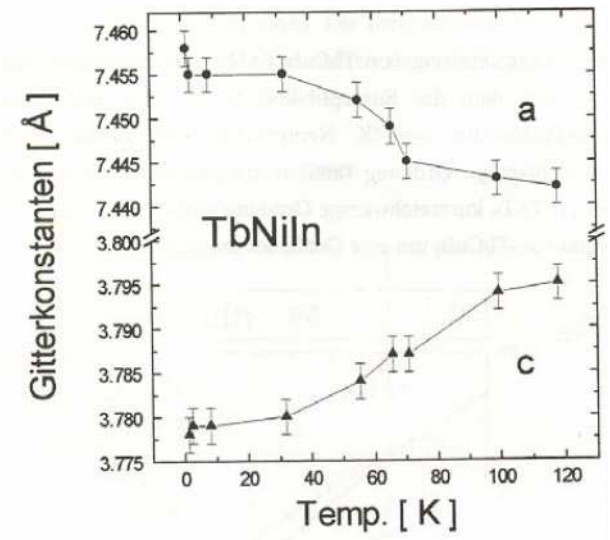

Figure 2.10: Temperature dependence of lattice parameters of TbNiIn at low temperature region [38].

3. Experimental details

3.1 Sample preparation

The polycrystalline $TbNiAl_{1-x}In_x$ (x = 0.0, 0.1,..., 1.0) samples were prepared by arc-melting of pure elements (3N for Tb, 4N5 for Ni, 5N for Al and 6N for In) in a mono-arc furnace under the protection of an argon atmosphere. The samples were turned and remelted four times to obtain better homogeneity. A higher evaporation of In (approximately two or three orders of magnitude) was considered before weighing individual elements - we add $\sim 5\%$ of In. The large samples used for the neutron diffraction experiment were additionaly sealed in silicon glass under pressure of 10^{-4} Pa and then annealed for 10 days at the temperature of 650°C.

3.2 EDX

The elemental composition of the selected samples x = 0.5 was checked by scanning electron microscope (SEM) Mira (Tescan) installed at the Department of Surface and Plasma Science. The microscope Mira is equipped with secondary electrons detector (SE), back-scattered electrons detector (BSE) and with Energy Dispersive X-ray analyzer (EDX) by Bruker Axs. The distribution of individual elements was investigated on the sample with x = 0.5. On this sample, the line scan mapping the majority and minority phase and their border was also realized.

3.3 X-ray diffraction

The X-ray diffraction at the room temperature was performed on the Bruker diffractometer using CuK_α radiation. The measurement was conducted for 2θ range of 10°- 80° with the step of 0.02°.

The low-temperature X-ray diffraction was performed on Bragg-Brentano diffractometer (Siemens D-500) equipped with helium gas flow cryostat (Oxford Instruments CF1108T) on powder samples fixed by acetone on the Si plate. The diffraction patterns were recorded for 2θ range of 20°- 140° with the step of 0.05° by using position-sensitive detector (Braun). Filtered radiation of the cobalt tube (CoK_α) was employed. The temperature of the samples was stabilized within 0.1 K by the ITC-503 temperature controller operating with the RhFe resistor. The diffraction patterns were taken for various temperatures: all samples at 300, 100 and 20 K, selected samples also at 200 and 5 K. Measurements were performed first at the room temperature in zero magnetic field. Consequently, permanent magnet made of sintered $Sm_2(Co, Fe, Cu, Zr)_{17}$ alloy (Vacomax 225HR, Vakuumschmelze) was placed under the sample holder (see Figure 3.1). It produced a magnetic field of approximately 0.3 T perpendicular to the sample surface. The room-temperature pattern was then taken again and revealed identical results as the zero-field measurement. The temperature was then gradually lowered to the selected temperatures and the diffraction patterns were taken

always at stabilized temperature.

Both diffractometers are installed at the Department of Condensed Matter Physics, Charles University in Prague.

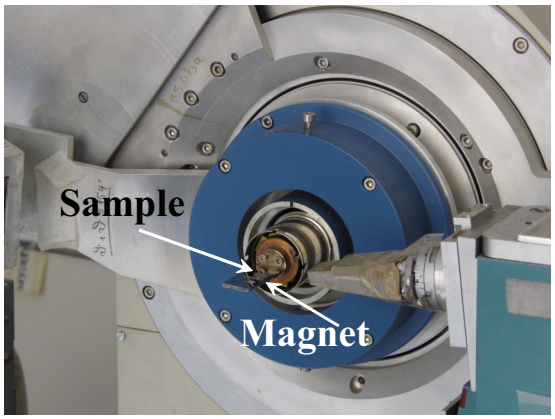

Figure 3.1: Siemens diffractometer. Si plate with the powder sample on the holder with the permanent magnet mounted under.

3.4 Magnetic measurements

The magnetization and AC-susceptibility measurements were performed using the Physical Property Measurement System (PPMS) and Magnetic Property Measurement System (MPMS), Quantum Design, installed in the Joint Laboratory for Magnetic Studies of the Charles University and the Institute of Physics of the Academy of Sciences of the Czech Republic. The MPMS was used only for magnetization measurement in the paramagnetic region for x = 0.1, 0.2, 0.6 and 0.9 samples. Powder samples ($\sim$ 10 mg) fixed in a random orientation by glue (Canagon) in a plastic capsule were used in all these measurements.

The temperature dependence of magnetization in the paramagnetic region was measured in magnetic fields of 1 and 2 T. The measurements in 1 T were performed during the cooling from 300 to 50 K, measurements in 2 T during the heating from 50 to 300 K for most of concentrations, the measurements with an opposite course (i.e. cooling in 2 T and heating in 1 T) were performed for x = 0.6 and 0.8. To exclude any effects that might arise from different temperature change regimes, the measurements in 1 T for both cooling and heating regimes were performed for x = 0.4. Each measurement was realized in the temperature sweep regime with the cooling/heating rate of 1 K/min.

The temperature dependence of magnetization in the magnetically ordered state was measured for constant fields under zero field cooled (ZFC) and field cooled (FC) conditions. The measurements were performed for all concentrations in fields of 0.005, 0.01, 0.05 T in both ZFC and FC regimes, in fields of 0.03 and 0.1 T under ZFC condition only and for selected concentrations in fields of 0.2 and 0.5 T under ZFC. The investigated temperature range was 3 - 70 K (80 K for TbNiIn) and the rate of temperature change was 1 K/min.

The magnetization curves (i.e. M vs H dependencies) were measured at constant selected temperatures. The field range was 0 - 14 T for 3 K and 0 - 5 T

for all other temperatures. The measurement was performed in the field sweep regime with the field change of 0.0025 T/s and 0.009 T/s below and above 1.2 T, respectively. The magnetization curve was always measured first for the highest temperature, then the temperature was gradually lowered to the selected temperatures (without the return above the magnetic ordering temperature) and measurement was taken at stabilized temperature. The measurements with the return above ordering temperature was made for x = 0.1 and 0.3. The difference between measurement with and without the return above ordering temperature is not distinguishable.

The AC-susceptibility measurements were performed in the temperature range of 3 - 70 K (up to 80 K for pure TbNiIn). The temperature dependence of the AC-susceptibility was measured under field-cooled (FC) condition for frequencies of 13, 113, 1113 Hz in the zero magnetic field and for the frequency 9993 Hz in magnetic fields of 0, 0.05, 0.1, 0.2 and 0.5 T for most of the samples. The cooling rate was 0.5 K/min.

3.5 Specific heat

The specific heat measurements were performed using the PPMS instrument employing the relaxation method. The temperature dependence of the specific heat was measured in the temperature range between 3 and 110 K for x = 0.4, 0.8 and 1.0 compounds and up to 250 K for x = 0.6 compound in zero magnetic field. Polycrystalline samples (mass $\sim$ 12 mg) were thermally attached to the sample platform by the Apiezon N grease. The heat capacity of the used amount of grease was subtracted from the measured data.

Certain difficulties occur when measuring the heat capacity of pure TbNiAl. Despite the relatively large number of studies using different experimental techniques, the specific heat of TbNiAl was not reported up to now. The structural transition observed in TbNiAl around 100 K [33] could be a reason. We have experienced that the thermal contact between the sample and the sample holder is usually strongly impaired when cooling below the transition. To avoid these difficulties with the structural transition, we have performed the heat capacity measurement with the sample covered on the bottom side by a Stycast epoxy. The Stycast coating does not affect the heat conduction to the sample significantly, as proved by numerous studies [39]. The measurement was done on $\sim$ 7.9 mg polycrystalline sample placed on $\sim$ 0.94 mg of Stycast 2850 FT. The heat capacity of the pure Stycast (and Apiezon N grease) was then subtracted from the measured data.

3.6 Transport properties

The temperature evolution of the electrical resistance was performed using two stage Closed cycle refrigerator (CCR, Janis Research/ Sumitomo Heavy Industries) with base temperature of 3 K, installed at the Department of Condensed Matter Physics, Charles University in Prague.

The electrical resistance was measured in the temperature range between 3.5 and 300 K with the rate of 0.3 K/min (in most cases the rate was 0.3 K/min

for range 3.5 - 70 K and 0.6 K/min for 70 - 300 K) in zero static magnetic field or in field of approximately 0.3 T produced by the permanent magnet made of Nd-Fe-B alloy. The measurement itself was preceded by one faster temperature cycle 300 - 4 - 300 K to stabilize the electrical contacts and then measured in more detail with slower heating/cooling rate of 0.3 K/min and 0.6 K/min respectively. The measurement with nonzero magnetic field followed immediately. The electrical contacts of the Cu wires (50 μm thickness, 5N purity) to the samples in prism shape - typically ($\sim$ 2 x 2 x 10 mm) - were provided using colloidal silver paste.

The temperature dependence of the resistance of the TbNiAl compound under hydrostatic pressure was measured using the clamped pressure cell made of annealed copper beryllium bronze. The inner diameter of the pressure cell was 7 mm and the cell allows measurements under pressures up to 1 GPa. The electrical contacts were provided same way as in the measurement without the cell. The spindle oil OL-3 was used as the exchange pressure medium and the manganin wire was used to determine the pressure inside the pressure cell. The first measurement was done in the pressure of 0.3 GPa then, the pressure was increased up to 0.75 GPa and subsequently gradually decreased to 0.55, 0.35 and 0.2 GPa. The pressure was then again increased to 0.25 GPa and at the end lowered for the measurement in the ambient pressure. The hydrostatic pressures of the exchange medium presented in the thesis are measured at room temperature. Because of the fact that the pressure decreases with decreasing temperature, the pressure at the temperature of structural phase transition ($\sim$ 110 K) is lower (approximately by 0.1 - 0.2 GPa) and in low temperature region is real pressure approximately zero for most of our pressure measurement, see Figure 3.2.

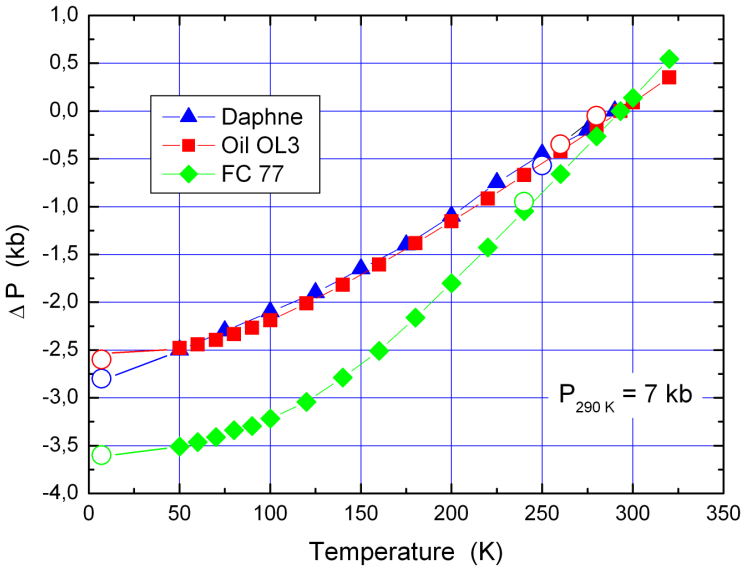

Figure 3.2: The temperature dependencies of pressure change for liquid exchange media. The pressure in the cell at room temperature was 0.7 GPa. Figure taken from [40].

3.7 Neutron diffraction

The neutron diffraction experiment was performed on D1B instrument in Institut Laue Langevin (ILL), Grenoble, France.

D1B is a two-axis powder diffractometer equipped with 3He/Xe position sensitive detector composed of a system of multi-electrodes with 400 cells, which scan a 2θ range of 80 degrees (see Figure 3.3). In our case the detector was set first in a position 3 (or 5) - 83 (or 85) degrees. We verified an absence of magnetic peaks in the low angle region. After the verification the detector was moved to the position of 11 (or 16) - 91 (or 96) degrees and the temperature dependence of diffraction patterns was performed. The neutrons with a wavelength of 2.53 Å were used in our experiment.

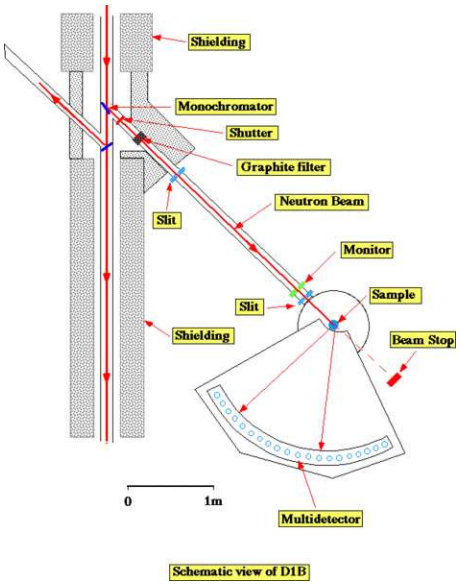

Figure 3.3: The schematic view of the D1B diffractometer, ILL, Grenoble, France.

The powder sample (the weight of the samples was 3 - 4 g) was placed in the cylindrical vanadium container with the diameter of 5.7 mm and with the height of 50 mm. The sample fills approximately three quarters of the container.

The diffraction patterns were obtained for 9 concentrations from $TbNiAl_{1-x}In_x$ series (not measured for x = 0.0 and 0.7). Patterns with a high statistics were measured in each magnetic phase as expected from the AC-susceptibility data (see Section 4.3.1). Additionally, except for samples with x = 0.1 and 0.6, diffraction patterns with slightly lower statistics were taken with 2 or 3 K steps from 2 K up to the paramagnetic state to follow the temperature development in more detail.

4. Results and discussion

4.1 Crystal structure and phase analysis

The pollycrystalline $TbNiAl_{1-x}In_x$ samples were prepared and annealed as described in chapter 3.1. The X-ray diffraction patterns were measured to verify the crystal structure and to refine the structural parameters. The refinement was done using the Fullprof program employing the Rietveld analysis [41]. The analysis showed the main phase with the ZrNiAl-type of structure (see Figure 2.1) and a few weak additional peaks that might indicate the presence of a small amount of impurity phase(s). The diffraction record and its fitting with Bragg's reflections for concentration with x = 0.3 can be seen in Figure 4.1.

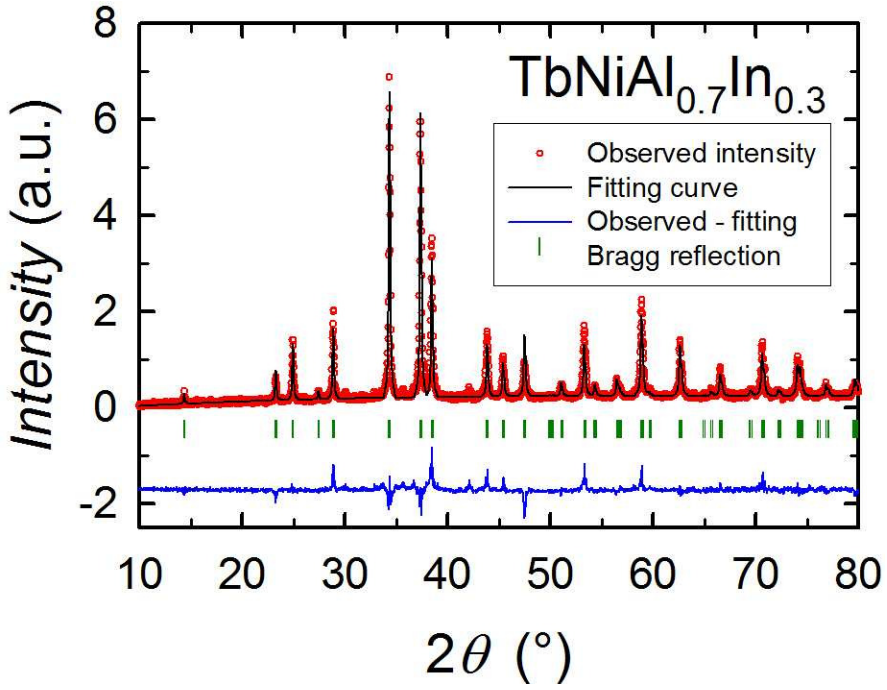

Figure 4.1: X-ray diffraction patterns, its fitting and Bragg's reflections of $TbNiAl_{0.7}In_{0.3}$ processed by Rietveld analysis.

The lattice parameters refined from diffraction data are placed in Table 4.1 and plotted in Figure 4.2. As can be seen the lattice parameter a increases linearly with increasing indium content, whereas the parameter c decreases linearly between concentrations x = 0.0 and 0.7 and for higher In concentrations remains almost unchanged. This observation can be well understood as the Al(In) atoms lie only within one of the two layers of the crystal structure (see Figures 2.1 and 2.2) and the replacement of Al by larger In atoms causes an expansion in this layer. The change of the lattice parameters when cooling to low temperatures is discussed in detail in Section 4.6. The c/a ratio consequently decreases almost linearly. Because of the fact that the parameter a increases faster (approximately four times) than c decreases, the volume per fundamental unit increases with increasing indium content. The distance between Tb-atoms in basal plane d_{BP} with the indium content increases, which could be expected from the values of lattice parameters of parent compounds. The distance between Tb-atoms in the

direction of the hexagonal c-axis (the lattice parameter c) is higher than the distance in the basal plane (d_{BP}) up to x = 0.6, Tb-atoms are closer in the direction of the c-axis for x > 0.6.

Table 4.1: Lattice parameters of $TbNiAl_{1-x}In_x$ compounds at 300 K compared with the literature data. The parameters from [42] were obtained from the electron microscopy. V is the volume of fundamental unit and d_{BP} is the distance between Tb-atoms in basal plane.

x	a(pm)	c(pm)	c/a	$V(10^6\mathrm{pm}^3)$	d_{BP}(pm)	R_{Bragg}
0.0 [43]	698.7(9)	386.9(5)	0.5537(8)	51.3(2)	362.5(9)	
0.0 [42]	700.3	387.7	0.5536	51.6016	363.3	
0.0	700.2(1)	388.0(1)	0.5541(1)	51.63(3)	363.3(1)	9.9
0.1	705.6(1)	386.2(1)	0.5473(1)	52.18(3)	366.1(1)	13.8
0.2	710.6(3)	384.7(2)	0.5415(3)	52.74(6)	368.7(3)	17.3
0.3	716.0(3)	383.5(2)	0.5356(3)	53.35(8)	371.5(3)	15.1
0.4	720.5(4)	382.4(2)	0.5308(3)	53.87(9)	373.8(4)	17.1
0.5	726.0(6)	381.6(3)	0.5256(5)	54.6(1)	376.7(6)	20.5
0.6	731.0(7)	380.5(4)	0.5205(6)	55.2(2)	379.3(7)	16.7
0.7	736.2(6)	379.7(3)	0.5158(5)	55.9(1)	382.0(6)	13.4
0.8	739.8(8)	379.4(4)	0.5129(6)	56.4(2)	383.8(8)	18.5
0.9	743.4(5)	379.1(3)	0.5099(4)	56.9(1)	385.7(5)	15.1
1.0	745.2(5)	379.5(3)	0.5093(4)	57.2(1)	386.6(5)	20.3
1.0 [21]	744.49(7)	379.80(4)	0.5101(1)	57.13(2)	386.3(7)	4.4

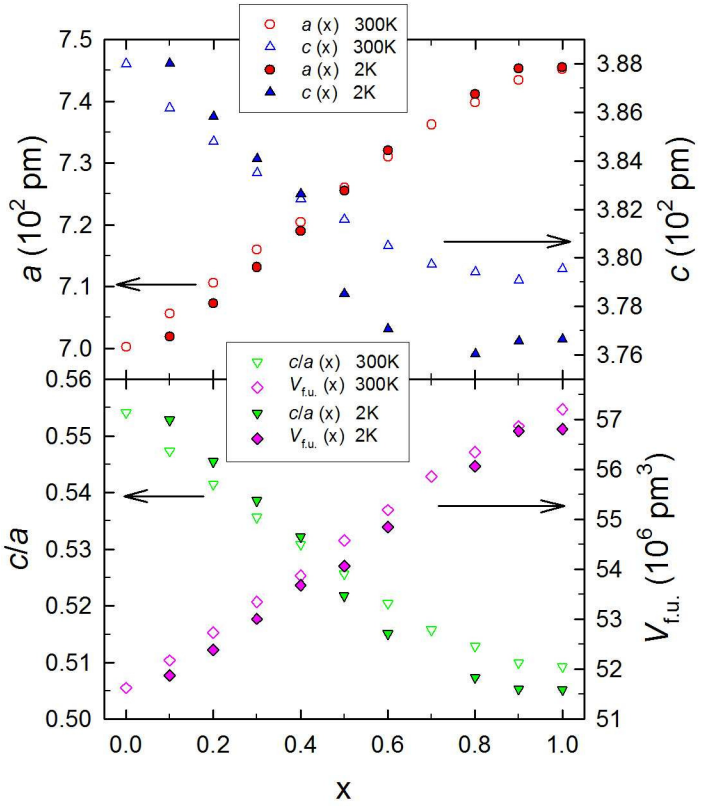

Figure 4.2: Lattice parameters of $TbNiAl_{1-x}In_x$ compounds refined from X-ray diffraction at room temperature and from powder neutron diffraction at temperature of 2 K. The scale of error bars is comparable with the size of the symbols.

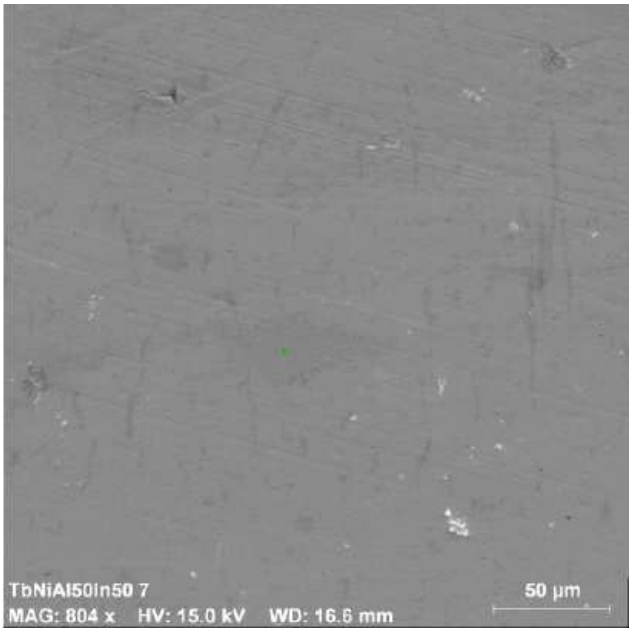

Figure 4.3: The surface of non-annealed $TbNiAl_{0.5}In_{0.5}$ sample. The horizontal lines are caused by polishing. The darker vertical line-shape ares are regions with an admixture of secondary phase. Bright islands are impurities adhering on the surface.

The verification of the phase purity and homogeneity by using the energy dispersive X-ray analysis was done on non-annealed $TbNiAl_{0.5}In_{0.5}$ sample. As can be seen on the picture of the surface of the sample (Figure 4.3), the sample is composed predominantly by one phase with small admixture of the second phase ($\leq 5\%$). We were able to identify only two different phases whose concentrations compositions are in the Table 4.2. The atomic concentrations of Tb and Ni determined from EDX seem to be incorrect because of a closeness of Tb and Ni peaks in the spectra. The program includes a part of Ni-contribution into Tb-contribution. The sum of terbium and nickel contributions gives the correct atomic concentration, i.e. $\frac{2}{3}$. Moreover the values for Tb and Ni from EDX are hardly probable because of the preparation of the samples, see section 3.1. The atomic concentrations of Tb and Ni were identical by weighting and the evaporation of these elements (arc-melting) is almost the same. On the other hand, the EDX measurement on the TbNiAl single crystal shows the correct representation of all three elements, i.e. $\frac{1}{3}$ of the atomic concentration for each of them.

Table 4.2: The composition of two phases observed in non-annealed sample $TbNiAl_{0.5}In_{0.5}$. c_A is the atomic concentration of elements in the phase and δc_A is its deviation.

	1. phase		**2. phase**	
Element	c_A (%)	δc_A (%)	c_A (%)	δc_A (%)
Tb	37.9	1.9	22.9	1.7
Ni	27.1	0.6	40.8	1.2
Al	17.2	0.3	33.7	0.7
In	17.8	0.7	2.6	0.2
Total	100.0		100.0	

The linescan on the sample was also made. On the boundary between majority and minority phase occurs nearly abrupt transition without interphase, this is well-showed in Figure 4.4. We can also see that the concentration composition of majority and minority phase is nearly constant. The Figure 4.5 shows homogeneous Al-In distribution in majority phase of $TbNiAl_{0.5}In_{0.5}$ sample. The replacement of In by Al in the minority phase is also well-shown. The presence of the minority phase can be identified in the pictures of distributions of all elements.

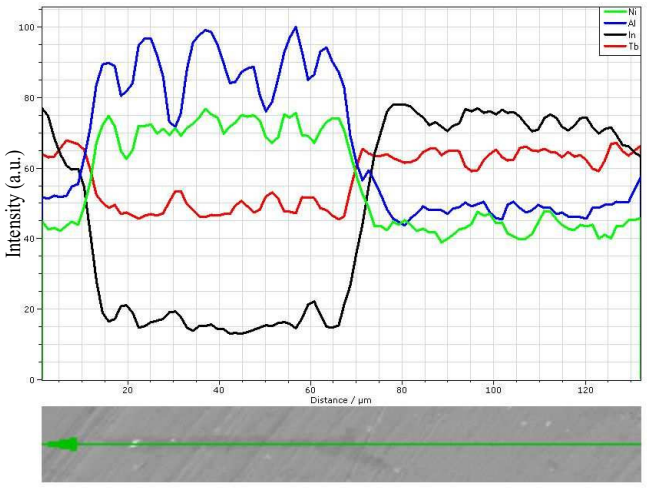

Figure 4.4: The linescan of the non-annealed $TbNiAl_{0.5}In_{0.5}$ sample. On the boundary between majority and minority phase occurs nearly abrupt transition without interphase.

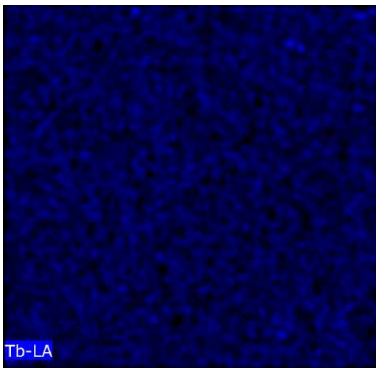

(a) Tb

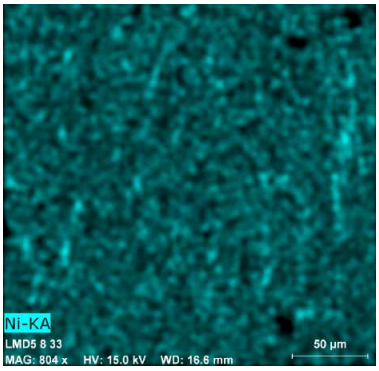

(b) Ni

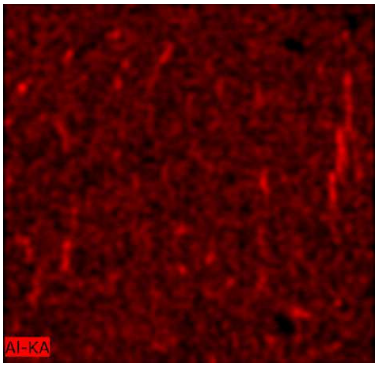

(c) Al

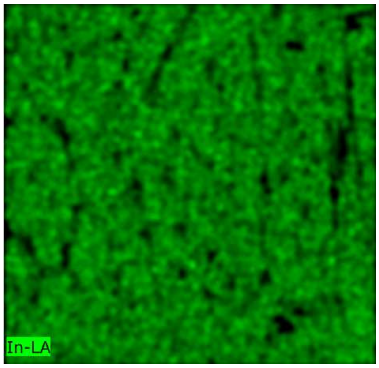

(d) In

Figure 4.5: The distribution of elements in the non-annealed $TbNiAl_{0.5}In_{0.5}$ sample. Minority phase is easy to see on all pictures as thin lines.

4.2 Low temperature X-ray diffraction in static magnetic field

Diffraction pattern of pure TbNiAl measured at 20 K (i.e. below T_N) in the presence of the magnetic field reveals (same as low indium content samples) a strongly textured powder (see Figure 4.6). Observed increase in the intensity of the (0 0 l) reflections (see Figure 4.7) indicates macroscopic ordering of crystallites with the c-axis parallel to the direction of the external magnetic field. This is in agreement with the results of neutron diffraction and magnetization data of TbNiAl showing a strong anisotropy and ferromagnetic order with moments aligned along the c-axis in the magnetic field of 0.3 T [14].

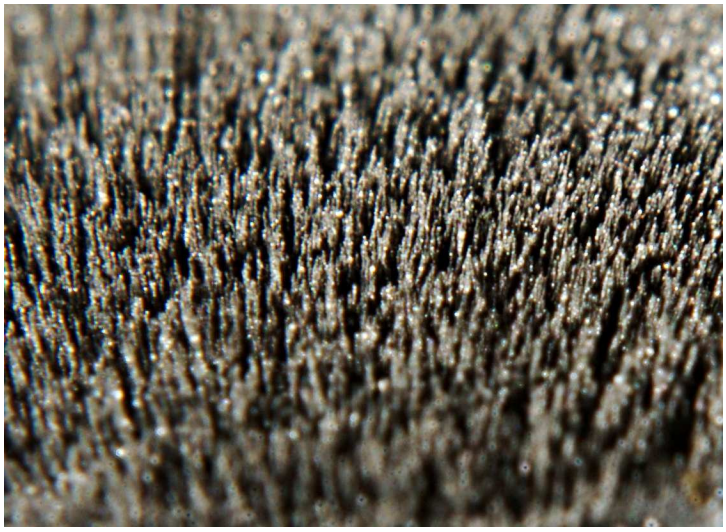

Figure 4.6: The textured powder of $TbNiAl_{0.9}In_{0.1}$ compound after the measurement in field of 0.3 T at the temperature of 20 K (i.e. below magnetic phase transition temperature T_{ord}). Picture taken at 300 K.

Diffraction patterns of In poor compounds (x $<$ 0.3) show similar behavior as pure TbNiAl, but the increase of intensity of the (0 0 l) peaks becomes less prominent (see Figure 4.8). We can observe also the strongest peaks other than (0 0 l) (see Figure 4.9). The intensity of (001) and (002) reflections are still clearly enhanced in the sample with 30% of In, but the preferred orientation is much weaker compared to TbNiAl (see Figures 4.7 and 4.8). Very small difference between the 300 and 20 K patterns is observed for the concentration with 40% of In and the texture seems to disappear completely for x $>$ 0.4, as can be seen from Figures 4.9, 4.10 and 4.11. This disappearance of the preferential orientation in the sample is in agreement with the complex non-collinear magnetic structure reported for TbNiIn [37, 38]. The magnetocrystalline anisotropy decreases with increasing In content and for that reason the grains in the sample orientate along the magnetic field less willingly. The behavior of preferential orientation indicates the flip of Tb moments from the direction parallel to the c-axis to the basal plane in concentration range between 40 and 50% of In.

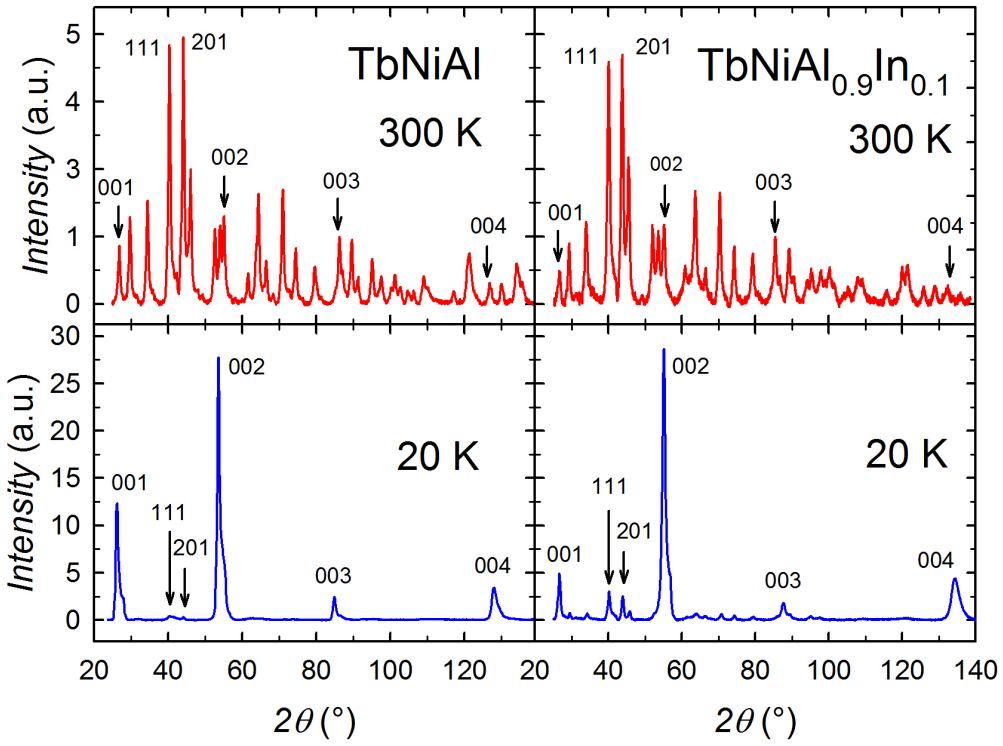

Figure 4.7: X-ray diffraction patterns in field of ≈ 0.3 T at temperatures above and below magnetic phase transition of TbNiAl and $TbNiAl_{0.9}In_{0.1}$ compounds. The strong peaks (0 0 l) in the direction of the magnetic field are marked.

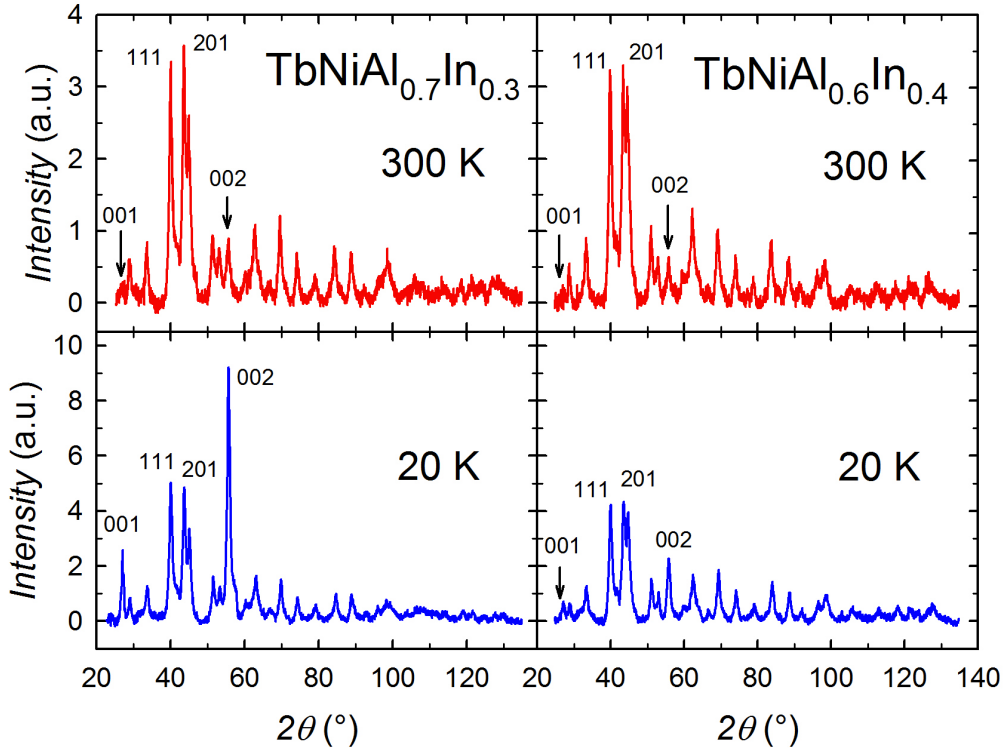

Figure 4.8: X-ray diffraction patterns in field of ≈ 0.3 T at temperatures above and below magnetic phase transition of $TbNiAl_{0.7}In_{0.3}$ and $TbNiAl_{0.6}In_{0.4}$ compounds. The difference between pattern above and below T_{ord} in $TbNiAl_{0.6}In_{0.4}$ is very small.

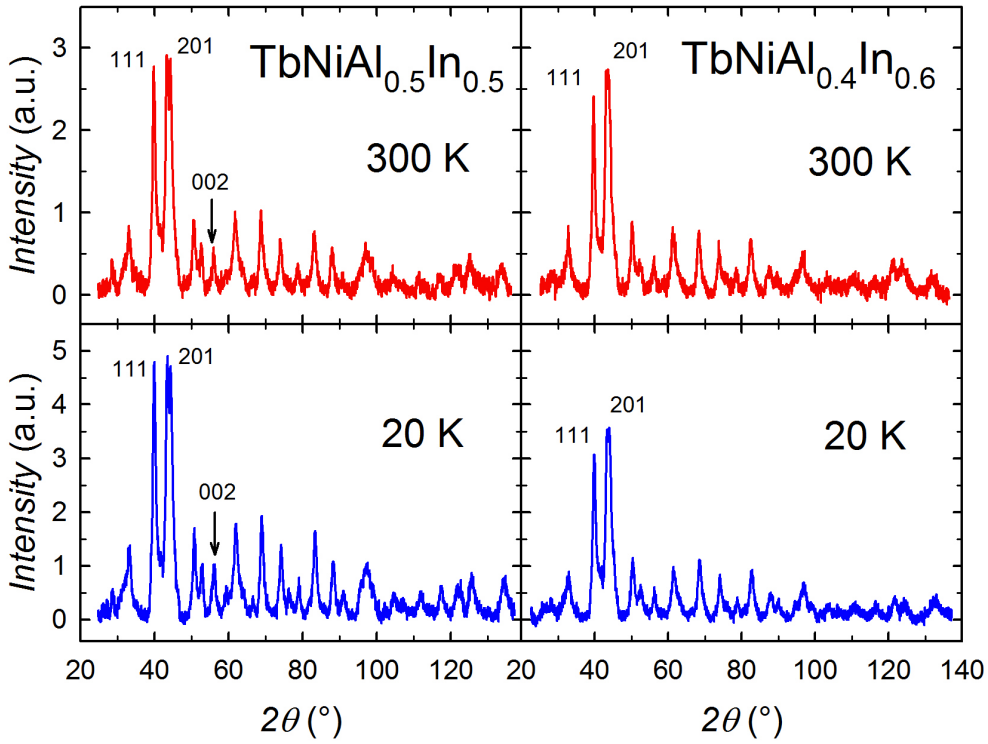

Figure 4.9: X-ray diffraction patterns in field of ≈ 0.3 T at temperatures above and below magnetic phase transition of $TbNiAl_{0.5}In_{0.5}$ and $TbNiAl_{0.4}In_{0.6}$ compounds.

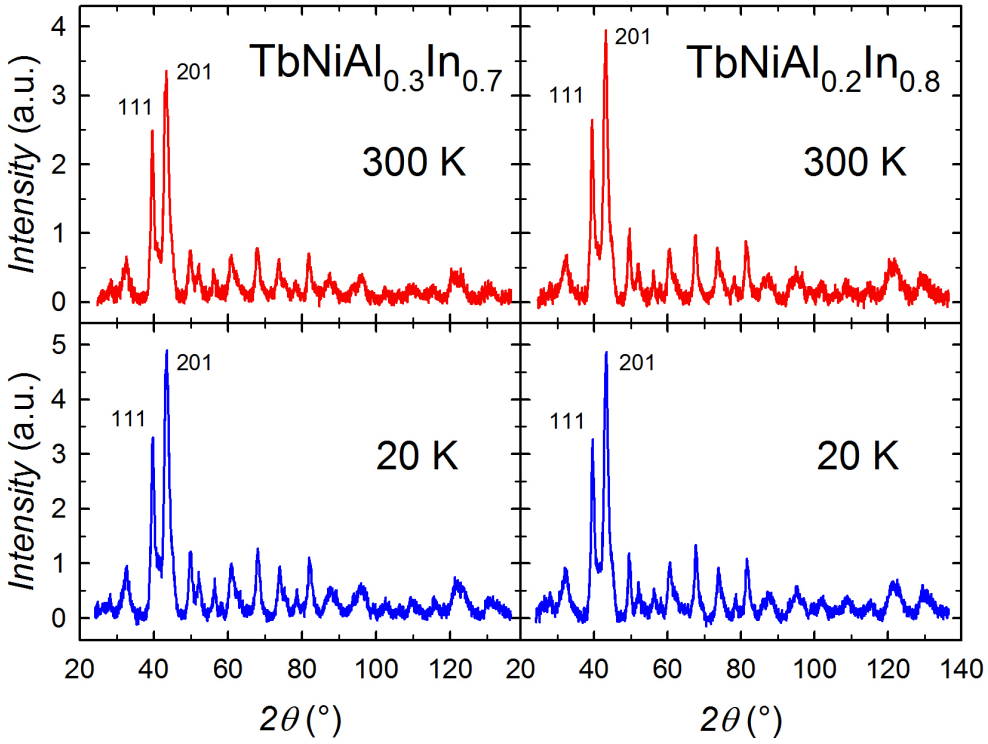

Figure 4.10: X-ray diffraction patterns in field of ≈ 0.3 T at temperatures above and below magnetic phase transition of $TbNiAl_{0.3}In_{0.7}$ and $TbNiAl_{0.2}In_{0.8}$ compounds.

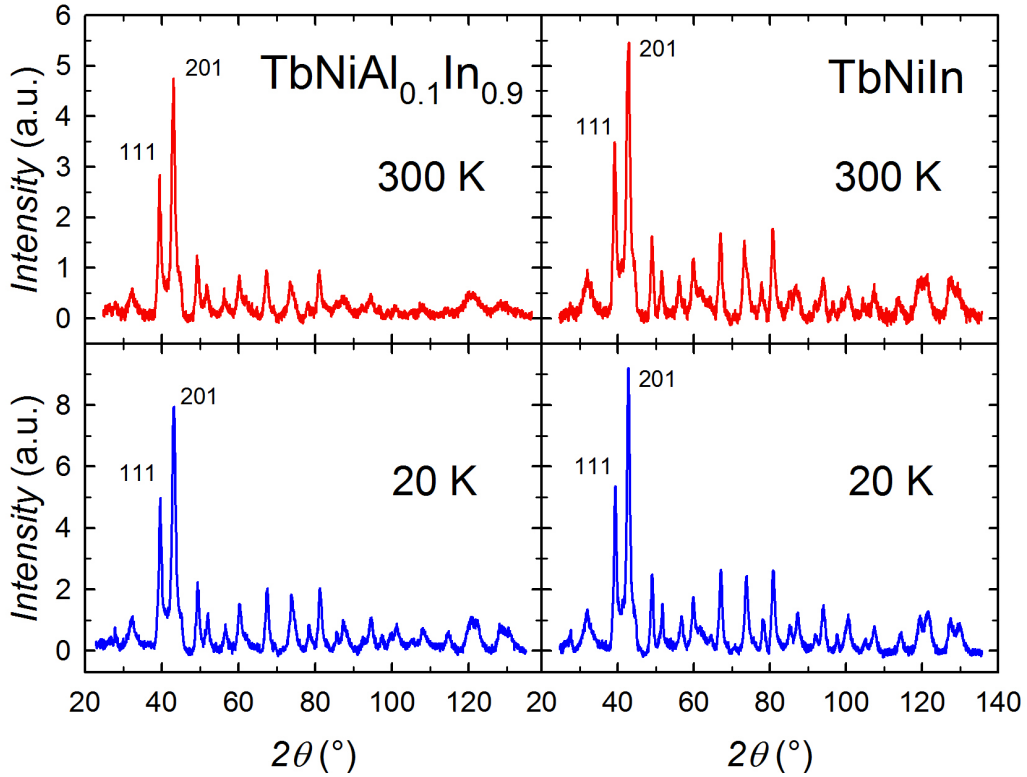

Figure 4.11: X-ray diffraction patterns in field of ≈ 0.3 T at temperatures above and below magnetic phase transition of $TbNiAl_{0.1}In_{0.9}$ and TbNiIn compounds.

4.3 Magnetic measurements

4.3.1 AC - susceptibility

The temperature dependence of AC-susceptibility reveals two or more magnetic phase transitions for all studied compounds (see the maxima in Figures below). The anomalies related to the temperature of the magnetic ordering are frequency independent which indicates the long-range magnetic ordering in the whole series, contrary to some R(Ni,Cu)Al compounds where the spin-glass state is manifested by frequency dependent signal [24].

The AC-susceptibility of aluminium rich compounds shows qualitatively similar behavior to the parent TbNiAl with a relatively sharp anomaly at T_{ord} and less pronounced maximum around T_1 (see Figures 4.12a, 4.13a, 4.14a, 4.15 and 4.17a). With increasing indium content, the anomaly around the ordering temperature becomes broader and the low-temperature anomaly becomes more pronounced, especially in the imaginary part of AC-susceptibility $\chi^{\prime\prime}$ (see Figures 4.19a, 4.20a, 4.21a and 4.22). The main maximum in the In rich compounds (x $\geq$ 0.8) is preceded by certain shoulder at higher temperatures (see Figure 4.20, 4.21 and 4.22,), which was observed also in the previous study on TbNiIn [21]. We label the anomaly appearing at higher temperature as T_{ord} and the other one as T' (see Table 4.3). Other maximum is observed in the low temperature region for concentrations with x = 0.0, 0.1 and 0.8. This maximum is described as T_{x}. The temperatures of all observed anomalies are summarized in Table 4.3. The microscopic nature of all the transitions will be discussed in Sections 4.6 and 4.7.

Table 4.3: Magnetic phase transition temperatures as determined from AC-susceptibility, the paramagnetic characteristics (not measured for x = 0.0, 0.3, 0.7 and 1.0) and the values of magnetic moment in field of 14 T at 3 K (not measured for x = 0.8) and the saturated magnetization in $TbNiAl_{1-x}In_x$ compounds.

x	T_{ord} (K)	T' (K)	T_1 (K)	T_{x} (K)	μ_{eff} (μ_{B})	θ_{P} (K)	$\mu_{14\mathrm{T}}^{3\mathrm{K}}$ (μ_{B})	μ_{sat} (μ_{B})
0.0 [8]	47	-	23	-	10.4	30		
0.0	46	-	24	18			7.5	8.6
0.1	48	-	25	18	9.9	36	7.1	8.1
0.2	48	-	22	-	10.0	32	8.0	9.0
0.3	45	-	15	-			7.6	9.1
0.4	42	-	12	-	10.1	34	7.9	8.9
0.5	42	-	12	-	9.6	34	7.6	8.2
0.6	45	-	14	-	9.9	36	6.7	7.1
0.7	47	-	20	-			7.0	7.4
0.8	56	52	20	13	9.7	40		
0.9	60	49	21	-	9.6	44	6.3	6.7
1.0	72	54	20	-			7.0	7.3
1.0 [21]	70	59	29	-	9.5	55		

The magnetic field generally suppresses all the anomalies but causes also a shift of some of them to lower temperatures which could indicate the antiferromagnetic character of the ordering (see Figures 4.18b and 4.21b). It is also possible that some of the anomalies at T_x are due to magnetic order in the minority phase (see Section 4.1).

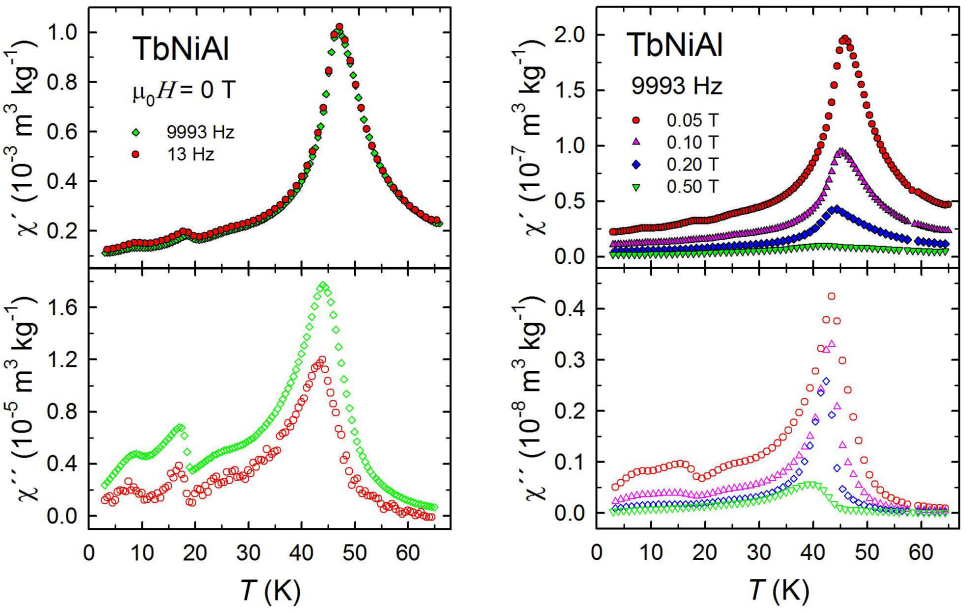

(a) (b)

Figure 4.12: The temperature dependence of AC-susceptibility of TbNiAl compound: (a) for frequencies of 13 and 9993 Hz in zero magnetic field and (b) for frequency of 9993 Hz in various magnetic fields. The field suppresses all the anomalies and causes a shift to lower temperatures.

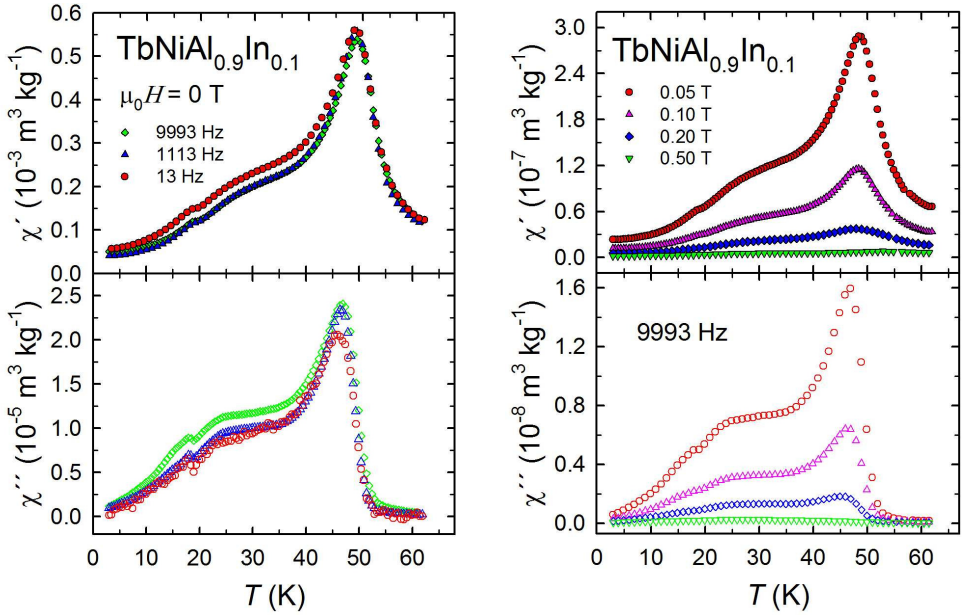

(a) (b)

Figure 4.13: The temperature dependence of AC-susceptibility of $TbNiAl_{0.9}In_{0.1}$ compound: (a) for various frequencies in zero magnetic field and (b) for the frequency of 9993 Hz in various magnetic fields.

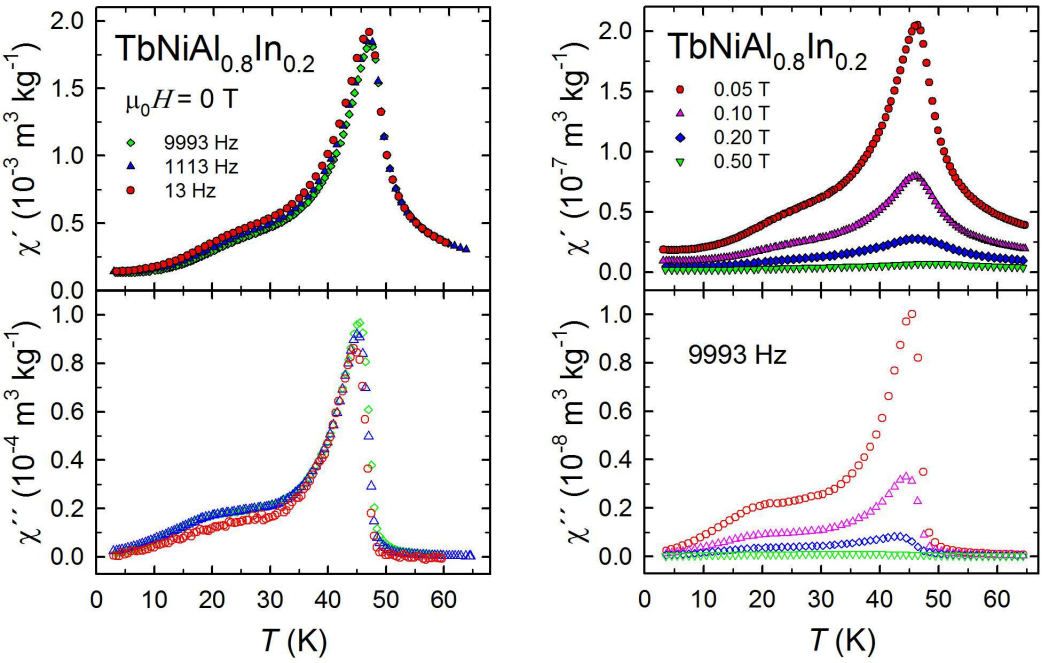

Figure 4.14: The temperature dependence of AC-susceptibility of $TbNiAl_{0.8}In_{0.2}$ compound: (a) for various frequencies in zero magnetic field and (b) for the frequency of 9993 Hz in various magnetic fields.

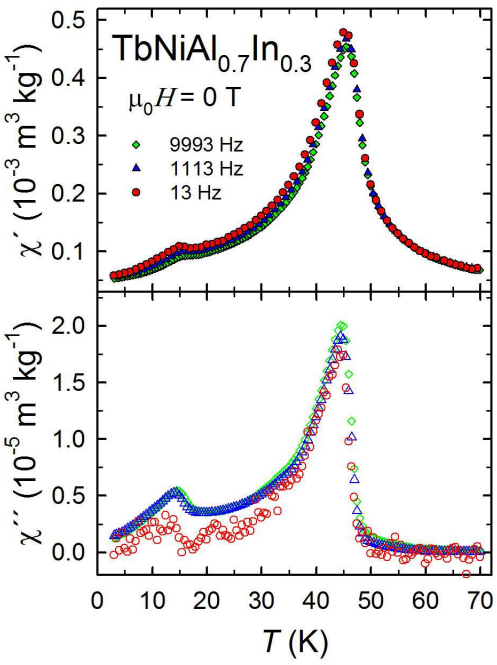

Figure 4.15: The temperature dependence of AC-susceptibility of $TbNiAl_{0.7}In_{0.3}$ compound for various frequencies in zero magnetic field.

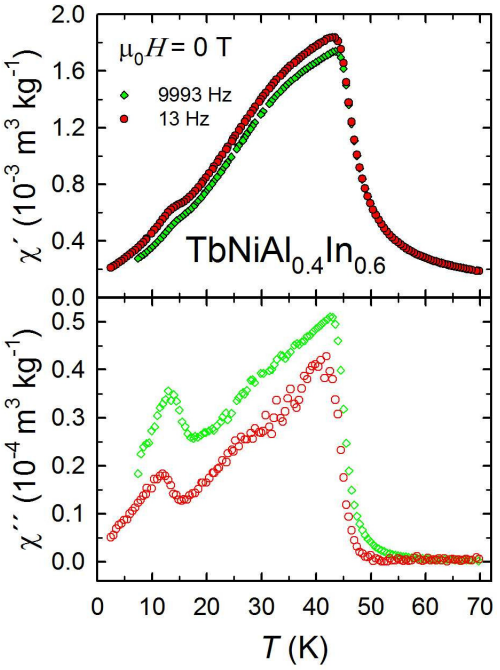

Figure 4.16: The temperature dependence of AC-susceptibility of $TbNiAl_{0.4}In_{0.6}$ compound for various frequencies in zero magnetic field.

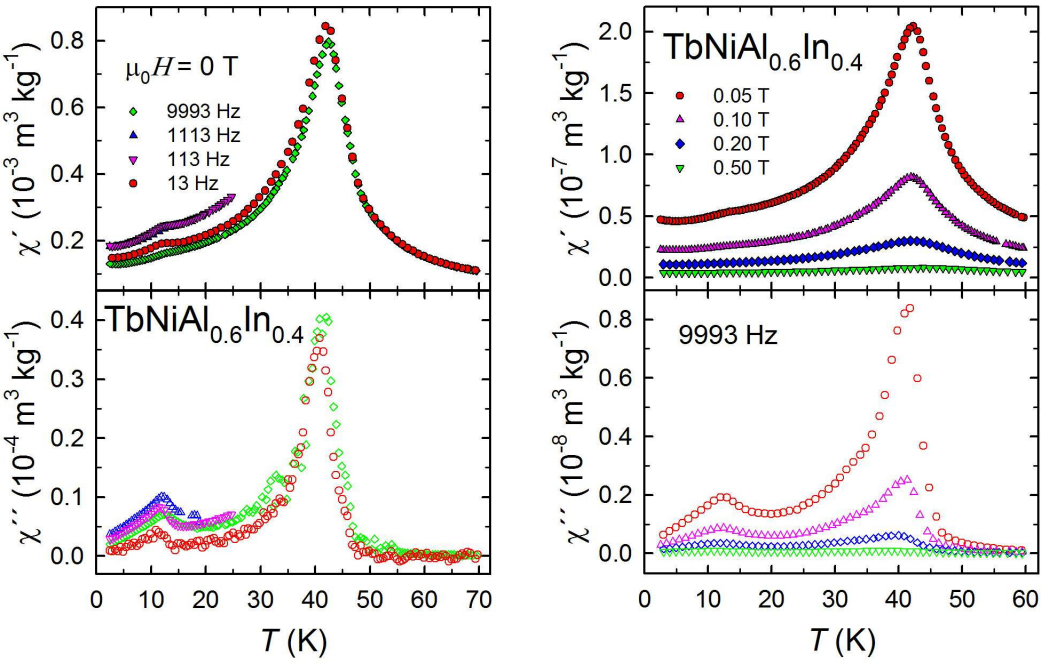

(a) (b)

Figure 4.17: The temperature dependence of AC-susceptibility of $TbNiAl_{0.6}In_{0.4}$ compound: (a) for various frequencies in zero magnetic field and (b) for the frequency of 9993 Hz in various magnetic fields.

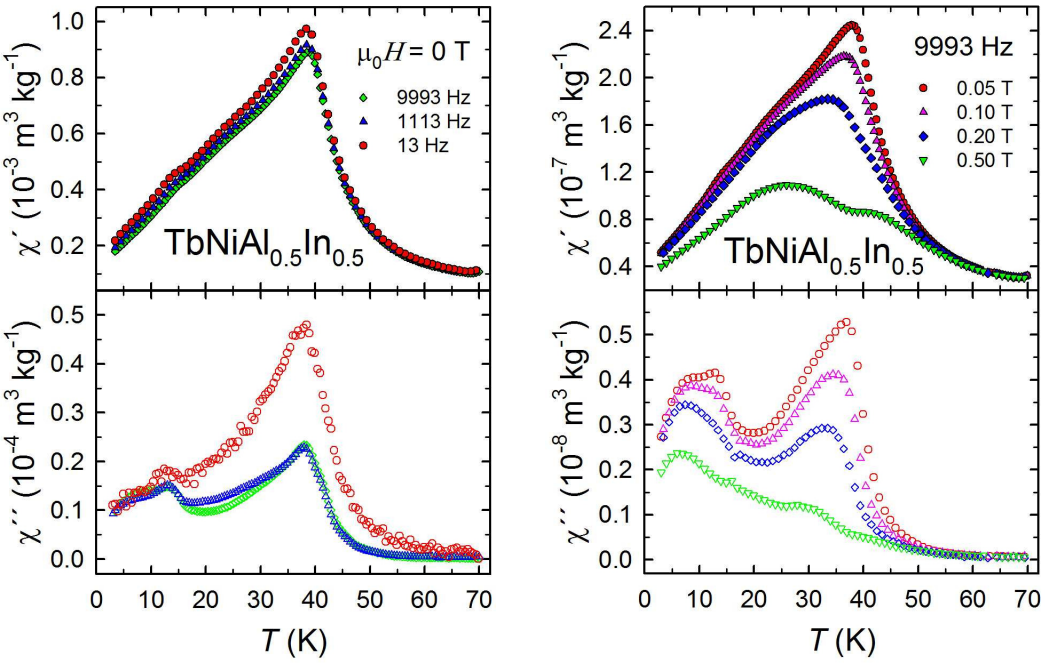

(a) (b)

Figure 4.18: The temperature dependence of AC-susceptibility of $TbNiAl_{0.5}In_{0.5}$ compound: (a) for various frequencies in zero magnetic field and (b) for the frequency of 9993 Hz in various magnetic fields. The field suppresses all anomalies and causes a considerable shift to lower temperatures.

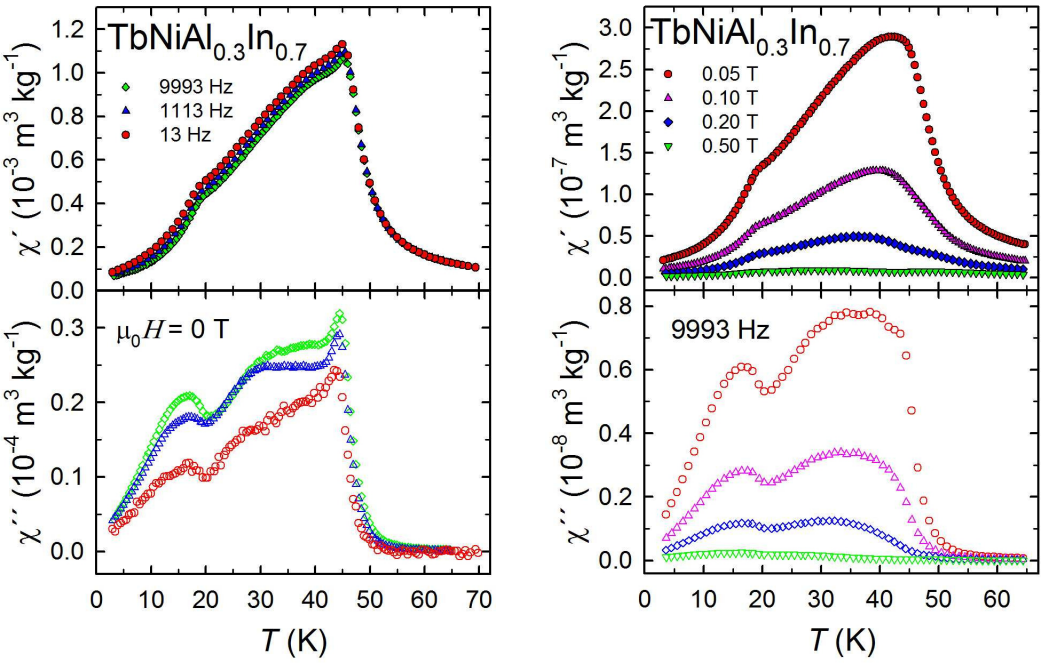

(a) (b)

Figure 4.19: The temperature dependence of AC-susceptibility of $TbNiAl_{0.3}In_{0.7}$ compound: (a) for various frequencies in zero magnetic field and (b) for the frequency of 9993 Hz in various magnetic fields.

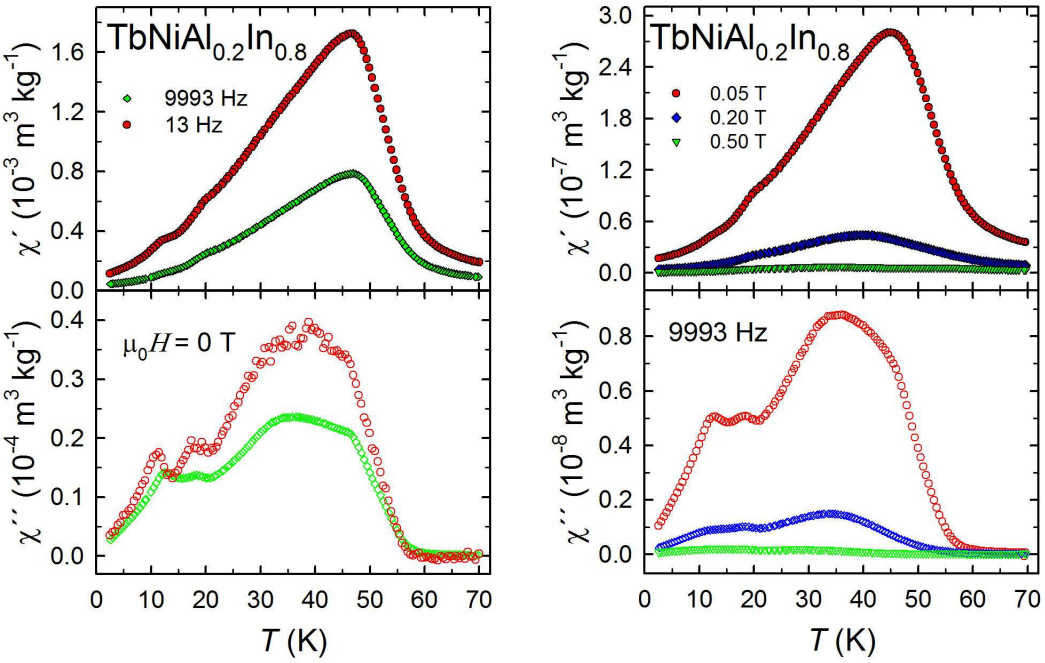

(a) (b)

Figure 4.20: The temperature dependence of AC-susceptibility of $TbNiAl_{0.2}In_{0.8}$ compound: (a) for various frequencies in zero magnetic field and (b) for the frequency of 9993 Hz in various magnetic fields. Two maxima in low-temperature region are well-shown especially in the imaginary part.

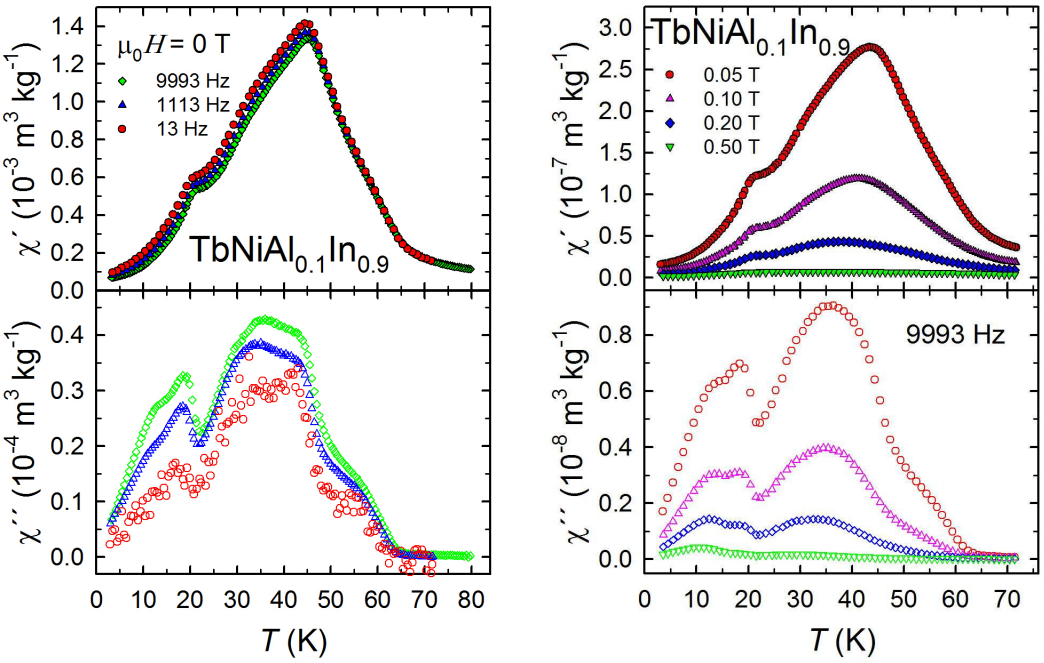

(a) (b)

Figure 4.21: The temperature dependence of AC-susceptibility of $TbNiAl_{0.1}In_{0.9}$ compound: (a) for various frequencies in zero magnetic field and (b) for the frequency of 9993 Hz in various magnetic fields. The field suppresses all anomalies and causes a considerable shift to lower temperatures.

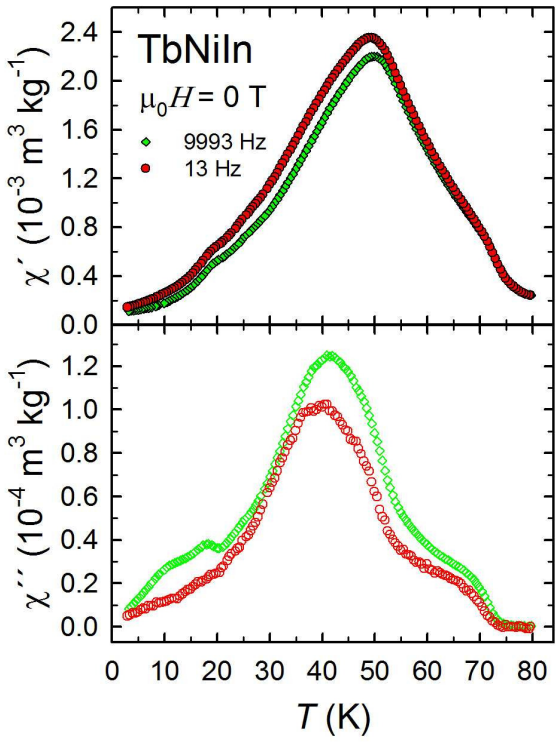

Figure 4.22: The temperature dependence of AC-susceptibility of TbNiIn compound for frequencies of 13 and 9993 Hz in zero magnetic field. Three maxima of magnetic phase transitions are clearly visible especially in the imaginary part.

4.3.2 DC - magnetization

The magnetic measurements were done as described in Section 3.4.

In the paramagnetic region, the $M/H(T)$ dependencies follow the Curie–Weiss behavior (see Equation (1.4) and Figure 4.23). The determined values of the effective moment, μ_{eff}, are close or slightly higher than the Tb^{3+} free ion value of 9.72 μ_{B} (see Table 4.3). The small enhancement can be attributed to the polarization of conduction electrons, similarly as in pure TbNiAl [34]. The paramagnetic Curie temperature, θ_{P}, is positive for all indium concentrations and weakly increases for the In rich compounds. The positive θ_{P} in TbNiAl compound despite its antiferromagnetic structure points to prevailed ferromagnetic interactions in the paramagnetic region [34]. The values of the paramagnetic Curie temperature are also placed in Table 4.3.

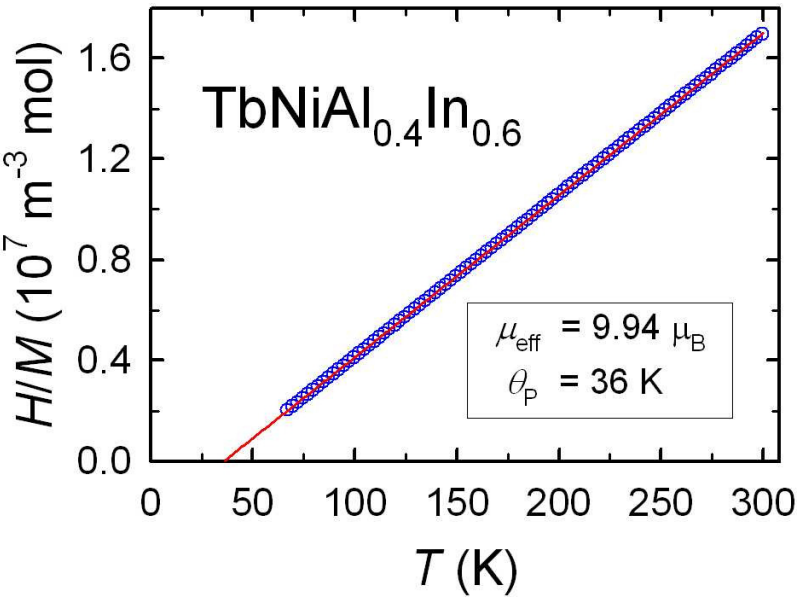

Figure 4.23: The ratio of magnetic field and magnetization in paramagnetic region of $TbNiAl_{0.4}In_{0.6}$ compound measured in the static magnetic field of 2 T. The temperature dependence is in accordance with the Curie-Weiss law (Equation (1.4)).

The temperatures of magnetic phase transitions can be well determined from $M/H(T)$ dependencies at lower temperatures, especially for the measurements under ZFC regime and for small fields. The temperatures of magnetic phase transitions very well correspond to temperatures obtained from AC-susceptibility measurement (see Table 4.3). The measured dependencies for various concentrations are shown in Figures 4.24 and 4.25. The magnetization curves for ZFC regime and small fields (in the case of the field of 0.005 T also for FC regime) show very interesting and surprising behavior, the magnetization under the temperature of magnetic ordering is negative. The negative temperature dependence of magnetization was found in several ternary or pseudoternary materials with ferro-, antiferro- and also ferri-magnetic ordering and crystallizing in various structures, for example in TbCoSi [44], UPdSb [45] and other. This phenomenon can be explained by an assumption that in the material exists another magnetic sublattice with a different temperature dependence and an orientation of magnetic moments. The total magnetization is then the difference between the magnetization of first

and second magnetic sublattice. In the case that only one magnetic sublattice is present in the material, the existing domain structure and/or anisotropy may act as the second magnetic sublattice, more in [46]. The second possible explanation of the negative magnetization in our measurement is the remanent field in the coil of PPMS. This remanent field can have a high influence on the value of the magnetization measured in the small magnetic fields. In our case, the remanent field should have the value of 0.01 T. Nevertheless, the magnetic phase transitions are clearly observed for all concentrations.

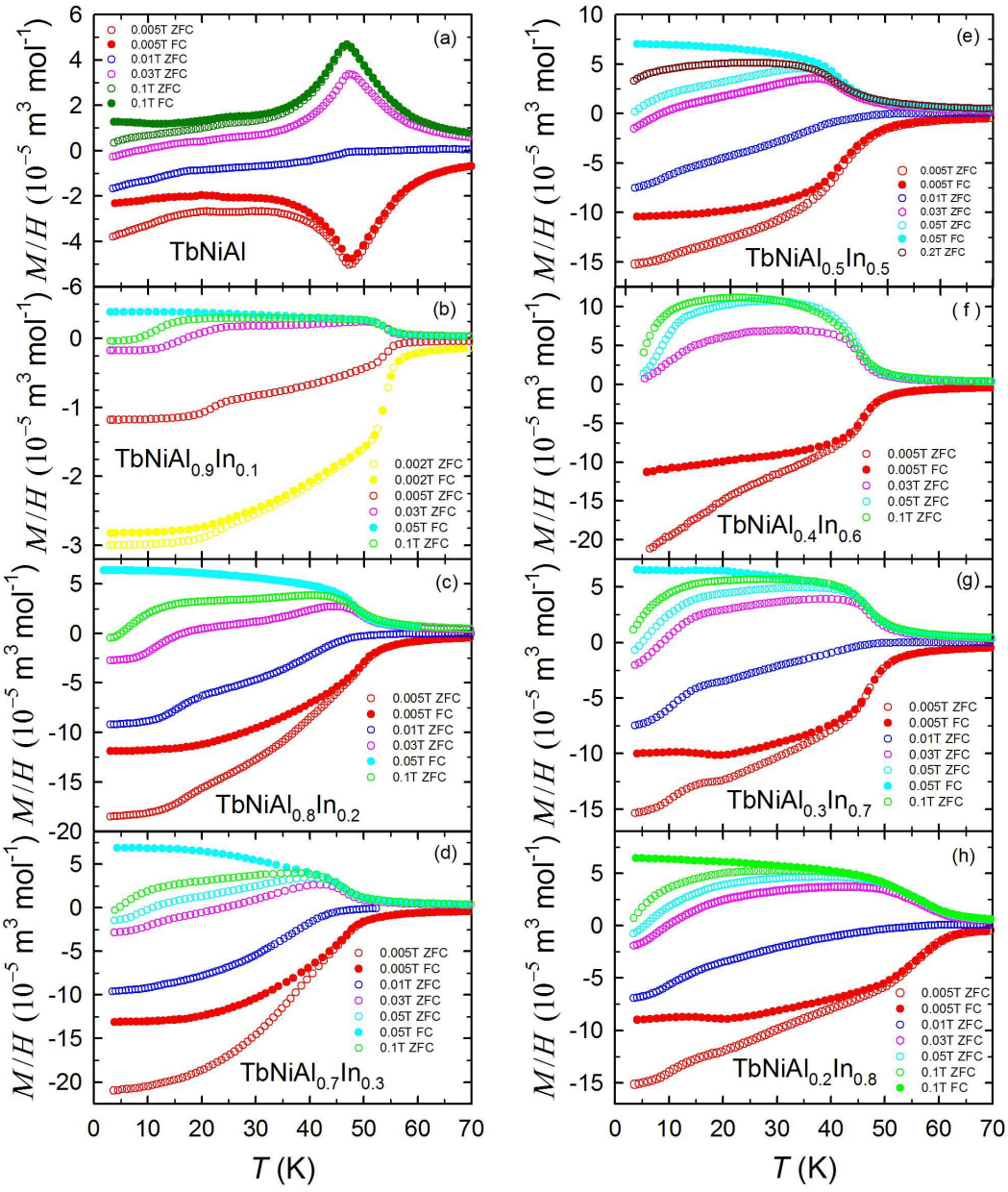

Figure 4.24: $M/H(T)$ dependencies of $TbNiAl_{1-x}In_x$ compounds in various magnetic fields and under ZFC and FC regimes.

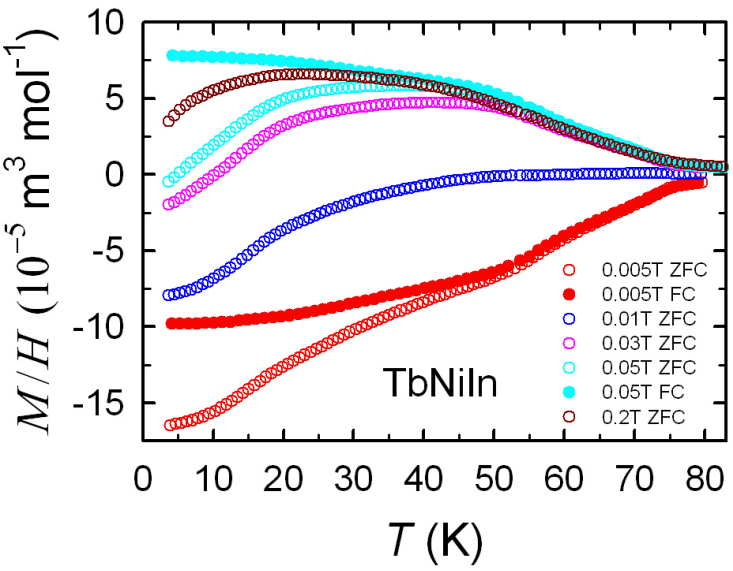

Figure 4.25: $M/H(T)$ dependencies of TbNiIn compound in various magnetic fields and under ZFC and FC regimes.

The saturated moment of the compounds is possible determine using the Akulov criterion [47]:

$$M = \mathrm{M_S}(1 - \frac{\mathrm{a}}{H} - \frac{\mathrm{b}}{H^2}), \tag{4.1}$$

where $\mathrm{M_S}$ is saturated magnetization and a and b are non-negative constants. The saturated magnetization reaching values between 7 and ∼9 μ_B for various concentrations (see Table 4.3). The Akulov criterion was used for the data from field region between 1.9 and 14 T measured at 2 K.

The antiferromagnetic ordering in pure TbNiAl demonstrates as s-shape curves for low temperatures in field dependencies of the magnetization $M(H)$. The highest values of magnetic moments are shown by the concentrations of x = 0.2, 0.3 and 0.4 (see Figures 4.26c-e). The $\mathrm{TbNiAl_{0.6}In_{0.4}}$ shows some signs of metamagnetic transition around 3.5 T. The magnetic moment decreases with the increasing temperature of measurement in accordance with the expectation. The measured curves for temperatures of 3 and 10 K are rather similar for the most of concentrations what means that no magnetic phase transition occurs in this temperature region (3 - 10 K). This is in accordance with the other experimental techniques.

The arrot plots ($M^2(H/M)$) were made from the magnetization data and are placed in Figures 4.27 and 4.28b. The data show a linear dependencies with the intersection with the x-axis for the temperatures from paramagnetic region. We can observe the antiferromagnetic component in the most of concentrations manifested as twisted curves (especially the curve for the temperature of 3 K) for low values of H/M.

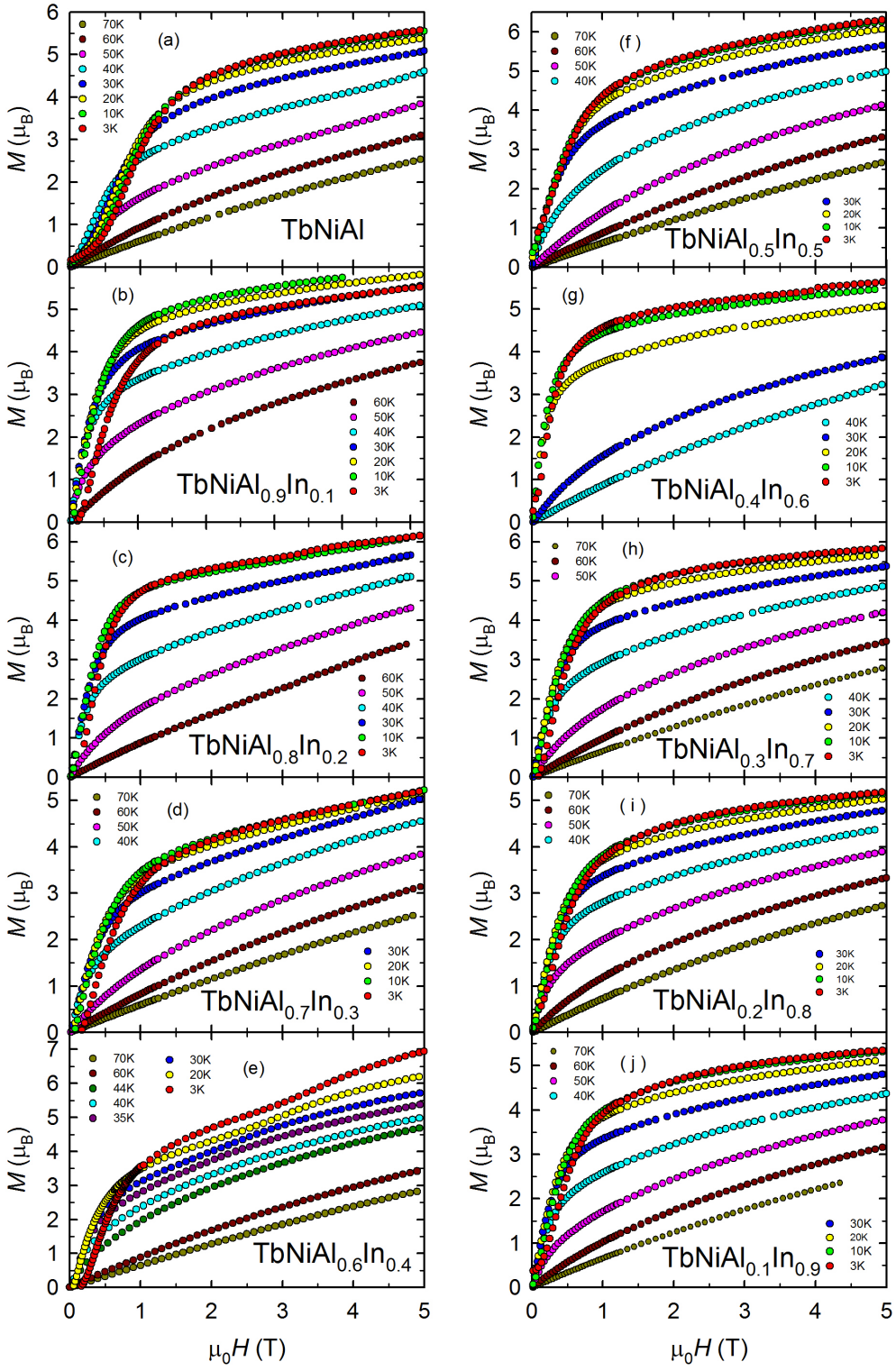

Figure 4.26: Field dependencies of the magnetization, $M(H)$, in various temperatures of $TbNiAl_{1-x}In_x$ compounds.

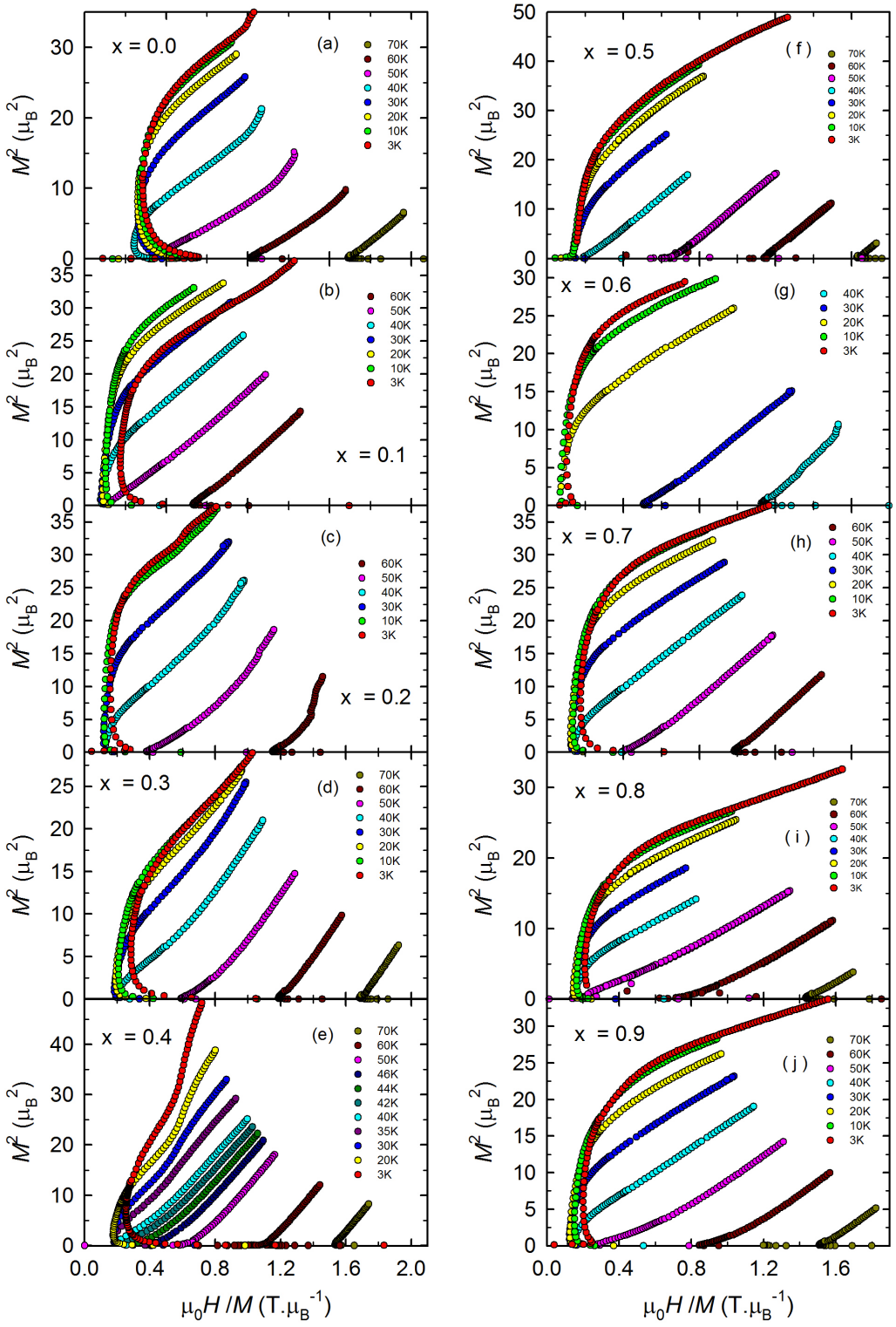

Figure 4.27: Arrot plots, $M^2(H/M)$, of $TbNiAl_{1-x}In_x$ compounds measured in various temperatures.

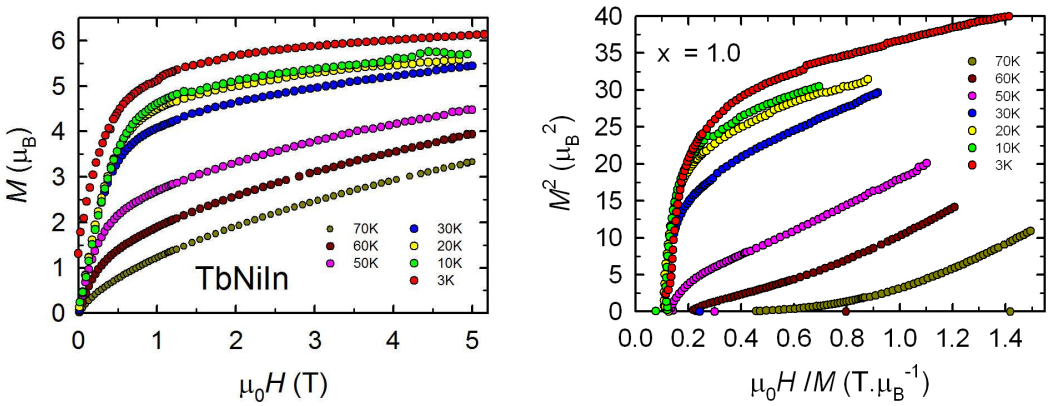

(a) (b)

Figure 4.28: (a) Field dependencies of the magnetization, and (b) the arrot plot in various temperatures of TbNiIn compound.

The measurements of field dependencies of the magnetization ($M(H)$) at 3 K show that the Tb magnetic moment in 14 T reaches the values between 6 and 8 μ_B for various concentrations (see Table 4.3). Some of magnetization curves are plotted in Figure 4.29.

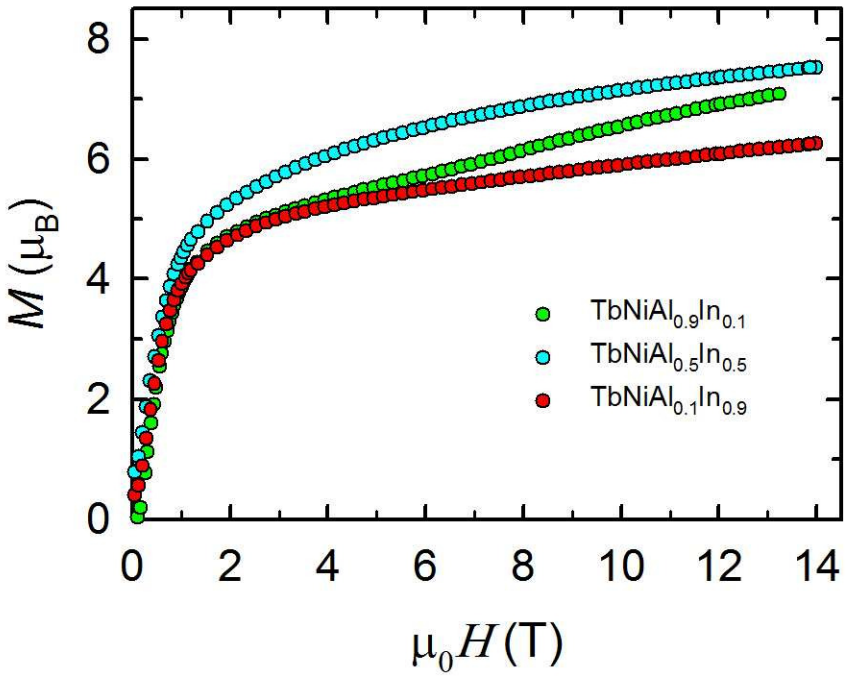

Figure 4.29: Field dependencies of the magnetization of $TbNiAl_{0.9}In_{0.1}$, $TbNiAl_{0.5}In_{0.5}$ and $TbNiAl_{0.1}In_{0.9}$ compounds. The rest of dependencies of other concentrations is not plotted in Figure for better lucidity.

4.4 Specific heat measurement

The measured temperature dependence of the specific heat of $TbNiAl_{1-x}In_x$ compounds is placed in Figures 4.30 and 4.31. We observe two sharp transitions for pure TbNiAl which well corresponds to the magnetic phase transitions observed by other experimental techniques. The anomaly at the ordering temperature loses its sharpness with increasing indium content. The additional magnetic phase transition as indicated by AC-susceptibility are not seen in specific heat data except $TbNiAl_{0.2}In_{0.8}$ where we can trace out the transitions at $\simeq 20$ K and $\simeq 50$ K (see Figure 4.31).

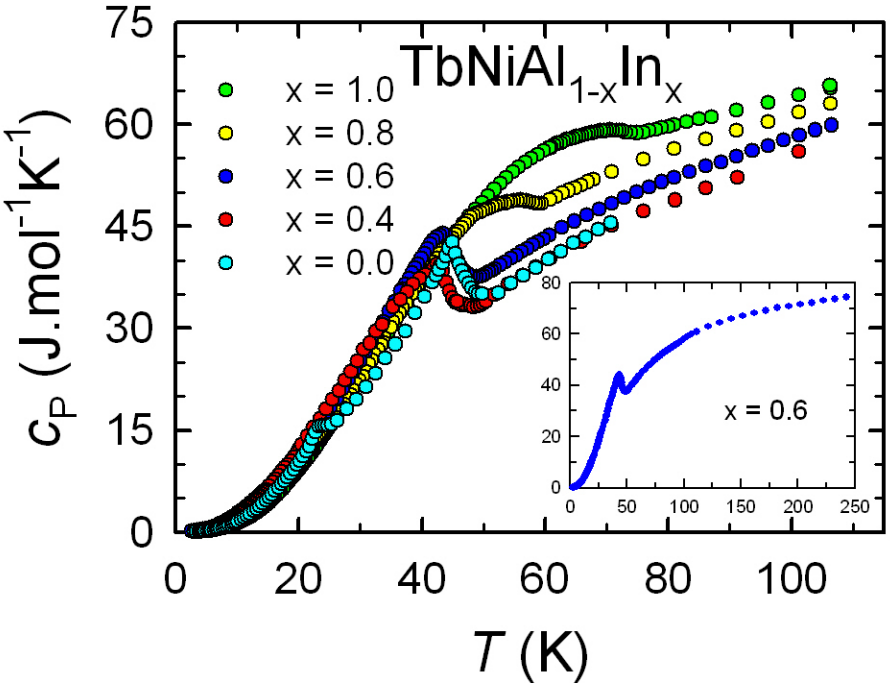

Figure 4.30: The temperature dependencies of specific heat for $TbNiAl_{1-x}In_x$ compounds. The subfigure has the same x-, y-labels.

In general, the specific heat of this type of materials in the studied temperature range can be described as the sum of several contributions:

$$c_p = c_{el} + c_{ph} + c_{mag}. \tag{4.2}$$

Specific heat of conduction electrons, c_{el}, is usually directly proportional to the temperature, the coefficient of proportionality γ is called as the Sommerfeld coefficient. Specific heat of lattice vibrations, c_{ph}, is usually well described in the Debye and Einstein approximation [48]. This contribution is dominant at high temperatures above ~ 50 K. The description of the magnetic contribution, c_{mag}, is generally more complex and depends on the magnetic behavior of the substance. Generally, the entropy of the compounds in which magnetism is due to rare earth ion depends on the corresponding magnetic quantum number J as:

$$S_{mag} = \mathrm{R.ln}(2J+1), \tag{4.3}$$

where R is universal gas constant.

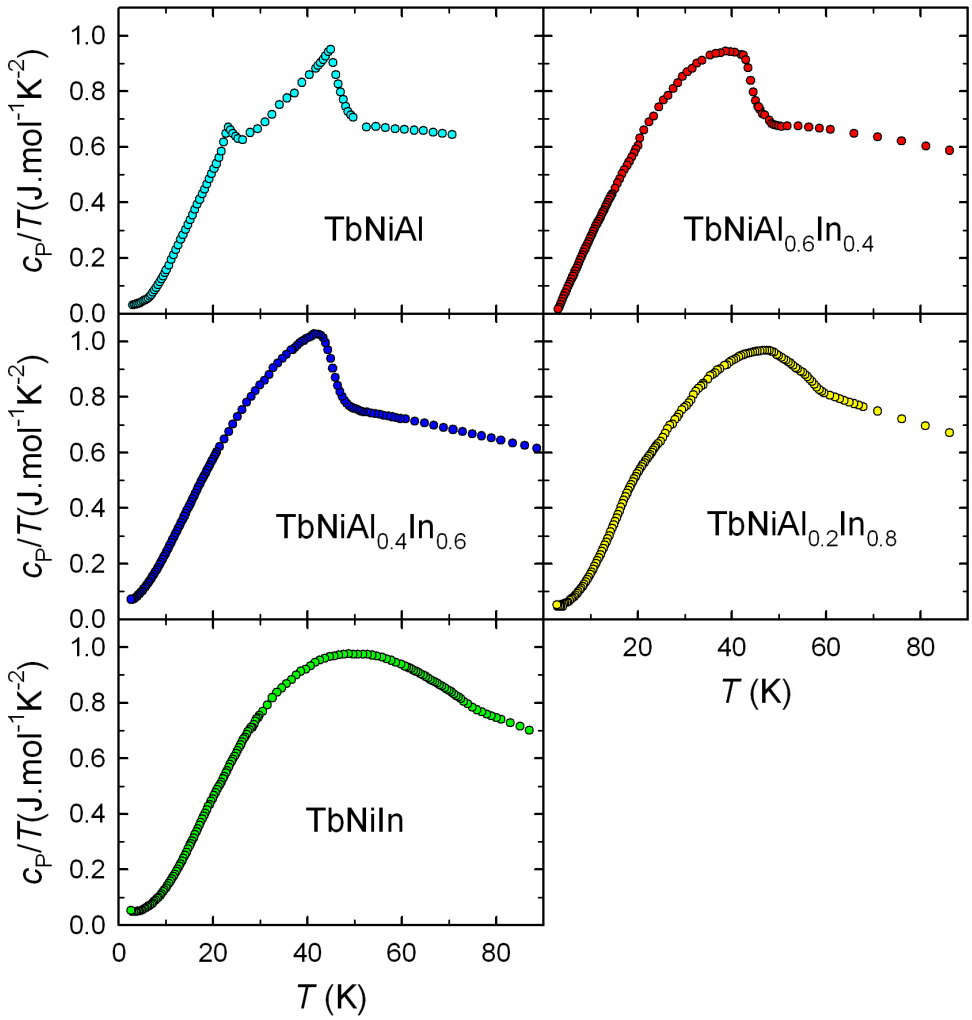

Figure 4.31: The temperature dependencies of the ratio of the specific heat and the temperature in $TbNiAl_{1-x}In_x$ compounds.

The magnetic contribution is zero for compounds with a non-magnetic rare earth ion ($J = 0$) and the total specific heat is the sum of electron and lattice contributions only. This is the case of compounds with yttrium, lanthanum or lutetium. Due to the same structure, similar lattice parameters and the mass of atoms we will consider the specific heat of LuNiAl [49] (see Figure 4.32) as a good estimate of these two contributions for TbNiAl. After the subtracting of LuNiAl data we got magnetic contribution to specific heat c_{mag} of TbNiAl. The temperature dependence of c_{mag} contribution obtained in this way is placed in Figure 4.32.

From the temperature dependence of c_{mag} contribution we then determined the magnetic entropy as:

$$S_{\mathrm{mag}}(T^*) = \int_0^{T^*} \frac{c_{\mathrm{mag}}}{T}\ \mathrm{dT}. \tag{4.4}$$

The magnetic contribution to specific heat in our unmeasured temperature range below 2 K is very small. For that reason we can assume that the $\frac{c_{\mathrm{mag}}}{T}$ ratio in this region in calculating of the entropy is equal to zero. The magnetic entropy S_{mag} calculated this way is shown in Figure 4.32.

The theoretical value of the magnetic entropy for Tb^{3+} ion ($J = 6$) is by Equation (4.3): $S_{mag} = 21.3$ J.mol^{-1}K^{-1}. In the measured temperature region up to 70 K S_{mag} reached the value of 18.3 J.mol^{-1}K^{-1} what correspond to 8 - 10 crystal-field levels. From Figure 4.32 we can assume that the value of magnetic entropy will increase for higher temperature to the value expected for all 13 levels.

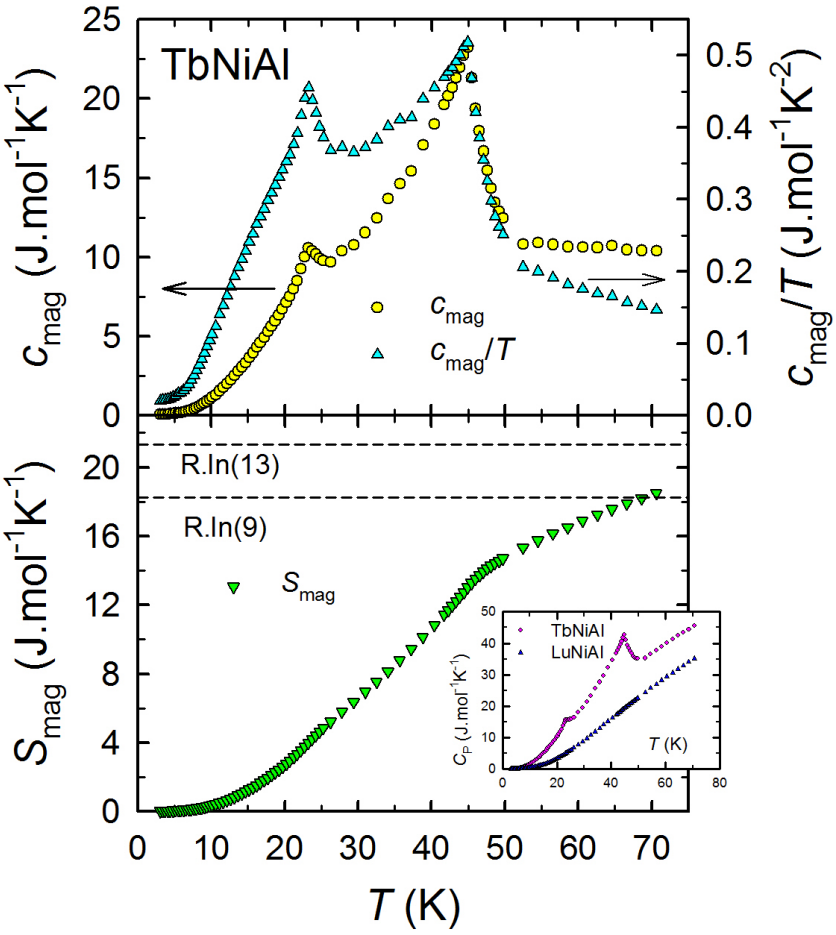

Figure 4.32: The magnetic part of the specific heat of TbNiAl obtained by subtracting non-magnetic analogue LuNiAl [49]. The magnetic entropy reaches the value of $\simeq 18.3$ J.mol^{-1}K^{-1} at 70 K. The specific heat data of LuNiAl are plotted in subfigure.

4.5 Transport properties

The electric current passing through the material is hindered by the non-periodicity of the system. This phenomenon is called as the electrical resistance. The conduction electrons of the material that mediate passage of the current are scattered on the errors in the periodic arrangement of the material.

The electrical resistance of metals is approximately described by Matthiessen rule:

$$\rho_{\mathrm{tot}} = \rho_0 + \rho_{\mathrm{ph}} + \rho_{\mathrm{mag}}. \tag{4.5}$$

This approximation states that the total resistance of the metal can be obtained by summing contributions from the individual scattering mechanisms. The contribution of the scattering of the conduction electrons on impurities and dislocations of the material, ρ_0, is temperature independent and it is the only contribution to the resistance for the temperature going to 0 K. The contribution due to the scattering of electrons on the lattice vibrations (phonons), ρ_{ph}, increases linearly with the increasing temperature. The magnetic contribution to the resistivity, ρ_{mag}, related to the scattering of the conduction electrons on the magnetic moments of the system increases with increasing temperature up to the temperature of magnetic ordering of the metal, then this contribution is constant with the temperature (in the absence of the crystal field). The Matthiessen rule is not valid in cases where there is a correlation between scattering processes, nevertheless, the rule is used for an approximate estimation of the resistivity of metals.

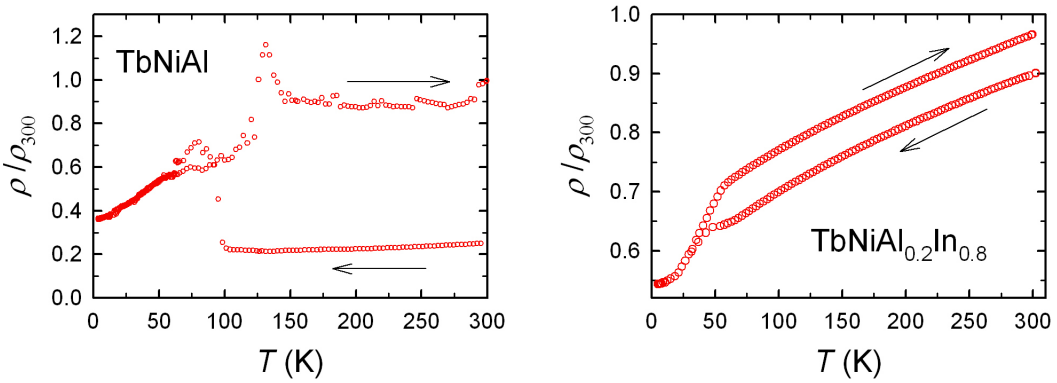

Figure 4.33: The temperature dependencies of the resistance of the (a) TbNiAl and (b) $TbNiAl_{0.2}In_{0.8}$ compounds. The resistivity measured in cooling regime has lower value.

The temperature dependencies of the resistivity were measured as described in Section 3.6. The structural phase transition was found on the polycrystalline sample of TbNiAl around 95 K or 120 K while cooling or heating process, respectively (see Figure 4.33a). Note, that exactly the same interval (95 - 120 K) was found as two-phase region where both phases are present according to the X-ray diffraction data (see Figure 2.4, [33, 12]). The temperature of this phase transition remains unchanged in applied magnetic field of 0.3 T. No such structural transition appears for the rest of $TbNiAl_{1-x}In_x$ compounds. We observe certain effect that could remind structural transition also for substituted compounds (especially the increase of the resistivity after temperature cycling), for

example $TbNiAl_{0.2}In_{0.8}$ (see Figure 4.33b). On the other hand, the development of the c/a ratio does not reveals any structural change in these compounds (see Figure 4.2 and Section 4.6). Therefore, we can speculate that observed effect originate in the measurement technique.

Some of the magnetic phase transitions are clearly seen as a kink in the $\rho(T)$ data (see Figure 4.34). The ordering temperatures, T_{ord}, are observable for most of concentrations. For the x $\geq$ 0.8, we do not observe any pronounced effect at T_{ord}, but we can see the transition corresponding to T'. The temperatures of observed magnetic phase transitions are in good agreement with the values obtained from magnetization measurements. The magnetic field of 0.3 T has minor effect on the resistivity. The temperatures of magnetic phase transitions are not influenced by applying the magnetic field.

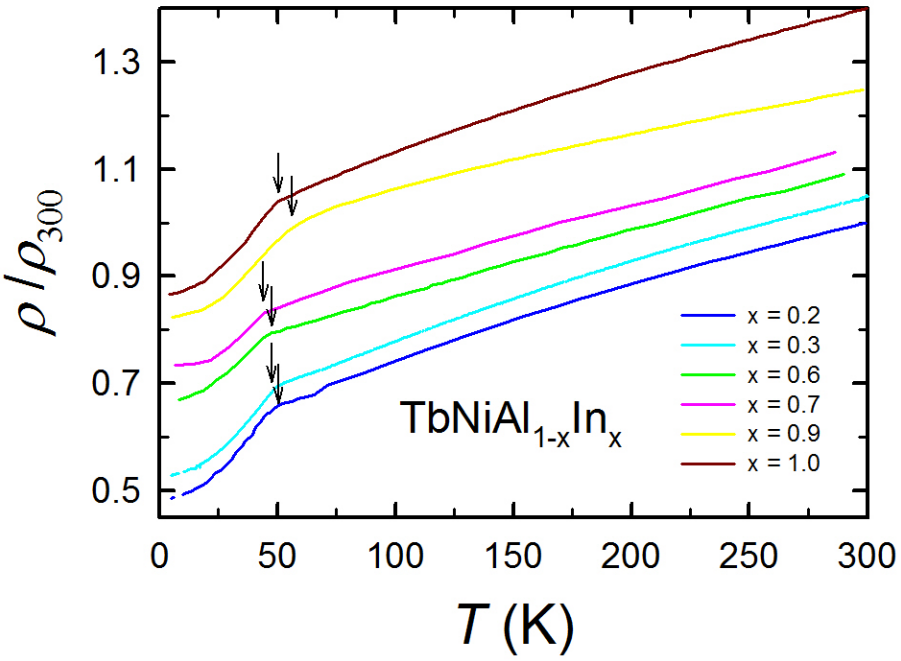

Figure 4.34: The temperature dependencies of the resistivity of the $TbNiAl_{1-x}In_x$ compounds measured in heating mode. The tick labels of the y-axis are related to x = 0.2 curve, resistance curves of further concentrations were shifted by 0.05 to higher values compared to the previous concentrations (except of TbNiIn compound where the shift was 0.15) for better lucidity of Figure.

The measurement of temperature dependence of the resistivity under hydrostatic pressure was done on the TbNiAl prism-shape sample as described in Section 3.6. The temperature dependencies of the electrical resistivity are placed in the Figure 4.35. The curves are plotted in the order they were measured. We can see the reducing quality of the sample with the experience of the structural phase transition. The quality of the sample is almost maintained for the pressures in which the structural transition does not occur (0.75 and 0.55 GPa). The measurement in the pressure of 0.75 GPa is not included in Figure because of the clarity (the curves of the pressures of 0.55 and 0.75 GPa are almost perfectly overlapped).

The temperature of structural phase transition is approximately 120 K for low pressures (0.2 and 0.25 GPa) and ambient pressure measurements in cooling

mode. The measurements in heating mode show slightly higher temperature of the transition. The temperature of the structural transition is lowered to 80 K for higher pressure of 0.3 GPa for the measurement in cooling mode, in heating regime the structural transition occurs on almost the same temperature as in the measurement in lowest pressures (see Figure 4.35). The structural transition for the pressure of 0.35 GPa is associated to the magnetic phase transition below 50 K, however, the structural transition is clearly identified (see Figure 4.35). The structural phase transition moves to the lower temperatures for higher pressures and it does not occur for pressures ≥ 0.55 GPa in the studied temperature range.

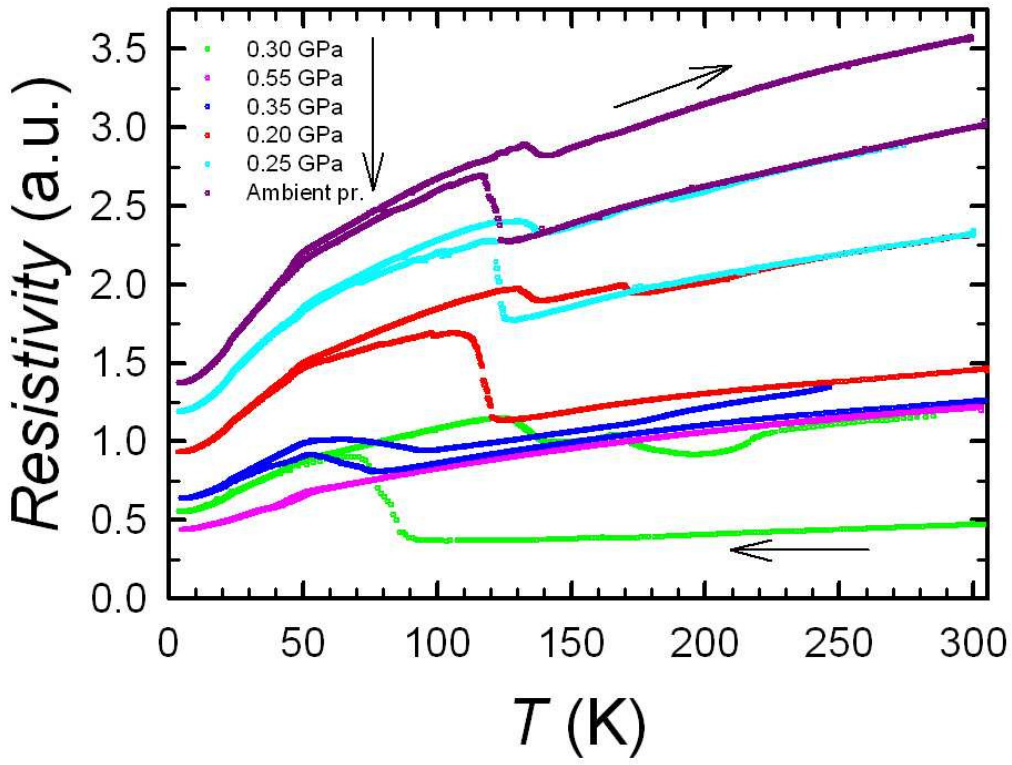

Figure 4.35: The temperature dependencies of the resistivity in the constant pressures of the TbNiAl compound. The arrow indicates the order in which individual curves were measured.

The kink around 170 - 180 K on the curves for the pressures of 0.2, 0.3 and less pronounced of 0.25 GPa for heating is not clearly identified (see Figure 4.35). Possible explanation of this kink could be a continuation of the structural phase transition caused by the application of the pressure. The pressure has the tendency to hold the sample in the structure with low c/a ratio. In the polycrystal, local variation of the element composition can appear, which can cause a small shift of the temperature of structural transition in different grains. Thus, for some grains it is energetically preferable to stay in the state with low c/a ratio and they undergo the structural transition at higher temperatures. This anomaly does not occur in the ambient pressure measurement.

The magnetic phase transitions corresponding to the temperatures T_{N} and T_1 for TbNiAl obtained from other experimental techniques are also clearly visible in Figure 4.35. Both observed ordering temperatures slightly increase with increasing pressure in the cell.

4.6 Neutron diffraction

The neutron diffraction patterns obtained as described in Section 3.7 were processed using the Fullprof program employing the Rietveld analysis [41].

4.6.1 Crystal structure

The refined diffraction patterns recorded at the paramagnetic state confirmed the hexagonal ZrNiAl-type of structure. Note that, the nuclear reflections (100) and (001) are very small in diffraction pattern (see Figure 4.36). Another weak peaks observed at small angles probably correspond to the presence of the minority phase in the sample (see Chapter 4.1). The peak around 72 degrees is due to vanadium sample container (the label 'V').

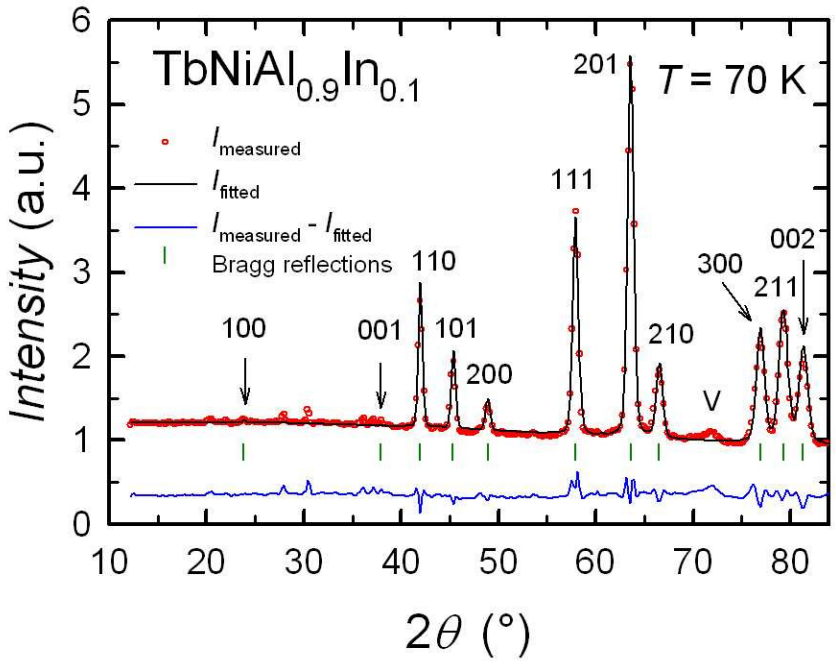

Figure 4.36: Diffraction pattern of $TbNiAl_{0.9}In_{0.1}$ recorded in the paramagnetic state (70 K). The peak around 72 degrees is due to vanadium sample container.

The refinement of our data revealed also some preferential orientation of the powder sample. We used the March function for the involvement of the preferential orientation into the refinement of diffraction data:

$$M_{hkl} = \int (f_{\mathrm{cor}}^2 \cos^2 \alpha + \frac{\sin^2 \alpha}{f_{\mathrm{cor}}})^{-\frac{3}{2}} \ \mathrm{d}\alpha. \tag{4.6}$$

The correlation factor f_{cor} expresses the degree of preferential orientation. The preferential orientation does not occur in the sample when $f_{\mathrm{cor}} = 1$, takes the plate-shape form for $f_{\mathrm{cor}} < 1$ and needle-shape for $f_{\mathrm{cor}} > 1$, more in [41]. The refinement of our data leads to a correlation factor slightly less than 1 (approximately 0.94 - 0.99) for most of measured concentrations, so the plate-shape form of the preferential orientation occurs in these compounds. This involvement of preferential orientation greatly improves the refinement of neutron diffraction

data (especially the magnetic refinement factor R_{M} corresponding to (000) propagation is improved by 7% in $TbNiAl_{0.8}In_{0.2}$, for example). There are only two exceptions, $TbNiAl_{0.5}In_{0.5}$ and TbNiIn compounds, where the preferential orientation does not occur ($f_{cor} = 1$).

Table 4.4: Lattice parameters of $TbNiAl_{1-x}In_x$ compounds in the paramagnetic state (i.e. 60 - 80 K) determined from powder neutron diffraction. x_{Tb} and $x_{\mathrm{Al(In)}}$ are fraction coordinates of Tb and Al(In) atoms in the fundamental unit (see Figure 2.1). R_{Bragg} is agreement factor for the nuclear fit.

x	T (K)	a (pm)	c (pm)	x_{Tb}	$x_{\mathrm{Al(In)}}$	R_{Bragg} (%)
0.1	70	703.0(2)	387.6(1)	0.582(1)	0.238(2)	4.1
0.2	60	708.2(3)	385.6(1)	0.580(1)	0.239(4)	5.9
0.3	60	714.1(3)	383.7(1)	0.579(1)	0.239(3)	6.0
0.4	70	720.0(3)	382.1(1)	0.584(1)	0.240(3)	4.7
0.5	70	724.5(3)	380.9(2)	0.579(2)	0.245(4)	6.9
0.6	70	730.7(3)	379.5(2)	0.583(2)	0.248(4)	5.5
0.8	70	740.3(3)	377.1(2)	0.588(1)	0.259(3)	6.7
0.9	80	744.3(3)	377.0(2)	0.585(2)	0.259(4)	6.4
1.0	80	744.9(2)	378.0(2)	0.592(1)	0.260(3)	4.8

The lattice parameters of each concentration refined from diffraction data measured above the ordering temperature are placed in Table 4.4. We can see that the lattice parameter a increases linearly with increasing indium content, whereas the parameter c decreases linearly between concentrations $x = 0.1$ and 0.6 and remains almost the same for higher In concentrations. This development of lattice parameters obtained by neutron diffraction at temperatures slightly above the magnetic phase transition is in agreement with results obtained at 300 K using the X-ray diffraction (see Chapter 4.1). Positions of Tb and Al(In) atoms (x_{Tb} and $x_{\mathrm{Al(In)}}$) slightly change for each concentration. We can observe roughly linear increase in $x_{\mathrm{Al,In}}$ in concentrations with x $\geq$ 0.5.

Temperature dependencies of the lattice parameters were in detail refined for $TbNiAl_{0.8}In_{0.2}$ and $TbNiAl_{0.1}In_{0.9}$ compounds. Obtained values are plotted in Figure 4.37. The recognizable change of the lattice parameters occurs in low In concentrations (x $\leq$0.4), but for higher In content compounds we can observe only a small alterations often only in the range of the error of the refinement (compare Figures 4.37a and 4.37b). In first concentration range, the c/a ratio increases with decreasing temperature below T_{ord}, whereas for x $\geq$ 0.5 this ratio slightly decreases with decreasing temperature. This behavior is observable also when comparing the lattice parameters at the room temperature and at 2 K (see Figure 4.2). This change of the temperature dependence of c/a ratio can be related to the change of the magnetocrystalline anisotropy in the series. The parent compounds have a different type of the anisotropy (uniaxial for TbNiAl and planar for TbNiIn) and their c/a ratios behave also conversely, thus we can assume that the change of the development of the c/a ratio is bound with the change of the anisotropy from uniaxial to planar type. On the other hand, the magnetocrystalline anisotropy can not be concluded solely from the behavior of the c/a ratio below the ordering temperature, for example the previous studies on

DyNiAl with the direction of magnetic moments along the c-axis and on TbPdIn with the moments oriented into the basal plane point very similar temperature dependencies of the c/a ratio (the increase with increasing temperature) [50].

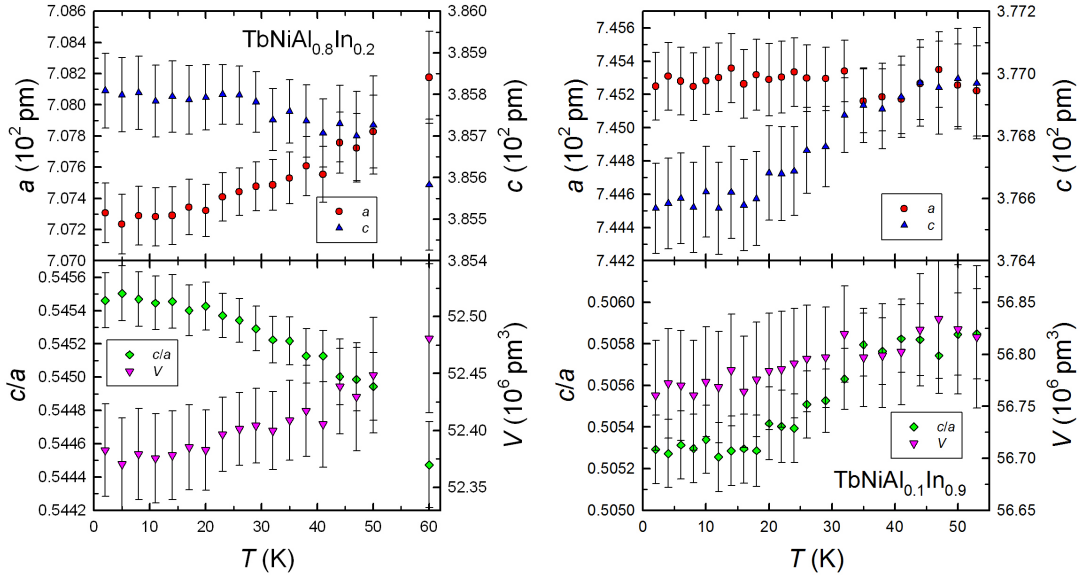

Figure 4.37: The temperature dependencies of lattice parameters of (a) $TbNiAl_{0.8}In_{0.2}$ and (b) $TbNiAl_{0.1}In_{0.9}$ compounds obtained from powder neutron diffraction.

4.6.2 Magnetic structures

Below the temperature of magnetic ordering, we observe several types of additional intensities as demonstrated in Figure 4.38. First, we observe increasing intensity on positions of nuclear reflections for decreasing temperature in the whole series. This behavior of the intensity means that magnetic reflections are on same angles as nuclear peaks what leads to the propagation vector $\vec{k} = (000)$. Some further magnetic peaks appear in diffraction patterns on positions which do not correspond to nuclear reflections. This observation implies another propagation vectors in TbNi(Al,In) series. Most of these purely magnetic peaks can be described by $(\frac{1}{2}\ 0\ \frac{1}{2})$ propagation vector. Moreover, another weak peaks appear on low-angle part of diffraction records (the symbol of '$*$'). These peaks can be in most cases described by $(0\ 0\ \frac{1}{2})$ and $(\frac{1}{2}\ 0\ 0)$ propagation vectors, but it is also possible that these peaks correspond to another phase. The presence of these peaks will be discuss in Section 4.7.

Qualitatively peaks of the same type are observed for all concentrations. Although the propagation vectors are the same for all compounds, the directions of Tb magnetic moments differ. This is well demonstrated on Figure 4.38. There is no magnetic intensity on the (001) reflection for $TbNiAl_{0.6}In_{0.4}$, whereas (001) is very strong magnetic peak for $TbNiAl_{0.5}In_{0.5}$ compound. Such observation immediately suggests an idea that Tb moments are parallel to the c-axis in $TbNiAl_{0.6}In_{0.4}$ and perpendicular to the c-axis in $TbNiAl_{0.5}In_{0.5}$ compound.

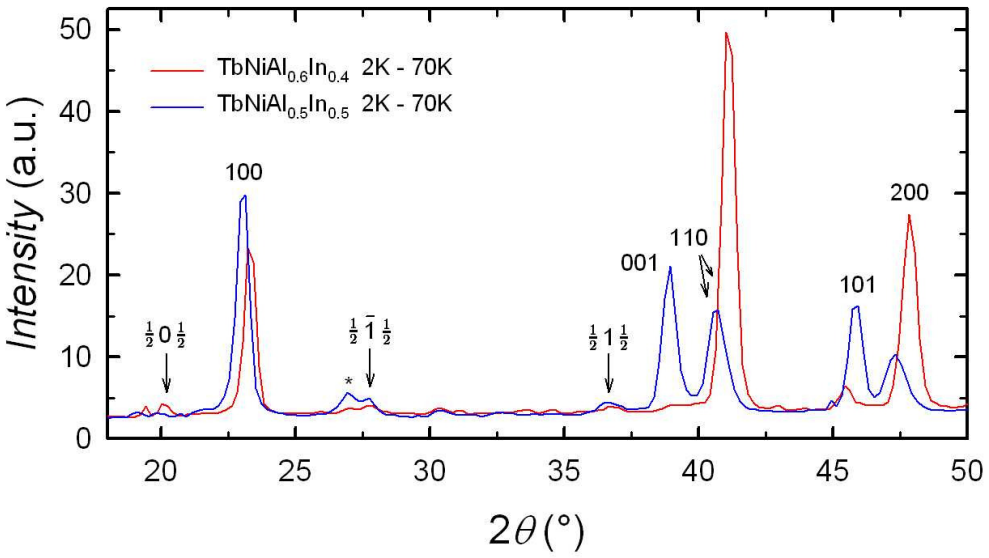

Figure 4.38: Diffraction patterns of $TbNiAl_{0.6}In_{0.4}$ and $TbNiAl_{0.5}In_{0.5}$ compounds. The diffraction patterns plotted in Figure were created by the subtracting of paramagnetic data from data obtained at 2 K. Observed reflections (h k l) belonging to propagation vectors of (000) and ($\frac{1}{2}$ 0 $\frac{1}{2}$) are described in Figure. Another weak magnetic peak is marked by the symbol '$*$'.

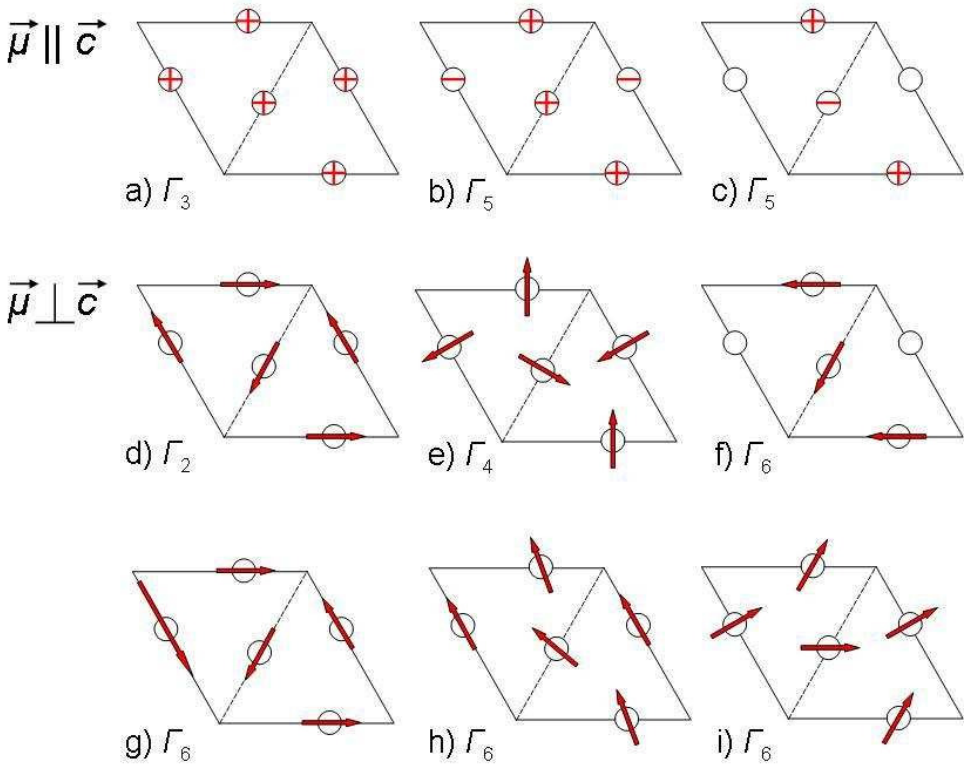

Figure 4.39: Possible magnetic moment orientations for the P$\bar{6}$2m space group and (000) propagation vector as derived from representation group theory employing the SARAh program [51].

The arrangements of the moments allowed by the symmetry are drawn in Figure 4.39 for propagation vector of (000) and in Figure 4.40 for $\vec{k}$ = ($\frac{1}{2}$ 0

$\frac{1}{2}$). Γ_5 and Γ_6 representations appear twice and four-times, respectively, in the results of the representation analysis of (000) propagation (similarly Γ_2 and Γ_4 for $\vec{k} = (\frac{1}{2}\ 0\ \frac{1}{2})$). It means that also any linear combination of the moments configurations corresponding to the same Γ is a possible solution of the magnetic structure.

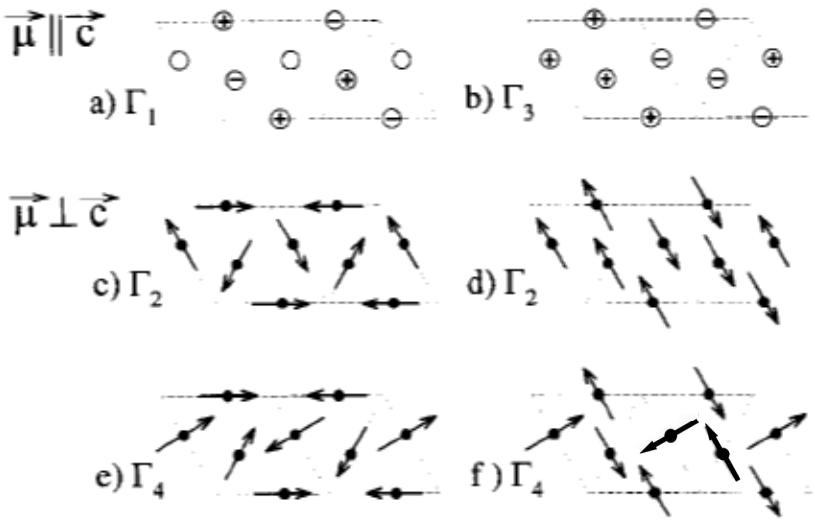

Figure 4.40: Possible magnetic moment orientations for the P$\bar{6}$2m space group and ($\frac{1}{2}$ 0 $\frac{1}{2}$) propagation vector as derived from representation group theory. The Figure taken from [14].

According to the type of magnetic order, we distinguish two concentration ranges x $\leq$ 0.4 and x $\geq$ 0.5.

Magnetic structure of $TbNiAl_{1-x}In_x$ with x $\leq$ 0.4

First concentration range includes compounds with x $\leq$ 0.4. The diffraction patterns of these concentrations are all very similar (compare Figures 4.41 and 4.42).

Let us first describe the magnetic structure of $TbNiAl_{0.9}In_{0.1}$ compound at 2 K. Magnetic moments that belong to the propagation vector $\vec{k} = (000)$ are parallel to the hexagonal c-axis in this concentration and form collinear ferromagnetic structure (see diffraction record in Figure 4.41). This ordering of magnetic moments corresponds to the Γ_3 structure in Figure 4.39. The value of magnetic moment is equal to 8.3 μ_B at 2 K (see Table 4.5).

Components of magnetic moments that propagate with $\vec{k} = (\frac{1}{2}\ 0\ \frac{1}{2})$ lie within the basal plane. The size of these components is about 2 μ_B, but the directions are very difficult to determine because of a small intensity of corresponding reflections. However, we can safely assume that their directions are not oriented parallel to the c-axis. The magnetic moment of one Tb^{3+} free ion is equal to 9 μ_B, thus the sum of components of moments (on one Tb atom) which propagate with $\vec{k} = (000)$ and ($\frac{1}{2}\ 0\ \frac{1}{2}$) should not be greater than this value. The best agreement of the fit (represented in Figure 4.41) with diffraction data with the respect to the allowed symmetry was obtained for the orientation of Tb moments $\Gamma_4$as drawn in Figure 4.40f.

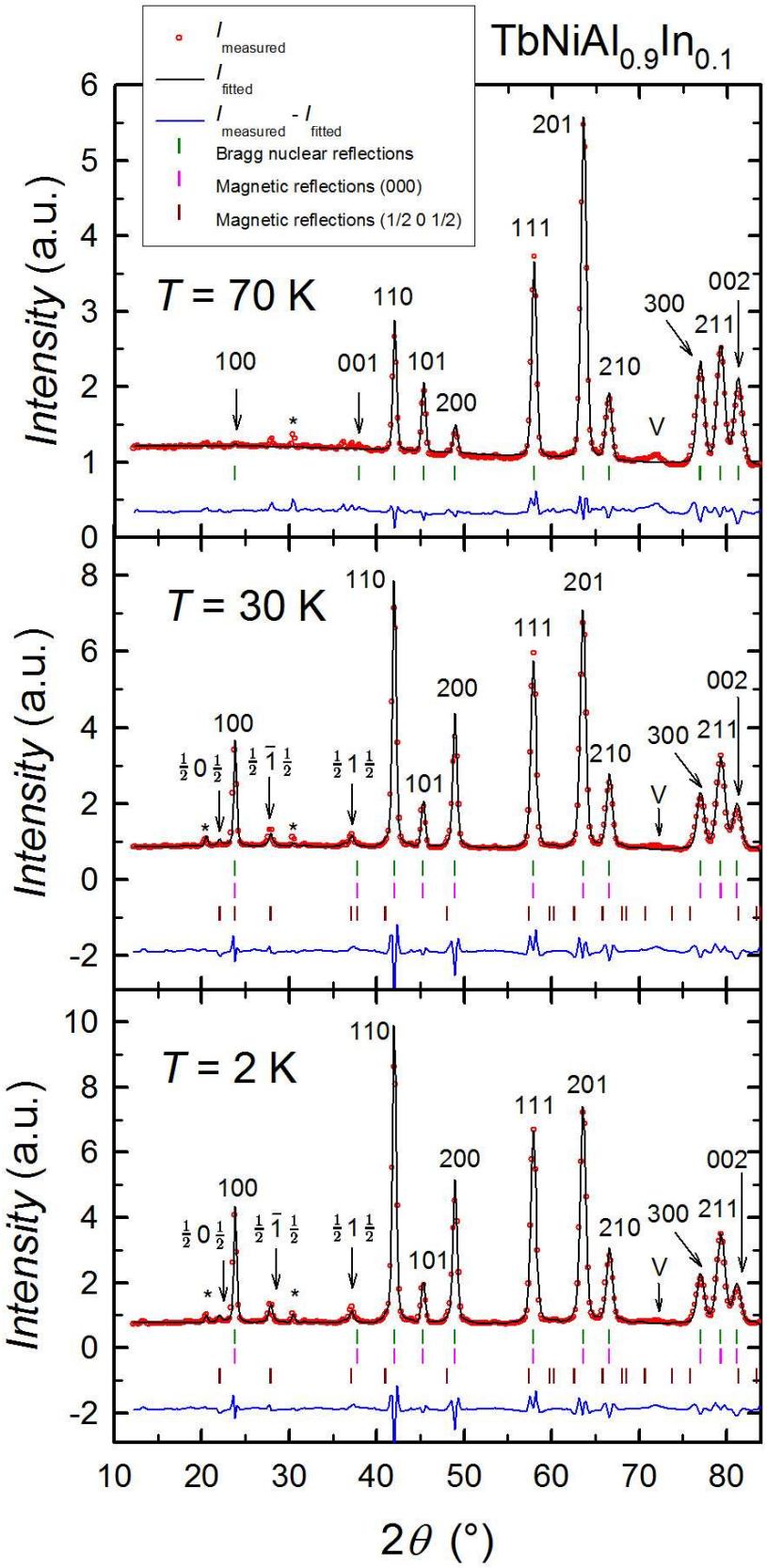

Figure 4.41: Diffraction patterns of $TbNiAl_{0.9}In_{0.1}$ compound at 2, 30 and 70 K. Observed reflections ($h\ k\ l$) belonging to propagation vectors of (000) and ($\frac{1}{2}\ 0\ \frac{1}{2}$) are described in Figure. Other weak magnetic peaks are marked by symbol '$*$'.

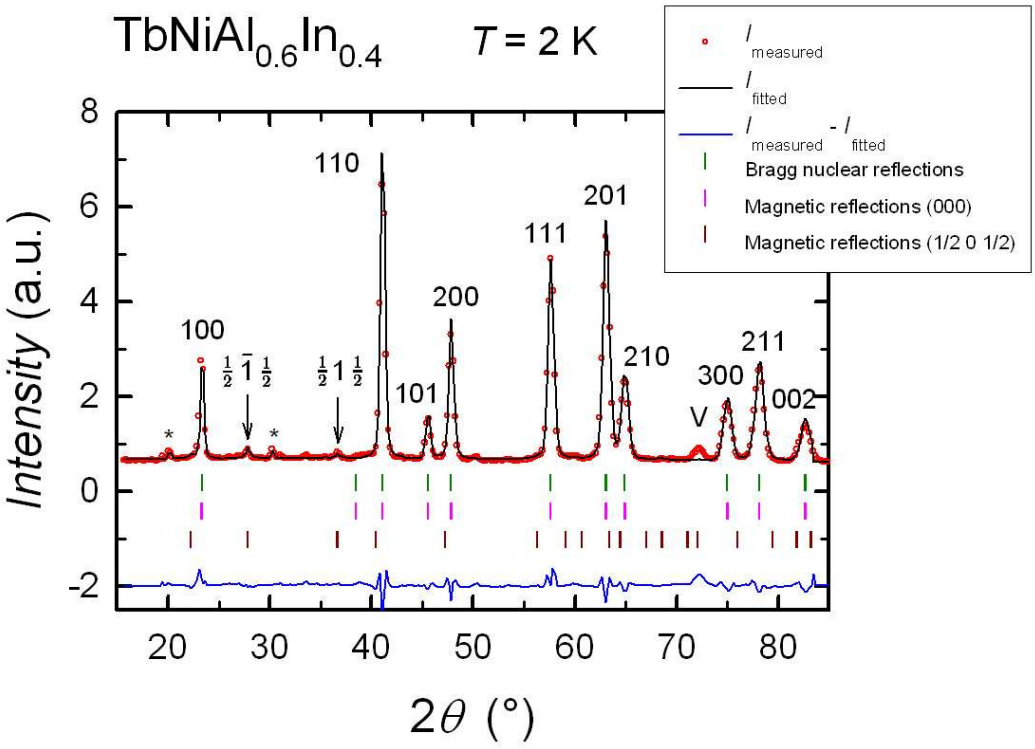

Figure 4.42: Diffraction patterns of $TbNiAl_{0.6}In_{0.4}$ compound at 2 K. Observed reflections ($h\ k\ l$) belong to propagation vectors of (000) and ($\frac{1}{2}\ 0\ \frac{1}{2}$) are described in Figure. Other weak magnetic peaks are marked by symbol '$*$'.

Other In poor concentrations behave similarly, Tb moments belonging to the (000) propagation order ferromagnetically along the c-axis. When we try refining also the direction of moments, we get slight deviation from the direction parallel to the c-axis (approximately 4, 6.5 and 7 degrees for concentration with x = 0.2, 0.3 and 0.4). The magnetic factor R_{M} is improved by $\sim 0.3\%$, but the value of magnetic moment is almost maintained for this involvement of the deviation from the c-axis. This deviation is in conflict with the allowed symmetry. Because of that and because the improvement of the fit is very small, we incline to magnetic structure with moments parallel to the c-axis for these In poor compounds.

Table 4.5: Parameters of magnetic structures of $TbNiAl_{1-x}In_x$ compounds determined from powder neutron diffraction at selected temperatures in individual magnetic phases as indicated by bulk measurements (see Table 4.3). μ is magnetic moment of the phase belonging to propagation vector $\vec{k}$. R_{M} is agreement factor for the fit of magnetic phase. Letters A - H mark the magnetic structures drawn in Figure 4.43. The symbol '?' means that magnetic peaks are too weak to determine the magnetic structure unambiguously.

x	T(K)	$\vec{k}$	*Structure type*	μ (μ_{B})	R_{M} (%)
0.1	2	(0 0 0)	$\vec{\mu} \parallel \vec{c}$, A	8.3(1)	3.4
		($\frac{1}{2}$ 0 $\frac{1}{2}$)	$\vec{\mu} \perp \vec{c}$, B?	2.0(2)	23.4
	30	(0 0 0)	$\vec{\mu} \parallel \vec{c}$, A	7.1(1)	2.8
		($\frac{1}{2}$ 0 $\frac{1}{2}$)	$\vec{\mu} \perp \vec{c}$, B?	1.1(3)	35.2

Continued on next page

Continuation of Table 4.5

x	T(K)	$\vec{k}$	*Structure type*	μ (μ_B)	R_M (%)
0.2	2	(0 0 0)	$\vec{\mu} \parallel \vec{c}$, A	7.8(1)	3.5
		$(\frac{1}{2}\ 0\ \frac{1}{2})$	$\vec{\mu} \perp \vec{c}$, B?	2.7(2)	19.4
	35	(0 0 0)	$\vec{\mu} \parallel \vec{c}$, A	5.7(1)	3.2
		$(\frac{1}{2}\ 0\ \frac{1}{2})$	$\vec{\mu} \perp \vec{c}$, B?	1.0(3)	48.3
0.3	2	(0 0 0)	$\vec{\mu} \parallel \vec{c}$, A	8.3(1)	3.3
		$(\frac{1}{2}\ 0\ \frac{1}{2})$	$\vec{\mu} \perp \vec{c}$, B?	2.4(2)	23.4
	30	(0 0 0)	$\vec{\mu} \parallel \vec{c}$, A	6.8(1)	4.4
		$(\frac{1}{2}\ 0\ \frac{1}{2})$	$\vec{\mu} \perp \vec{c}$, B?	0.9(3)	51.7
0.4	2	(0 0 0)	$\vec{\mu} \parallel \vec{c}$, A	8.4(1)	3.3
		$(\frac{1}{2}\ 0\ \frac{1}{2})$	$\vec{\mu} \perp \vec{c}$, B?	1.8(2)	46.0
	30	(0 0 0)	$\vec{\mu} \parallel \vec{c}$, A	6.0(1)	4.5
		$(\frac{1}{2}\ 0\ \frac{1}{2})$	$\vec{\mu} \perp \vec{c}$, B?	0.7(2)	70.9
0.5	2	(0 0 0)	$\vec{\mu} \perp \vec{c}$, C	8.2(1)	4.9
		$(\frac{1}{2}\ 0\ \frac{1}{2})$	$\vec{\mu} \perp \vec{c}$, D?	3.1(3)	15.1
	30	(0 0 0)	$\vec{\mu} \perp \vec{c}$, C	5.7(1)	7.5
		$(\frac{1}{2}\ 0\ \frac{1}{2})$	$\vec{\mu} \perp \vec{c}$, D?	1.3(3)	59.2
0.6	2	(0 0 0)	$\vec{\mu} \perp \vec{c}$, E	8.1(1)	2.8
		$(\frac{1}{2}\ 0\ \frac{1}{2})$	$\vec{\mu} \perp \vec{c}$, F?	2.4(3)	24.2
	30	(0 0 0)	$\vec{\mu} \perp \vec{c}$, E	6.1(1)	7.3
		$(\frac{1}{2}\ 0\ \frac{1}{2})$	$\vec{\mu} \perp \vec{c}$, F?	1.0(3)	50.8
0.8	2	(0 0 0)	$\vec{\mu} \perp \vec{c}$, G	6.8(1)	3.4
		$(\frac{1}{2}\ 0\ \frac{1}{2})$	$\vec{\mu} \perp \vec{c}$, H	5.1(1)	8.7
	34	(0 0 0)	$\vec{\mu} \perp \vec{c}$, G	5.2(1)	5.6
		$(\frac{1}{2}\ 0\ \frac{1}{2})$	$\vec{\mu} \perp \vec{c}$, H	1.7(2)	57.2
	54	(0 0 0)	$\vec{\mu} \perp \vec{c}$, G?	1.0(2)	14.4
0.9	2	(0 0 0)	$\vec{\mu} \perp \vec{c}$, G	5.8(2)	5.7
		$(\frac{1}{2}\ 0\ \frac{1}{2})$	$\vec{\mu} \perp \vec{c}$, H	6.2(1)	11.4
	35	(0 0 0)	$\vec{\mu} \perp \vec{c}$, G	4.2(1)	4.9
		$(\frac{1}{2}\ 0\ \frac{1}{2})$	$\vec{\mu} \perp \vec{c}$, H	2.1(2)	66.2
	53	(0 0 0)	$\vec{\mu} \perp \vec{c}$, G?	2.0(2)	8.2
1.0	2	(0 0 0)	$\vec{\mu} \perp \vec{c}$, G	8.2(1)	4.9
		$(\frac{1}{2}\ 0\ \frac{1}{2})$	$\vec{\mu} \perp \vec{c}$, H?	2.9(2)	20.0
	34	(0 0 0)	$\vec{\mu} \perp \vec{c}$, G	6.7(1)	2.5
		$(\frac{1}{2}\ 0\ \frac{1}{2})$	$\vec{\mu} \perp \vec{c}$, H?	1.7(2)	44.3
	60	(0 0 0)	$\vec{\mu} \perp \vec{c}$, G?	2.5(2)	11.6

End of Table

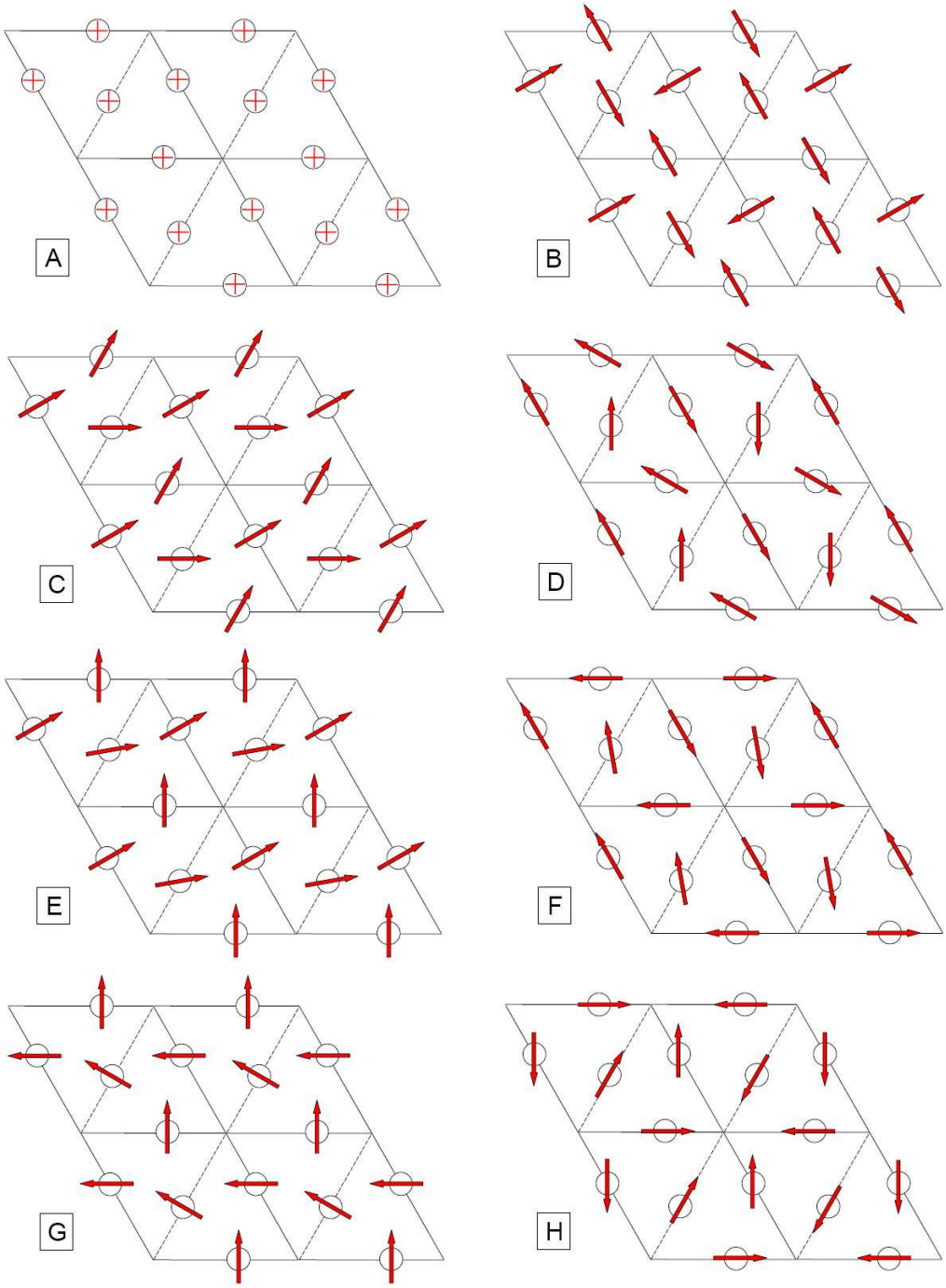

Figure 4.43: Magnetic structures occurring in TbNi(Al,In) series. The arrangement of the moments drawn in the first column belong to propagation vector $\vec{k} = (000)$, in the second column to $\vec{k} = (\frac{1}{2}\ 0\ \frac{1}{2})$. The A - H labels correspond to notation in Table 4.5. The basal plane of the structures is drawn in Figures.

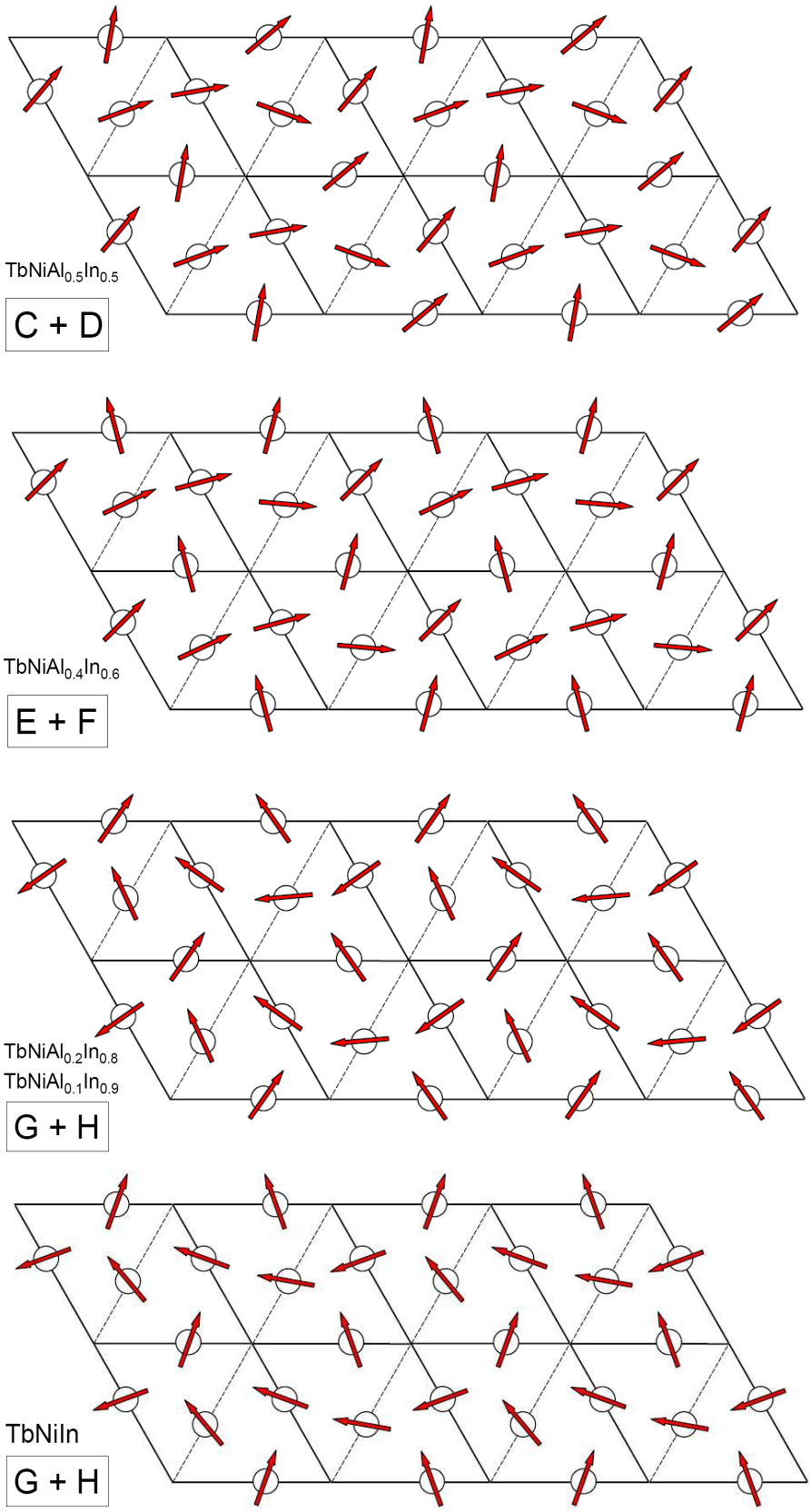

Figure 4.44: Magnetic structures occurring in TbNi(Al,In) series. Each structure was obtained as the sum of structures corresponding to propagation vectors $\vec{k}$ = (000) and ($\frac{1}{2}$ 0 $\frac{1}{2}$) taking into account the actual values of both components of each Tb moment at 2 K. The letters label the summed structures in notation from Table 4.5 and Figure 4.43.

The temperatures of magnetic phase transitions should be reflected by temperature dependencies of intensities of individual reflections ($h\ k\ l$) for given concentration. The temperature dependencies of intensities of selected significant peaks were plotted in Figure 4.45. Vertical dashed lines in Figures represent temperatures of magnetic phase transitions T_1 and T_{ord}, as determined from the AC-susceptibility and the DC-magnetization measurements (see Table 4.3).

We can confirm the magnetic ordering below temperature (T_{ord}) determined from AC-susceptibility and DC-magnetization measurements (see Table 4.3). The increase of the intensity described by (000) propagation below T_{ord} is rather clear. On the other hand, there is no clear change of the intensity around T_1. In the $TbNiAl_{0.8}In_{0.2}$ and $TbNiAl_{0.6}In_{0.4}$ compounds, the intensity of (000) peaks is almost maintained below T_1 and above T_1 quite sharply decreases. However, the direction of magnetic moments described by $\vec{k} = (000)$ does not change in the whole temperature region between 2 K and T_{ord}.

In the $TbNiAl_{0.7}In_{0.3}$ compound, this 'saturation' of the intensity occurs rather at $\approx$ 30 K than at $T_1 = 15$ K.

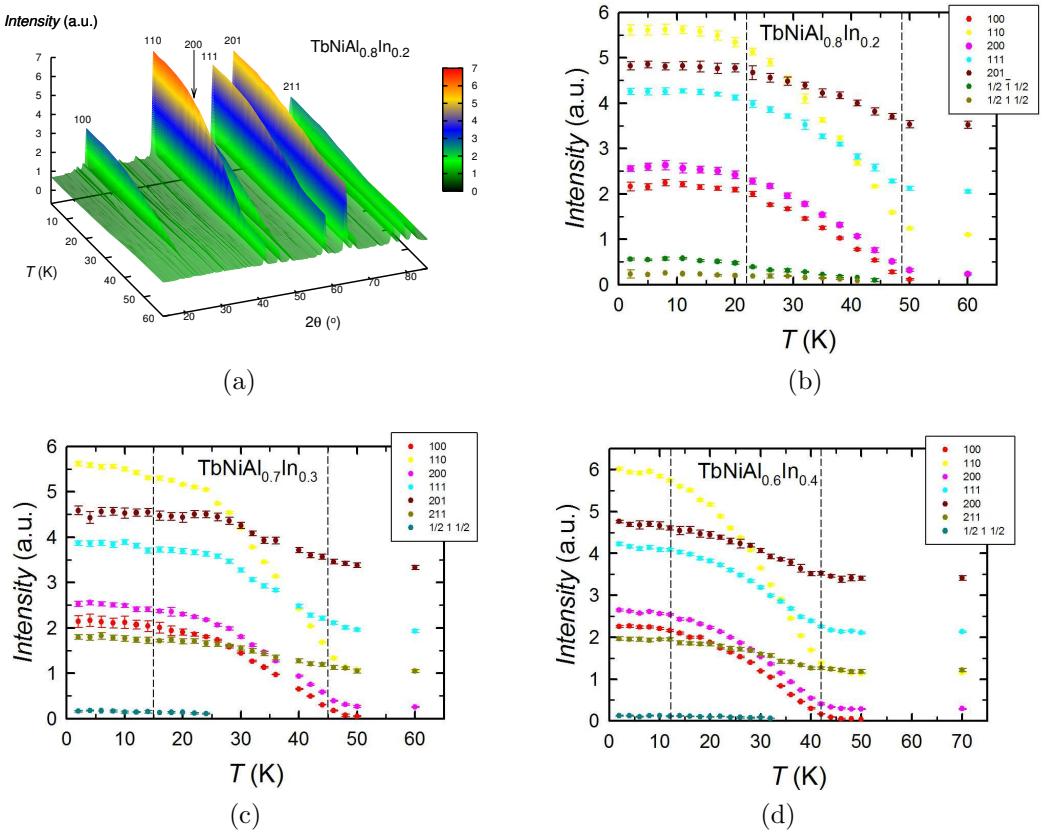

Figure 4.45: (a) The 3D plot of temperature and angular dependence of the intensity of (a) $TbNiAl_{0.8}In_{0.2}$ compound and the temperature dependencies of the intensity of significant ($h\ k\ l$) reflections of (b) $TbNiAl_{0.8}In_{0.2}$, (c) $TbNiAl_{0.7}In_{0.3}$ and (d) $TbNiAl_{0.6}In_{0.4}$ compounds. Vertical lines represent temperatures of magnetic phase transitions as determined from the AC-susceptibility and the DC-magnetization.

Most probably, certain changes occur for the components described by $(\frac{1}{2}\ 0\ \frac{1}{2})$ propagation at T_1. One can see that the ratio of the intensities of $(\frac{1}{2}\ \bar{1}\ \frac{1}{2})$

and $(\frac{1}{2}\ 1\ \frac{1}{2})$ changes below T_1 in $TbNiAl_{0.8}In_{0.2}$ compound. This observation can be associated with the change of the direction of magnetic moments at this temperature. However, the reflections corresponding to this propagation vector have too small intensities to refine the change of the direction of Tb moments at T_1. It is also possible that this change of intensities is caused by the presence of another magnetic phase. The nature of magnetic phase transitions will be discussed in Section 4.7.

The temperature dependence of the magnetic moment value refined for the $TbNiAl_{0.8}In_{0.2}$ compound is plotted in Figure 4.46a. We do not show the development of the magnetic moment of components propagating with $\vec{k} = (\frac{1}{2}\ 0\ \frac{1}{2})$, because its value is very small and has a very high error. The value of magnetic moment belonging to (000) propagation vector is almost unchanged up T_1 (see Table 4.3). For higher temperatures the moment decreases very fast and is equal to zero above ordering temperature T_{ord}. The total magnetic moment on one Tb atom determined as the vector sum of two perpendicular components with $\vec{k} = (000)$ and $(\frac{1}{2}\ 0\ \frac{1}{2})$ takes a value of 8.5 μ_{B} and its direction deviates from the c-axis by $\sim 13°$ at 2 K. The magnetic structure can be thus considered as slightly canted ferromagnetic. The behavior of the value of magnetic moment is very similar for all compounds with x $\leq$ 0.4.

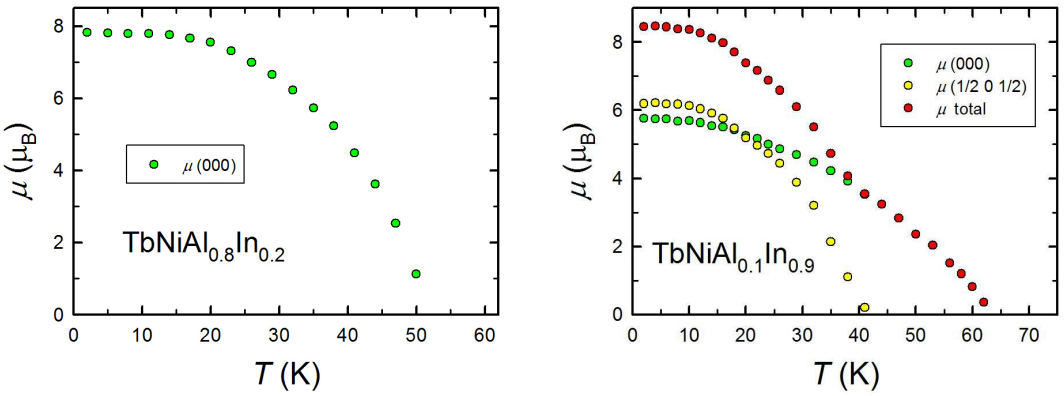

(a) (b)

Figure 4.46: The temperature dependencies of the value of the magnetic moment of (a) $TbNiAl_{0.8}In_{0.2}$ and (b) $TbNiAl_{0.1}In_{0.9}$ compounds obtained from the powder neutron diffraction. The error of the determined value of magnetic moments is between 0.1 and 0.2 μ_{B}.

Magnetic structure of $TbNiAl_{1-x}In_x$ with x $\geq$ 0.5

The significant change of the diffraction patterns compared with low In concentrations occurs in $TbNiAl_{0.5}In_{0.5}$ compound (see Figure 4.38). We can observe the sudden increase of the (001) magnetic reflection in diffraction data (see Figure 4.47). The presence of this reflection means that Tb magnetic moments are not oriented along the hexagonal c-axis. Moreover, the change in the intensity of some reflections occurs. The reflections of (100) and (101) have considerably higher intensity compared to concentration range with x $\leq$ 0.4, whereas peaks (110), (200) and (210) are much weaker. From this behavior of the intensity we can assume that the magnetocrystalline anisotropy between the concentra-

tions with In content of 40 and 50% changes from the uniaxial type of In poor concentrations to planar ordering of magnetic moments as in TbNiIn [37].

The intensity of reflections belonging to $\vec{k} = (\frac{1}{2}\ 0\ \frac{1}{2})$ retained very small also for this concentration. Nevertheless, the reflection of $(\frac{1}{2}\ 0\ \frac{1}{2})$ appears on almost the same angle as the stronger (100) reflection and we can see only one peak corresponding to both reflections. Considerable overlap occurs also for many other peaks belonging to $\vec{k} = (000)$ and $(\frac{1}{2}\ 0\ \frac{1}{2})$ propagation (see Figure 4.47).

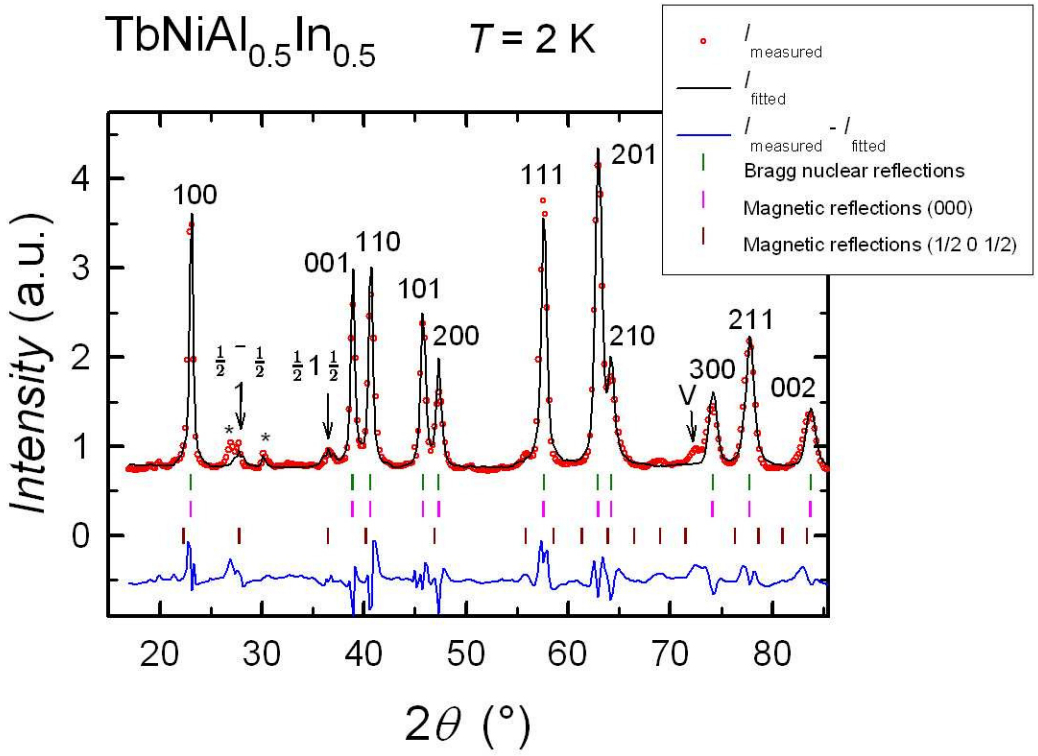

Figure 4.47: The refined diffraction patterns of $TbNiAl_{0.5}In_{0.5}$ compound at 2 K. Observed reflections ($h\ k\ l$) belonging to propagation vectors of (000) and $(\frac{1}{2}\ 0\ \frac{1}{2})$ are described in Figure. Other weak peaks are marked by symbol '$*$', see text for details.

The peak marked by the symbol of '$*$' appears on angle $\sim 27°$ in diffraction data of $TbNiAl_{0.5}In_{0.5}$ compound (see Figure 4.47). This reflection is certainly magnetic because its intensity decreases with the increasing temperature and the peak disappears around 28 K. However, this reflection can not be described by $(0\ 0\ \frac{1}{2})$ or $(\frac{1}{2}\ 0\ 0)$ propagation vectors in contrast with the rest of unfamiliar magnetic peaks occurring in neutron diffraction patterns of the whole series. We ascribe it to magnetic order in the impurity phase.

We found correlation factor (f_{cor}) nearly equal to 1 during the refinement, the preferential orientation does not occur in this sample.

We determined during the refinement that the magnetic moments propagating with $\vec{k} = (000)$ in $TbNiAl_{0.5}In_{0.5}$ compound lie within the basal plane and they order in agreement with the allowed structure Γ_6 obtained from representation analysis, see Figures 4.39i or 4.43C. The arrangement of components of magnetic moments with propagation vector $\vec{k} = (\frac{1}{2}\ 0\ \frac{1}{2})$ is very difficult to find because of the small intensity of corresponding reflections (same as in low In concentrations).

The best agreement of the fit with measured data was obtained for the magnetic structure remotely similar to the Γ_2 arrangement determined from the group theory (see Figure 4.40d). Our structure is drawn in Figure 4.43D. It is possible to find another arrangement of these components of magnetic moments (propagating with $\vec{k} = (\frac{1}{2}\ 0\ \frac{1}{2})$) which will have the same or better agreement with the measured data, but we are strictly limited by total magnetic moment on one Tb atom (9 μ_B for Tb^{3+} free ion). The arrangement of total moments (the vector sum of components with $\vec{k} = (000)$ and $(\frac{1}{2}\ 0\ \frac{1}{2})$) on Tb atoms is presented in Figure 4.44C+D. The components propagating with $\vec{k} = (\frac{1}{2}\ 0\ \frac{1}{2})$ disappears in lower temperature than the component with $\vec{k} = (000)$ and because of that the magnetic structure in the compound slightly below T_{ord} looks like in Figure 4.43C.

The comparison of the intensities of reflections belonging to $\vec{k} = (\frac{1}{2}\ 0\ \frac{1}{2})$ at 2 and 30 K does not indicate the significant change of the magnetic structure. The origin of the anomalies around T_1 obtained from AC-susceptibility and DC-magnetization measurements is not clear. The microscopic studies does not show any pronounced difference between intensity ratios below and above T_1 for significant reflections (see Figure 4.48). It is possible that some magnetic impurities in the sample cause this anomaly at T_1. This phenomenon will be discuss in Section 4.7.

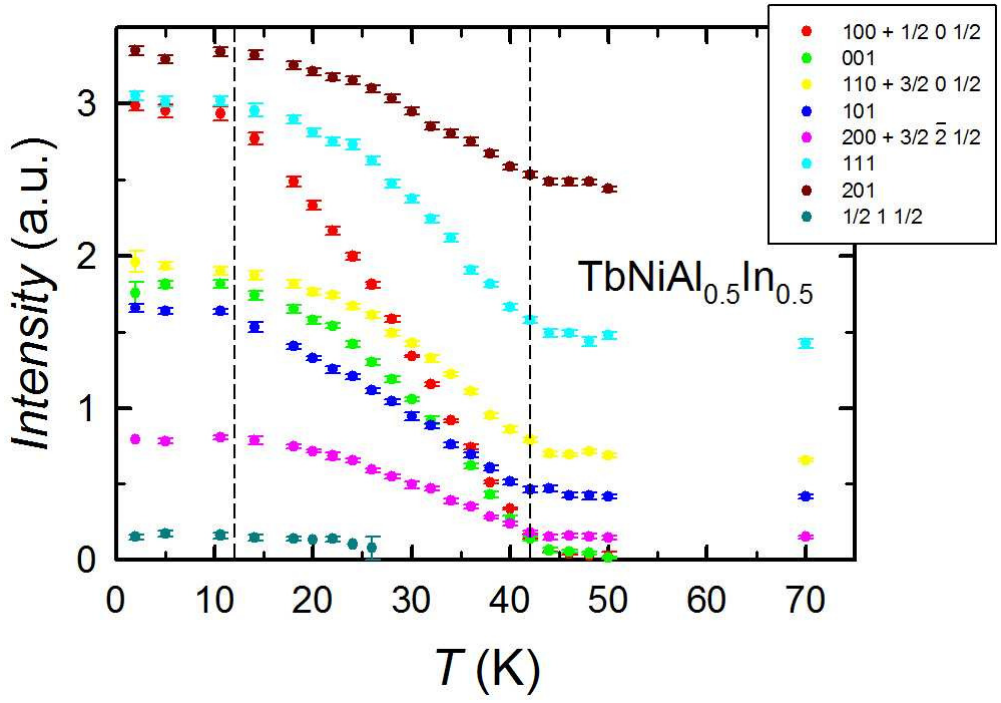

Figure 4.48: The temperature dependencies of the intensity of individual peaks (h k l) of $TbNiAl_{0.5}In_{0.5}$ compound. Vertical lines represent temperatures of magnetic phase transitions determined from the AC-susceptibility and the DC-magnetization measurement.

The diffraction patterns of $TbNiAl_{0.5}In_{0.5}$ and $TbNiAl_{0.4}In_{0.6}$ compounds are very similar. However, one can observe some differences in the intensity of some reflections, especially (100) and (101) peaks have significantly higher intensity in concentration with In content of 60% (compare Figures 4.47 and 4.49). This different intensity reflects different ordering of magnetic moments in the compound

with 60% of In. Tb moments are still oriented within the basal plane, but they form a magnetic structure which is in conflict with the allowed symmetry. This magnetic structure (see Figure 4.43E) is very similar to the 'allowed' structure of $TbNiAl_{0.5}In_{0.5}$ compound with label Γ_6, as can be seen in Figure 4.39i. We incline to this ordering of magnetic moments even though that this magnetic structure is not allowed by the symmetry, in contrast with low In concentrations where we adhered to allowed ordering of Tb moments. The main reason is the great improvement of the fit of diffraction data. The magnetic refinement factor R_M is improved by $\sim 10\%$ in comparison with the 'allowed' structures that give the best agreement with observed data (see Figures 4.39e and 4.39i). We can assume that the arrangement of the magnetic moments of this concentration is some transition between structures of $TbNiAl_{0.5}In_{0.5}$ compound and concentrations with In content $\geq 80\%$.

The magnetic structure corresponding to $\vec{k} = (\frac{1}{2}\ 0\ \frac{1}{2})$ is very similar to arrangement in $TbNiAl_{0.5}In_{0.5}$ compound, but we can observe some deviation of the direction of magnetic moments on positions Tb_1 and Tb_3 (see Figure 2.1). The intensities of corresponding reflections are still too small for precise determination, but the best agreement of the fit was obtained for structure drawn in Figure 4.43F. The arrangement of total magnetic moments is shown in Figure 4.44E+F.

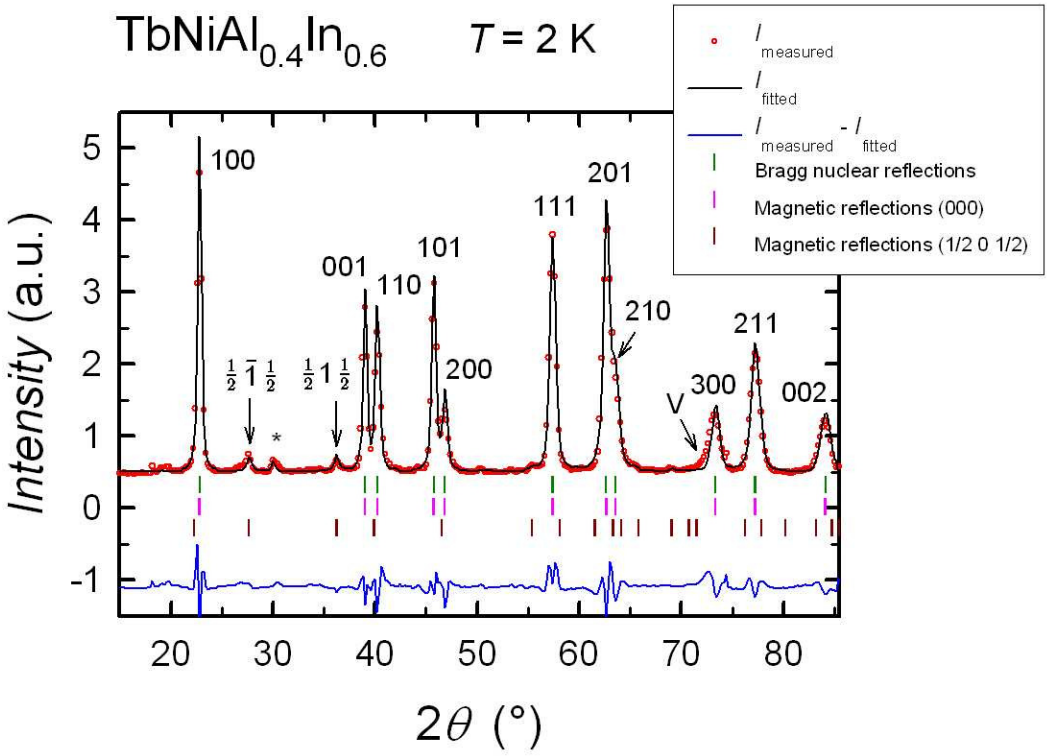

Figure 4.49: The refined diffraction patterns of $TbNiAl_{0.4}In_{0.6}$ compound at 2 K. Observed reflections ($h\ k\ l$) belonging to propagation vectors of (000) and ($\frac{1}{2}\ 0\ \frac{1}{2}$) are described in Figure. Other weak magnetic peak marked by symbol '$*$' can be indexed by ($\frac{1}{2}\ 0\ 0$) propagation.

Another significant change of diffraction patterns can be observed for concentrations with x = 0.8 and 0.9, see Figure 4.50. The intensity of reflections belonging to propagation vector $\vec{k} = (\frac{1}{2}\ 0\ \frac{1}{2})$, small for x $\leq$ 0.6 concentrations,

extremely increases in these two compounds. The increase in the intensity is well-seen especially for $(\frac{1}{2}\ \bar{1}\ \frac{1}{2})$ and $(\frac{1}{2}\ 1\ \frac{1}{2})$ reflections (compare Figures 4.49 and 4.50). Moreover, another peaks corresponding to $(\frac{1}{2}\ 0\ \frac{1}{2})$ propagation are well visible on diffraction patterns, for example $(\frac{5}{2}\ \bar{1}\ \frac{1}{2})$, $(\frac{1}{2}\ \bar{1}\ \frac{3}{2})$ and $(\frac{3}{2}\ \bar{1}\ \frac{3}{2})$. Other magnetic reflections belonging to $\vec{k} = (\frac{1}{2}\ 0\ \frac{1}{2})$ develop on almost same angles as reflections of (000) propagation, so we can find only one common peak for these reflections. Both magnetic reflections are strong, in contrast with concentrations with lower In content, what greatly complicates the refinement of diffraction patterns of these compounds. The reflections of (001) and (200) appear on almost same angles as reflections (110) and (101), respectively, in concentrations with x $\geq$ 0.8 (see Figure 4.50). We observe just one common asymmetric peak instead of two peaks as in previous concentrations. This phenomenon makes the refinement of diffraction patterns more difficult.

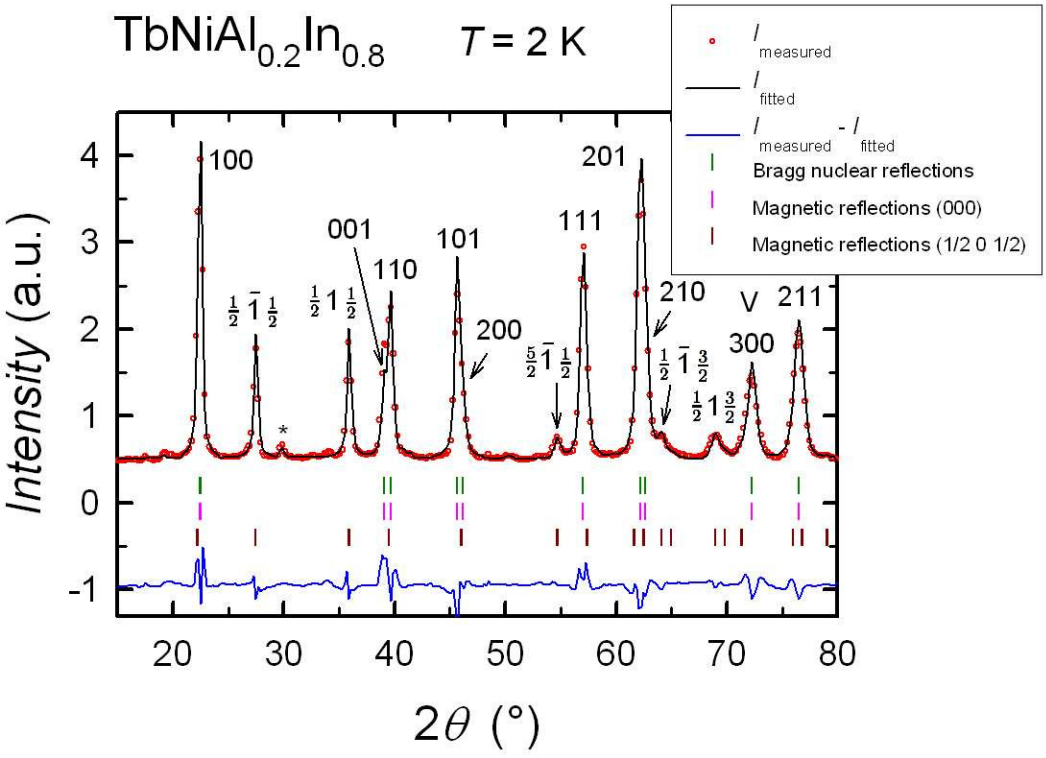

Figure 4.50: The refined diffraction patterns of $TbNiAl_{0.2}In_{0.8}$ compound at 2 K. Observed reflections $(h\ k\ l)$ belonging to propagation vectors of (000) and $(\frac{1}{2}\ 0\ \frac{1}{2})$ are described in Figure. Other weak peak marked by symbol '$*$' can be indexed by propagation vector of $(\frac{1}{2}\ 0\ 0)$.

The refinement of 2 K data leads to the identical magnetic structures in both $TbNiAl_{0.2}In_{0.8}$ and $TbNiAl_{0.1}In_{0.9}$ compounds, only the value of magnetic moment of phase with $\vec{k} = (\frac{1}{2}\ 0\ \frac{1}{2})$ is higher for second concentration (see Table 4.5). The arrangement of Tb moments is in disagreement with the 'allowed' symmetry also in these concentrations. One can observe the similarity of the occurring structure for $\vec{k} = (000)$ (see Figure 4.43G) with the arrangement Γ_4 in Figure 4.39 determined employing the group theory, but the directions of moments on atoms with positions Tb_2 and Tb_3 differ.

It is possible to determine the arrangement of the components of magnetic

moments with propagation ($\frac{1}{2}$ 0 $\frac{1}{2}$) much more precisely in these two concentrations than in the rest of the series due to the strong corresponding reflections. The best agreement of the fit with the measured data was obtained for magnetic structure drawn in Figure 4.43H. This arrangement of the magnetic moments is quite similar to the Γ_4 structure determined from the representation analysis (see Figure 4.40e), but the direction of the moment on the atom with the position Tb_2 is significantly different. Again, we note that both components described by (000) and ($\frac{1}{2}$ 0 $\frac{1}{2}$) propagation, respectively, are perpendicular to each other. Such arrangement keeps the total moment below the maximum Tb^{3+} free ion value of 9 μ_B. We could find also somewhat different magnetic structures for both components, but the total moment would than considerably exceed 9 μ_B.

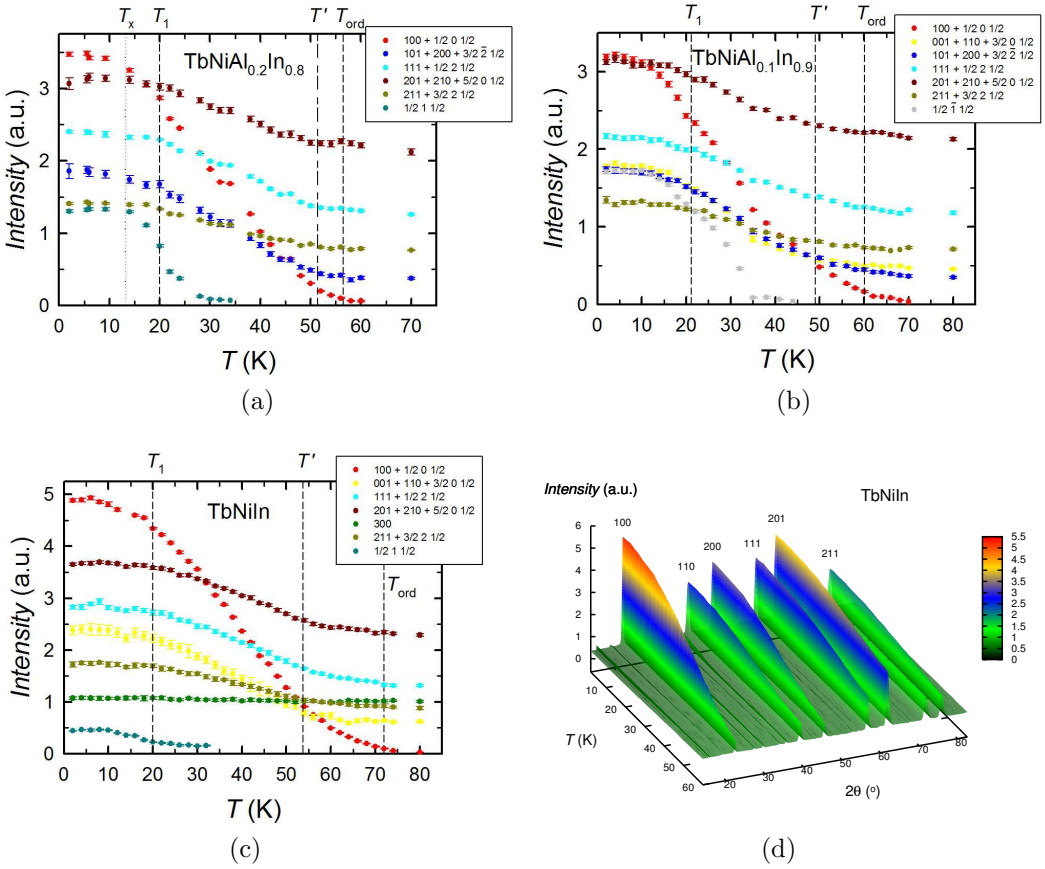

Figure 4.51: The temperature dependencies of the intensity of significant (h k l) reflections of (a) $TbNiAl_{0.2}In_{0.8}$, (b) $TbNiAl_{0.1}In_{0.9}$ and (c) TbNiIn compounds. Vertical lines represent temperatures of magnetic phase transitions determined from the AC-susceptibility and the DC-magnetization. (d) The 3D plot of temperature and angular dependence of the intensity of TbNiIn compound.

The temperature dependencies of the intensity of several representative peaks of these two concentrations are placed in Figures 4.51a and 4.51b. One can observe the significant decrease in the intensity around T_1, especially for the reflections corresponding to $\vec{k} = (\frac{1}{2}\ 0\ \frac{1}{2})$ in $TbNiAl_{0.2}In_{0.8}$. These magnetic reflections completely disappear between T_1 and T'. In $TbNiAl_{0.1}In_{0.9}$, the decrease and disappearance of ($\frac{1}{2}$ 0 $\frac{1}{2}$) reflections are shifted to temperature that is something

above T_1 (as obtained from AC-susceptibility measurement, see Table 4.3). We do not observe any pronounced change in the intensity around T_{ord} (see Table 4.3), only the intensity of (100) reflection starts to increase considerably below T_{ord}. This behavior of the intensity we will discuss in Section 4.7.

The magnetic structure between T' and T_{ord} is described by (000) propagation only. The exact arrangement of Tb moments at these temperatures can not be determined because the magnetic intensities are very small.

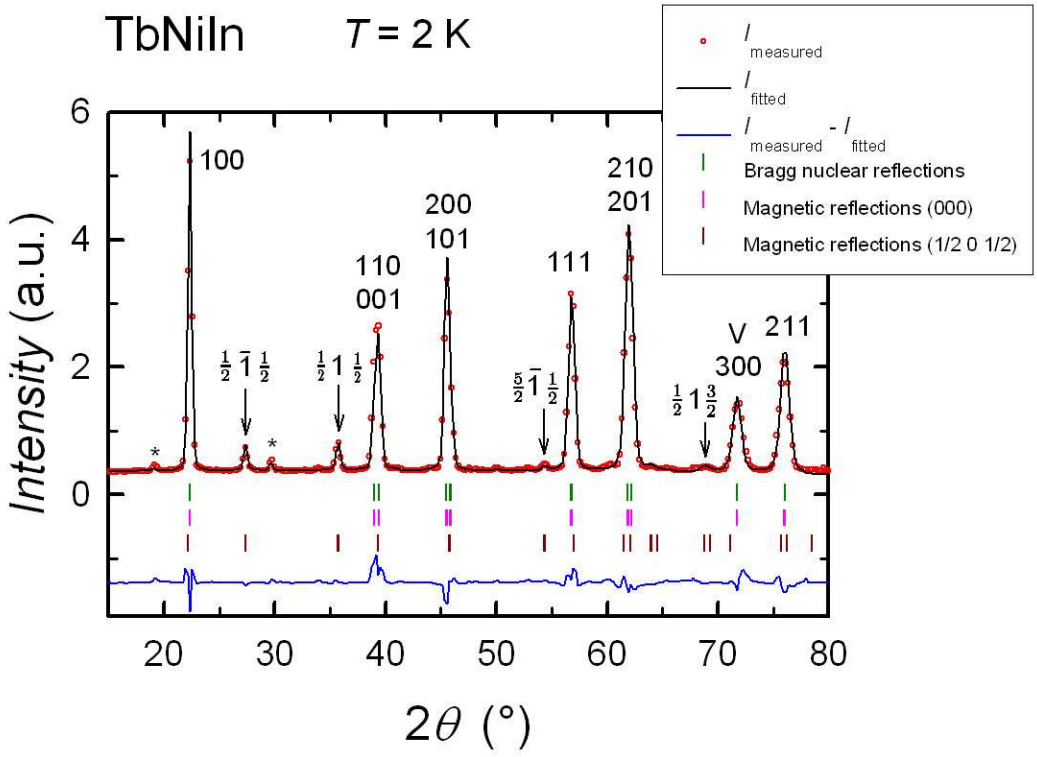

Figure 4.52: The refined diffraction patterns of TbNiIn compound at 2 K. Observed reflections ($h\ k\ l$) belonging to propagation vectors of (000) and ($\frac{1}{2}\ 0\ \frac{1}{2}$) are described in Figure. Other weak peaks are marked by '$*$'.

The magnetic structure in TbNiIn is generally the same as for concentrations with x = 0.8 and 0.9. The only difference represents the ratio between the size of both magnetic components. The intensity of reflections belonging to $\vec{k} = (\frac{1}{2}\ 0\ \frac{1}{2})$ is much smaller for this compound, indicating much smaller component propagating with ($\frac{1}{2}\ 0\ \frac{1}{2}$) (compare Figures 4.50 and 4.52). The preferential orientation does not occur in TbNiIn sample (same as in the concentration with In content of 50%).

As concern the part of the magnetic structure described by (000) propagation, it is very similar to the magnetic structure in TbNiIn shown by Ehlers in Reference [38] (see Figure 2.9b). Only difference between these two arrangements is in the orientation of magnetic moment on the atom with the position Tb_2, the direction differs by 30° (compare Figures 4.43G and 2.9b). This difference may be sample dependent. However, both structures are in conflict with the 'allowed' symmetry Γ_4 (see Figure 4.39e) as obtained from representation analysis, the reason is the opposite direction of magnetic moment on position Tb_3.

The arrangement of the total magnetic moments is drawn in Figure 4.44G+H. The directions of total magnetic moments little differ (approximately by about 20 degrees) when comparing $TbNiAl_{0.2}In_{0.8}$ or $TbNiAl_{0.1}In_{0.9}$ and pure TbNiIn, although the magnetic structures corresponding to the propagations (000) and $(\frac{1}{2}\ 0\ \frac{1}{2})$ are the same for all three concentrations. The value of magnetic moment of the components propagating with $\vec{k} = (\frac{1}{2}\ 0\ \frac{1}{2})$ is much lower for TbNiIn compared to other two concentrations and for that reason the magnetic structure of the total moment so differs for these concentrations. The magnetic structure between T' and T_{ord} is not affected by the presence of the components of magnetic moments with propagation vector $\vec{k} = (\frac{1}{2}\ 0\ \frac{1}{2})$ and might look like in Figure 4.43G, but the magnetic intensities are too small to determine the magnetic structure unambiguously.

The temperature dependencies of the intensity of significant peaks in TbNiIn compound are plotted in Figure 4.51c and the temperature and angular dependence of the intensity (3D plot) is showed in Figure 4.51d. The slight decrease of the intensity is seen around T_1, but we do not observe any pronounced change of magnetic structure. The magnetic reflections belonging to $(\frac{1}{2}\ 0\ \frac{1}{2})$ propagation strongly decrease around T_1 and completely disappear in temperature region between T_1 and T'.

4.7 General discussion

In the first instance we have to comment the phase analysis of TbNi(Al,In) series. Two phases appear in the $TbNiAl_{0.5}In_{0.5}$ sample by EDX measurement. The atomic concentrations of elements in the majority phase should be $\frac{1}{3}$ of total concentration for each element (Tb, Ni and Al(In)), but the used program miscalculated Tb and Ni contributions (see Table 4.2). The sum of these two concentrations gives the correct value, i.e. $\frac{2}{3}$ of total atomic concentration. So, we can assume that the program includes a part of Ni-contribution into Tb-contribution because of the closeness of Tb and Ni peaks in the spectra. This explanation seems to be acceptable with respect to the preparation of the samples. The atomic concentrations of Tb and Ni were identical by weighting and the evaporation of these elements (arc-melting) is almost the same. On the other hand, the EDX measurement on the TbNiAl single crystal shows, from this point of view somewhat surprisingly, the correct representation of all three elements, i.e. $\frac{1}{3}$ of the atomic concentration for each of them. The content of the minority phase in the sample volume was approximately 5%. This impurity phase is reflected in the diffraction patterns as unfamiliar peaks, especially in neutron diffraction data we can easily observe the presence of the minority phase. The hexagonal structure of majority phase was confirmed by X-ray and neutron diffraction, the data analysis in the paramagnetic state confirms the correct stoichiometry.

We were able verify the existence of the 'forbidden c/a' region ([12]) in pure TbNiAl compound (see Figure 4.33a). Moreover, the resistivity measurement in the hydrostatic pressure on TbNiAl compound showed a shift of this structural transition to lower temperatures with increasing pressure. The structural phase transition does not appear in pressures ≥ 0.55 GPa (see Figure 4.35). This disappearance of the structural transition is probably caused by an approach of the layers (lattice parameter c decreases) in ZrNiAl-type of structure. The pressure has similar effect as the substitution of Al by larger In on the interatomic distances along the hexagonal c-axis in the structure. The 10% In substitution causes such a change of lattice parameters that shifts the c/a ratio far from the 'forbidden' region. We do not observe any discontinuity in the c/a ratio in the substituted compounds.

The refinement of neutron diffraction data revealed the magnetic structures with two propagtion vectors in the $TbNiAl_{1-x}In_x$ compounds. The components of magnetic moments with propagation vector $\vec{k} = (000)$ are oriented parallel to the hexagonal c-axis in $TbNiAl_{0.9}In_{0.1}$ compound. The magnetic structure of this concentration corresponds to the results of the representation analysis (group Γ_3), see Figure 4.39b. Low In content compounds ($x \leq 0.4$) behave similarly, but we obtain better agreement of the fit and measured data when we try refining also the direction of magnetic moments. Nevertheless, we inline to the 'allowed' structure determined from the group theory because of the very small improvement of the refinement with the slight deviation from the direction parallel to the c-axis. The arrangement of the components of magnetic moments with $\vec{k} = (000)$ in $TbNiAl_{0.5}In_{0.5}$ compound significantly differs from lower In content concentrations. Tb moments lie in the basal plane and form the magnetic structure marked as Γ_6 (see Figure 4.39i). The magnetic structure of the concentration with 60% of In (see Figure 4.43E) somewhat resembles the same arrangement but the mo-

ments on Tb_1 and Tb_3 positions are slightly turned. We incline to this ordering of magnetic moments even though that this magnetic structure is not allowed by the symmetry, in contrast with low In concentrations where we adhered to allowed ordering of Tb moments. The main reason is the great improvement of the fit of diffraction data compared to the nearest 'allowed' structures. Similarly in the rest of measured concentrations ($x \geq 0.8$), we chose the arrangement of magnetic moments in disagreement with the results of the group theory because of the improvement of the fit. The magnetic structure (components described by (000) propagation) of these three compounds is the same (see Figure 4.43G) and is very similar to the arrangement of TbNiIn shown by Ehlers in Reference [38] (see Figure 2.9b).

The refinement of the phase with propagation vector $\vec{k} = (\frac{1}{2}\ 0\ \frac{1}{2})$ was very difficult because of the very small intensity of corresponding reflections in most of concentrations. In compounds with $x = 0.8$ and 0.9, these reflection are much stronger, but most of them lie on almost same angles as reflections of $\vec{k} = (000)$. One can see only common peaks belonged to these two propagations what very complicates the refinement of diffraction patterns. The refined magnetic structures of $\vec{k} = (\frac{1}{2}\ 0\ \frac{1}{2})$ with the best agreement with the measured data are drawn in Figure 4.43. With the respect to the small intensity of reflections it is possible to find another suitable arrangement of magnetic moments, but we are limited to a maximum value of magnetic moment on one Tb atom (the magnetic moment of Tb^{3+} free ion is equal to 9 μ_B). Moreover, one can expect two perpendicular components of magnetic moment which propagate with different vectors. The sums of two components of magnetic moments with $\vec{k} = (000)$ and $(\frac{1}{2}\ 0\ \frac{1}{2})$ (the total magnetic moments) are drawn in Figure 4.44. Note that the approximately collinear magnetic structure in $TbNiAl_{0.5}In_{0.5}$ behaves more and more non-collinear with increasing In content and for pure TbNiIn we can observe nearly triangle arrangement of Tb moments.

We observe the change of the antiferromagnetic arrangement of Tb moments in TbNiAl to predominantly ferromagnetic order with the substitution of 10% of Al by In. The disruption of antiferromagnetic structure of TbNiAl compound was previously found also in $Tb_{1-x}Y_xNiAl$ ([36]) and $TbNi_{1-x}Cu_xAl$ ([13]) series. The substitution of Tb by few percent of nonmagnetic Y disturbs the balance of magnetic moments in the compound and from the antiferromagnetic ordering becomes the ferromagnetic one. The substitution of Ni by Cu has the same effect, but the change of the magnetic structure is caused by additional *d*-electrons which are brought by copper into the system (*d*-elements are presented in both crystallographic layers in hexagonal ZrNiAl-type of structure). The change of the magnetic structure of TbNiAl compound is induced by isoelectronic substitution of Al by larger In atoms in our case. The substitution causes an expansion of the layer with the *p*-metal and an approach to the second layer consequently. The change of the magnetic structure is thus most probably induced by the change of the structure parameters. It is further corroboration of the fact that the antiferromagnetic structure in TbNiAl is very unstable and can exist only in 'perfect' structure with certain Tb-Tb distances.

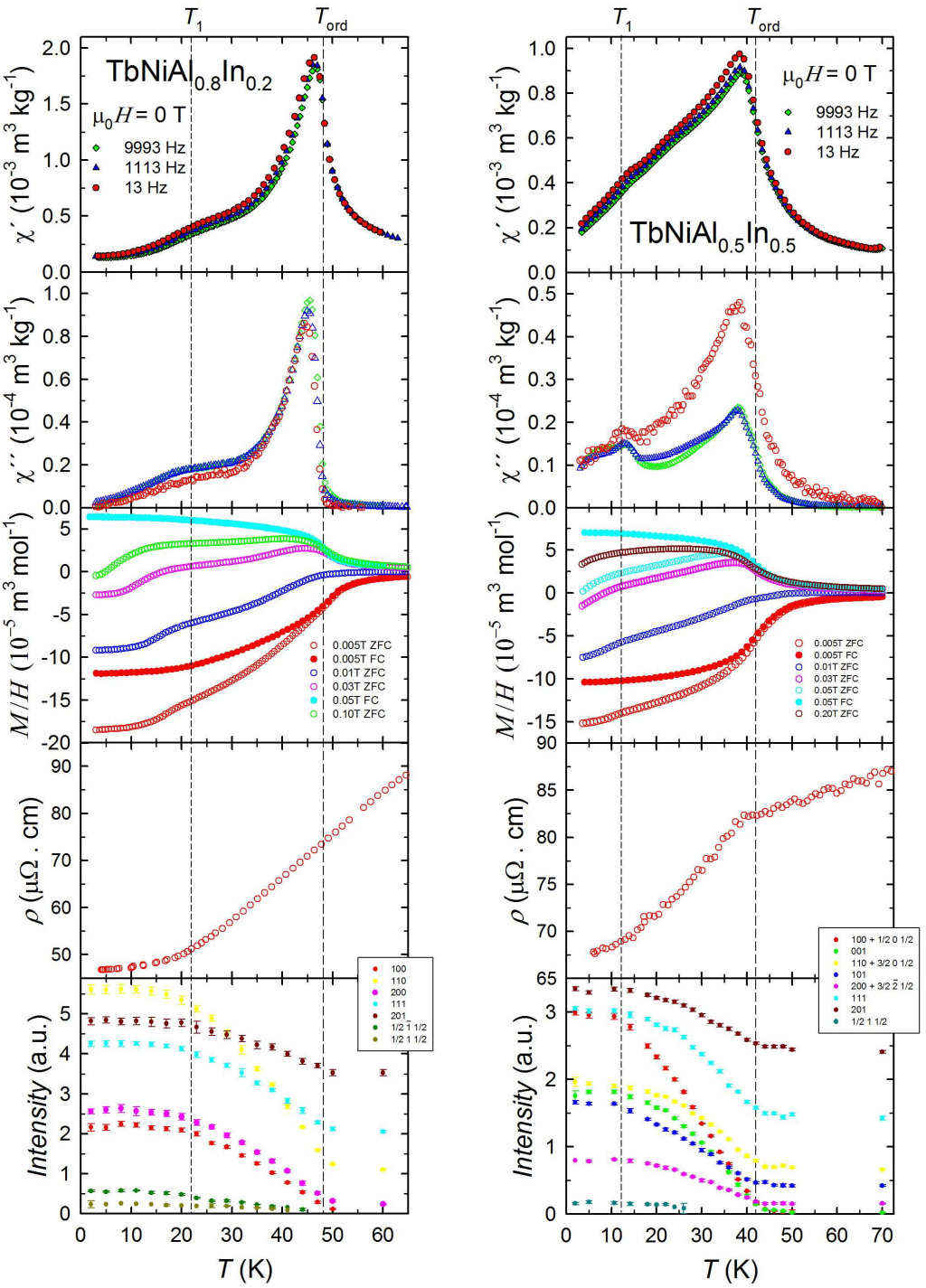

Figure 4.53: Temperature dependencies of AC-susceptibility, DC-magnetization, electrical resistivity and intensity of significant (h k l) reflections obtained by neutron powder diffraction of (a) $TbNiAl_{0.8}In_{0.2}$ and (b) $TbNiAl_{0.5}In_{0.5}$ compounds. Dashed lines represent founded temperatures of magnetic phase transitions from susceptibility measurements.

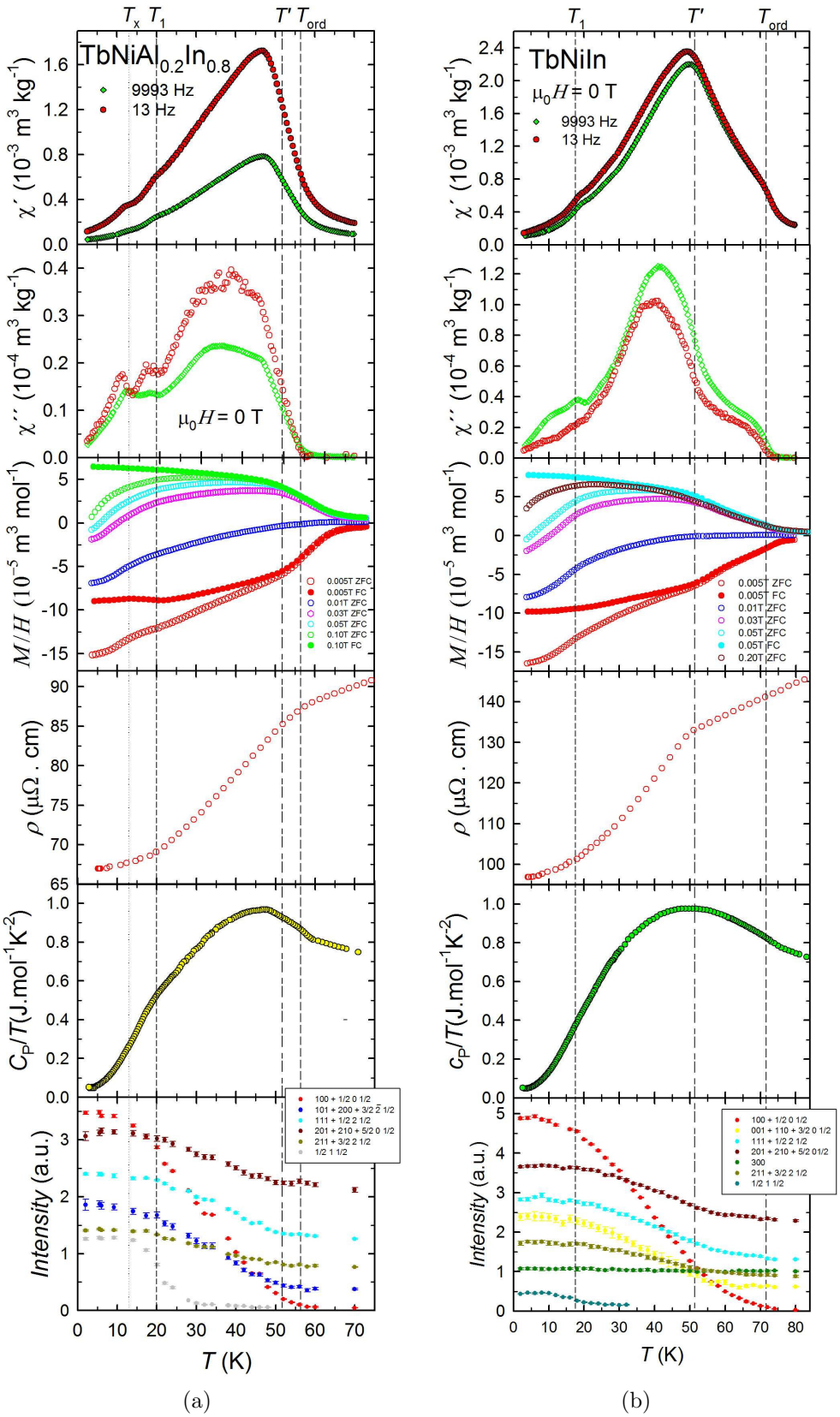

(a) (b)

Figure 4.54: Temperature dependencies of AC-susceptibility, DC-magnetization, electrical resistivity, specific heat and intensity of significant (h k l) reflections obtained by neutron powder diffraction of (a) $TbNiAl_{0.2}In_{0.8}$ and (b) TbNiIn compounds. Dashed lines represent founded temperatures of magnetic phase transitions from susceptibility measurements.

Two or more anomalies corresponding to magnetic phase transitions were observed for all TbNi(Al,In) compounds in AC-susceptibility measurement. Especially, the imaginary part of the susceptibility χ'' shows clear maxima. The temperatures of these anomalies are in very good agreement with temperatures obtained from magnetization measurement, as can be seen in Figures 4.53 and 4.54. The resistivity measurement reveals only one magnetic phase transition for each concentration. The temperature of this anomaly corresponds to T_{ord}, as marked from AC-susceptibility measurement in Table 4.3, for most of concentrations (see Figure 4.53). But for compounds with In content ≥ 0.8, the resistivity kinks belong better to temperature T' instead of T_{ord} (see Figure 4.54). This behavior of the resistivity is very interesting and one can ask what temperature is the real ordering temperature. The specific heat measurement votes rather T_{ord} as real ordering temperature in the In rich compounds. The anomaly around T_1 is less prominent in the c_{p}(T) data (except $TbNiAl_{0.2}In_{0.8}$ compound). The temperature dependencies of the intensity of significant reflections obtained from powder neutron diffraction very well confirm ordering temperature T_{ord} in concentrations x ≤ 0.5 ($TbNiAl_{0.4}In_{0.6}$ was measured only in three temperatures and $TbNiAl_{0.3}In_{0.7}$ was not measured by powder neutron diffraction). The magnetic phase transitions appear rather at T' for In rich compounds, as can be seen in Figure 4.54. However, the magnetic reflection of (100) shows considerable magnetic intensity already between T' and T_{ord}. This phenomenon is probably a consequence of the configuration of Tb moments in basal plane. The anomaly around T_1 observed in AC-susceptibility and magnetization measurements is bound with the change on the intensity curve obtained by neutron diffraction. In the case of the phase with $\vec{k} = (000)$, we can be sure that the magnetic structure is maintained, only the intensity of some reflections starts often sharp decrease. The transition at T_1 is bound with the components with $\vec{k} = (\frac{1}{2}\ 0\ \frac{1}{2})$, as can be seen in $TbNiAl_{0.2}In_{0.8}$ (Figure 4.54a). A certain sign of the change of magnetic structure of components with $\vec{k} = (\frac{1}{2}\ 0\ \frac{1}{2})$ below T_1 can be also observed in $TbNiAl_{0.8}In_{0.2}$ compound. For $TbNiAl_{0.7}In_{0.3}$ and $TbNiAl_{0.1}In_{0.9}$ compounds, this change shifts to higher temperatures than T_1 determined from susceptibility data. The magnetic structures of this phase ($\vec{k} = (\frac{1}{2}\ 0\ \frac{1}{2})$) above T_1 can not be distinguished because of a small intensity of the reflections, but the best agreement of the fit with the measured data is for the identical structure in whole ordered state. The origin of the anomaly in AC-susceptibility measurement at T_{x} is probably bound with the presence of the minority phase in our samples.

Very similar behavior, meaning non-collinear structure with Tb moments lying in the basal plane and several phase transitions, manifests itself in many TbTIn compounds. The antiferromagnetic order with a second magnetic phase transition to complex metamagnetism was reported in TbPtIn [19]. In TbCuIn, both, the short- and long-range magnetic ordering appear below Néel temperature [16, 38]. Similarly in the case of TbAuIn, the change of the magnetic order from an antiferromagnetic one through a spin-glass-like short-range magnetic ordering to a paramagnetic state occurs [17]. For TbPdIn, AC-susceptibility measurement on polycrystalline sample indicates three magnetic phase transitions [52] and powder neutron diffraction two components of magnetic moments with different propagation vectors at 2 K [53]. On the other hand, the neutron diffraction measurement on single crystal shows unambiguously only one magnetic transition

bound with single propagation vector [18]. As the crystal structure in the single crystal is presumably closer to an ideal arrangement than for polycrystalline samples, we can speculate that the very complex behavior might be often consequence of certain structural disorder. This speculation holds also for compounds studied in this series.

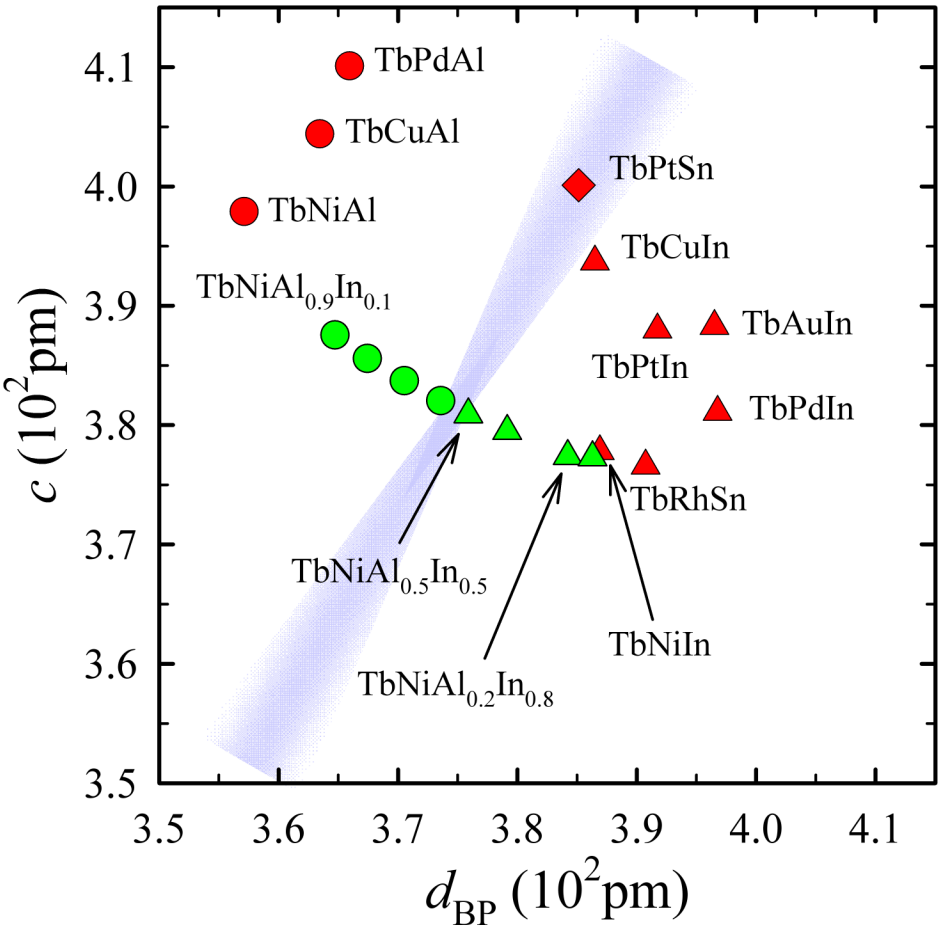

Figure 4.55: Magnetocrystalline anisotropy in TbTX compounds studied until now. d_{BP} is the distance between Tb atoms in the basal plane. The symbol '$\circ$' means Tb moments along the c-axis, the symbol '$\triangle$' Tb moments perpendicular to the c-axis and '$\diamond$' more complex behavior of magnetic moments pointing out of any principal crystallographic direction. The 'green' symbols indicate data measured by neutron diffraction at 2 K in this work with the correct type of magnetocrystalline anisotropy. The gray area indicates assumed flipping magnetic moments from the direction parallel to c-axis to basal plane. The compounds occurring in the Figure were previously studied by X-ray and neutron diffraction: TbPdAl [12], TbCuAl [13], TbNiAl (16 K) [14] TbPtSn [15], TbCuIn [16], TbAuIn [17], TbPdIn [18], TbPtIn [19], TbRhSn [20], TbNiIn (68 K) [21].

The observed magnetic ordering results from the competition between exchange interactions of the RKKY type, the geometrical frustration of the rare-earth magnetic moments and the influence of the crystal field. The latter affects the direction of magnetic moments and is responsible for the magnetocrystalline anisotropy. The refinement of the neutron diffraction patterns shows us the orientation of the magnetic moments, thus also the change of the magnetocrystalline

anisotropy in TbNi(Al,In) series. The direction of magnetic moments of the components with propagation vector $\vec{k} = (000)$ in low In concentrations ($x \leq 0.4$) remains parallel with the hexagonal c-axis whereas in concentrations with $x \geq 0.5$ the Tb moments lie within the basal plane. The change of the c/a ratio due to the Al-In substitution causes the change of the magnetocrystalline anisotropy from the uniaxial to a planar type. We can observe the decrease of the magnetocrystalline anisotropy with increasing In content up to $x = 0.4$ in the low temperature X-ray diffraction in static magnetic field (see Figures 4.7 and 4.8). The value of the magnetocrystalline anisotropy of the uniaxial ordering decreases and for $TbNiAl_{0.5}In_{0.5}$ compound is energetically preferable to flip the magnetic moments into the basal plane. The exact size of the anisotropy is possible determine from the single crystal measurement, but unfortunately we have the polycrystalline samples only. Thank to the knowledge where the magnetocrystalline anisotropy changes from the uniaxial to planar type in TbNi(Al,In) series, we can estimate the region where one can expect the change of the anisotropy in TbTX compounds in general. TbPtSn compound ([15]) with more complex magnetic structure should belong to this region. We can redraw Figure from the beginning of the work (Figure 2.3 from Section 2.1) to obtain Figure 4.55.

5. Conclusions

This thesis has been focused on the change of the magnetocrystalline anisotropy in pseudo-ternary TbTX compounds, on structural and magnetic properties and the relationship between them in TbNi(Al,In) series respectively. The hexagonal ZrNiAl-type of structure of this series was verified by X-ray and neutron diffraction experiments.

The magnetic properties of TbNi(Al,In) series were closely investigated by AC-susceptibility, magnetization, specific heat and electrical resistivity measurements in the temperature region between 2 and 300 K. TbNiAl orders as collinear antiferromagnet. This antiferromagnetic ordering can be easily disrupted by the substitution of 10% of Al by In. We found evidences of a ferromagnetic arrangement of magnetic moments in low In concentrations by magnetization measurements. The ferromagnetic order was confirmed by powder neutron diffraction. The magnetic ordering in In rich concentrations can not be easily described as antiferro- or ferro- magnetic, but as complex non-collinear structure.

The magnetic structure of the series was studied by powder neutron diffraction. The magnetic arrangement is characterized by two propagation vectors $\vec{k} = (000)$ and $(\frac{1}{2}\ 0\ \frac{1}{2})$ in the whole series. Stronger magnetic reflections are observed for $\vec{k} = (000)$ and weaker for $\vec{k} = (\frac{1}{2}\ 0\ \frac{1}{2})$, except the concentrations with 80 and 90% of In where both components of magnetic moment have approximately the same value at 2 K. The magnetocrystalline anisotropy changes from the uniaxial type of In poor concentrations to planar type in In rich compounds. The change occurs in concentration range between 40 and 50% of In. The flip of the components of magnetic moment with the propagation vector $\vec{k} = (000)$ from the direction parallel to the hexagonal c-axis to basal plane happens only, the component with $\vec{k} = (\frac{1}{2}\ 0\ \frac{1}{2})$ remains within the basal plane for all concentrations. An additional magnetic phase transition was observed in the ordered state in TbNi(Al,In) series. This transition is most probably related to certain change of the arrangement of components described by $(\frac{1}{2}\ 0\ \frac{1}{2})$ propagation.

From the knowledge where the change of the magnetocrystalline anisotropy in TbNi(Al,In) series occurs, we can estimate the region where the type of anisotropy changes for hexagonal TbTX compounds in general. The knowledge of the structural parameters allows us to estimate the change of the magnetic anisotropy in these compounds.

Bibliography

[1] V. M. Goldschmidt, *Geochemische Verteilungsgesetze Der Elemente, Part V: Isomorphie Und Polymorphie Der Sesquioxyde. Die Lanthaniden-Kontraktion Und Ihre Konsequenzen*, Oslo, 1925.

[2] N. N. Greenwood, A. Earnshaw, *Chemistry of the Elements (2nd ed.)*, Oxford, 1997.

[3] N. W. Ashcroft, N. D. Mermin, *Solid State Physics*, Philadelphia, 1976.

[4] I. A. Campbell, *J. Phys. F: Metal Phys.*, **2** (L47) 1972.

[5] V. F. Sears, *Neutron News*, **3** (26) 1992.

[6] V. Sechovský, L. Havela, E. P. Wolfhart, K. H. J. Buschow, *Handbook of Ferromagnetic Materials*, Prague, 1988.

[7] B. Bandyopadhyay, K. Ghoshray, A. Ghoshray, N. Chatterjee, *Phys. Rev. B*, **38** (8455) 1988.

[8] G. Ehlers, H. Maletta, *Z. Physik B*, **101** (317) 1996.

[9] A. Dönni, G. Ehlers, H. Maletta, P. Fischer, H. Kitazawa, M. Zolliker, *J. Phys.: Condens. Matter*, **8** (11213) 1996.

[10] P. Javorský, P. C. M. Gubbens, A. M. Mulders, K. Prokeš, N. Stüsser, T. J. Gortenmulder, R. W. A. Hendrikx, *J. Magn. Magn. Mater.*, **251** (123) 2002.

[11] E. Morosan, S. L. Buďko, P. C. Canfield, *Phys. Rev. B*, **71** (014445) 2005.

[12] J. Prchal, H. Kitazawa, T. Furubayashi, P. Javorský, K. Koyama, V. Sechovský, *Physica B*, **378-380** (1102–1104) 2006.

[13] G. Ehlers, D. Ahlert, C. Ritter, W. Miekeley, H. Maletta, *Europhys. Lett.*, **37** (269) 1997.

[14] P. Javorský, P. Burlet, V. Sechovský, A. V. Andrejev, J. Brown, P. Svoboda, *J. Magn. Magn. Mater.*, **166** (133–140) 1997.

[15] A. Szytuła, M. Kolenda, J. Leciejewicz, N. Stüsser, *J. Magn.Magn. Mater.*, **164** (377–380) 1996.

[16] A. Szytuła, A. Arulraj, S. Baran, T. Jaworska-Gołąb, B. Penc, N. Stüsser, Yu. Tyvanchuk, A. Zarzycki, *Acta Phys. Polonica A*, **113** (4) 2008.

[17] A. Szytuła, W. Bażela, Ł. Gondek, T. Jaworska-Gołąb, B. Penc, N. Stüsser, A. Zygmuntd, *J. Alloys and Compounds*, **336** (11–17) 2002.

[18] P. Javorský, J. Fikáček, J. Prokleška, S. Nishigori, G. J. Mc Intyre, *Acta Physica Polonica A*, **118** (879) 2010.

[19] E. Morosan, S. L. Buďko, P. C. Canfield, *Phys. Rev. B*, **72** (014425) 2005.

[20] S. Baran, M. Bałanda, P. Fischer, W. Sikora, A. Szytuła, *J. Magn.Magn. Mater.*, **261** (369–376) 2003.

[21] Yu. B. Tyvanchuk, Ya. M. Kalyczak, Ł. Gondek, M. Rams, A. Szytuła, Z. Tomkowicz, *J. Magn. Magn. Mater.*, **277** (368) 2004.

[22] J. Prchal, P. Javorský, V. Sechovský, M. Dopita, O. Isnard, K. Jurek, *J. Magn. Magn. Mater.*, **283** (34) 2004.

[23] J. Prchal, P. Javorský, J. Poltierová Vejpravová, O. Isnard, B. Detlefs, S. Daniš, V. Sechovský, *Intermetalics*, **18** (2109–2118) 2010.

[24] J. Prchal, E. Šantavá, D. Schmoranzer, *Physica B*, **404** (3056–3058) 2009.

[25] J. Fikáček, P. Javorský, M. Klicpera, E. Šantavá, *Acta Physica Polonica A*, **118** (884) 2010.

[26] P. Javorský, *Phd. Thesis*, Prague, 1997.

[27] J. Prchal, *Phd. Thesis*, Prague, 2006.

[28] A. V. Andreev, P. Javorský, A. Lindbaum, *J. Alloys and Compounds*, **290** (10–16) 1999.

[29] J. Prchal, and B. Detlefs P. Javorský, S. Daniš, O. Isnard, *J. Magn. Magn. Mater.*, **310** (589) 2007.

[30] J. Prchal, P. Javorský, J. Rusz, F. de Boer, M. Diviš, H. Kitazawa, A. Dönni, S. Daniš, V. Sechovský, *Phys. Rev. B*, **77** (134106) 2008.

[31] Y. Isikawa, T. Kuwai, T. Mizushima, T. Abe, G. Nakamura, J. Sakurai, *Physica B*, **281-282** (365) 2000.

[32] P. Javorský, J. Prokleška, O. Isnard, J. Prchal, *J. Phys.: Condens. Matter*, **20** (104223) 2008.

[33] P. Javorský, J. Prchal, D. Adroja, *J. Phys.: Condens. Matter*, **146** (21–24) 2008.

[34] G. Ehlers, H. Maletta, *Z. Physik B*, **99** (145–150) 1996.

[35] G. Ehlers, C. Ritter, J. R. Stewart, A. D. Hillier, H. Maletta, *Phys. Rev. B*, **75** (024420) 2007.

[36] G. Ehlers, C. Ritter, A. Kurtjakow, W. Miekeley, N. Stüsser, Th. Zeiske, H. Maletta, *Phys. Rev. B*, **59** (8821) 1999.

[37] Ł. Gondek, A. Szytuła, S. Baran, J. Hernandez-Velasco, *J. Magn. Magn. Mater.*, **272-276** (e443–e444) 2004.

[38] G. Ehlers, *Phd. Thesis*, Berlin, 1996.

[39] P. Javorský, F. Wastin, E. Colineau, J. Rebizant, P. Boulet, G. Stewart, *J. Nucl. Mat.*, **344** (50) 2005.

[40] J. Kamarád, Z. Machátová, Z. Arnold, *Rev. Sci. Instrument*, **75** (5022–5025) 2004.

[41] J. Rodriguez–Carvajal, *Physica B*, **192** (55) 1993.

[42] C. M. Andrei, J. Walmsley, Y. D. Yu, H. W. Brinks, R. Holmestad, B. C. Hauback, *J. Magn.Magn. Mater.*, **356-357** (658–663) 2003.

[43] N. K. Singh, K. G. Suresh, R. Nirmala, A. K. Nigam, S. K. Malik, *J. Magn.Magn. Mater.*, **302** (302–305) 2006.

[44] W. Suski, B. Bielan, R. Gladyshevskii, O. I. Bodak, A. Gilewski, T. Mydlarz, K. Wochowski, *J. Magn. Magn. Mater.*, **300** (221) 2006.

[45] K. Gofryk, D. Kaczorowski, *J. Phys.: Condens. Matter*, **18** (3887) 2006.

[46] W. Suski, *Materials Science - Poland*, **25** (2) 2007.

[47] S. Chikazumi, *Physics of Magnetism*, New York, 1964.

[48] C. Kittel, *Solid State Physics*, **22** (1–26) 1969.

[49] P. Daniel, P. Javorský, J. Prchal, E. Šantavá, S. Daniš, *Acta Physica Polonica A*, **113** (1) 2008.

[50] S. Daniš, P. Javorský, D. Rafaja, *J. Alloys and Compounds*, **345** (10–15) 2002.

[51] SARAh, refinement program, available at http://www.ucl.ac.uk/chemistry/.

[52] M. Bałanda, A. Szytuła, M. Guillot, *J. Magn.Magn. Mater.*, **247** (345) 2002.

[53] P. Javorský, P. Svoboda, S. Nishigori, M. Hofmann, N. Stüsser, *Acta Physica Slovaca*, **48** (767) 1998.

List of symbols

a	lattice parameter
a.u.	arbitrary units
b_c	coherent scattering length
BSE	back scattered electrons
c	velocity of light
c	lattice parameter
C	Curie constant
c_A	atomic concentration
c_p	specific heat
$c_{el,ph,mag}$	electronic, phonon, magnetic specific heat
CF	crystal field
d	interplane spacing (diffraction)
e	electron charge
EDX	energy dispersive X-ray diffraction
f_{cor}	parameter describing preferred orientation
FC	field cooled
f.u.	formula unit
F_{hkl}	(nuclear) structure factor
F_M	magnetic structure factor
$f_{at}(\vec{q})$	atomic dispersion factor
$f(\vec{q})$	magnetic formfactor
h,k,l	Miller indices
H	magnetic field
$\hat{H}$	Hamiltonian
I	intensity of diffracted beam
J	total angular quantum number
J_{ij}	exchange integral
$\vec{k}$	propagation vector
L	total orbital quantum number
m	magnetic moment
m_e	electron mass
M	magnetization
M_S	saturated magnetization
M_{hkl}	March function (Fullprof program)
MPMS	Magnetic Property Measurement System
N_A	Avogadro constant
PPMS	Physical Property Measurement System
$\vec{q}$	scattering vector

R	gas constant
$\vec{r}$, $\vec{R}$	position vector
R	any rare earth
R_{Bragg}	refinement factor (nuclear intensities)
R_{M}	refinement factor (magnetic intensities)
RKKY	Ruderman-Kittel-Kasuya-Yosida interaction
S	total spin quantum number
S_{mag}	magnetic entropy
SE	secondary electrons
SEM	scanning electron mikroscope
T	temperature
T	any transition metal
T_{ord}	magnetic ordering temperature
$T_{\mathrm{C,N}}$	Curie, Néel temperature
T', T_1, T_{x}	temperatures of additional magnetic phase transitions
$V_{\mathrm{f.u.}}$	volume of formula unit
W	Debye-Waller displacement factor
x	fraction coordinate
x	number from interval (0.0; 1.0), studied concentrations
X	any p-metal
ZFC	zero field cooled

γ	Somerfeld coeficient (electronic contribution to specific heat)
Γ	representation
$\delta_{c_{\mathrm{A}}}$	error of atomic concentration
λ	wavelength
$\lambda_{1,2}$	relaxation rates (muon spectroscopy)
μ	magnetic moment
μ_0	vacuum permeability
μ_{eff}	effective magnetic moment
μ_{B}	Bohr magneton
μ_{SAT}	saturation moment
μSR	muon spectroscopy
θ	scattering angle
θ_{p}	paramagnetic Curie temperature
χ	magnetic susceptibility
χ', χ''	real, imaginary part of the AC-susceptibility
ρ, ρ_{tot}	electrical resistivity
$\rho_{\mathrm{0,ph,mag}}$	residual, phonon, magnetic contribution to electrical resistivity
$\rho(\vec{r})$	electronic charge density

Published results:

Magnetic Phase Transitions in TbNi(Al,In) Compounds,
M. Klicpera, P. Javorský, E. Šantavá, *Acta physica Polonica A* **118** 2010 (881).

Magnetocaloric Effect of the $Tb_{1-x}Y_x$ and $TbNiAl_{1-y}In_y$ Series,
J. Kaštil, P. Javorský, M. Klicpera, *Acta physica Polonica A* **118** 2010 (888).

The Change of Anisotropy in TbNi(Al,In) Compounds Studied by Low Temperature X-ray diffraction,
M. Klicpera, P. Javorský, S. Daniš, *Journal of Physics: Conference series*, in press.